UNIVERSITY OF OKLAHOMA

GRADUATE COLLEGE

CHARACTERIZATION OF THE SECOND-HALF REACTION OF *O*-ACETYLSERINE SULFHYDRYLASE-A AND THE REACTION OF *O*-ACETYLSERINE SULFHYDRYLASE-B FROM *SALMONELLA TYPHIMURIUM*

A Dissertation

SUBMITTED TO THE GRADUATE FACULTY

in partial fulfillment of the requirements for the

degree of

Doctor of Philosophy

By

Wael Mhd-Rabeh Rabeh

Norman, Oklahoma
2004

UMI Number: 3148885

UMI®

UMI Microform 3148885

Copyright 2005 by ProQuest Information and Learning Company.
All rights reserved. This microform edition is protected against
unauthorized copying under Title 17, United States Code.

ProQuest Information and Learning Company
300 North Zeeb Road
P.O. Box 1346
Ann Arbor, MI 48106-1346

CHARACTERIZATION OF THE SECOND-HALF REACTION OF *O*-ACETYLSERINE SULFHYDRYLASE-A AND THE REACTION OF *O*-ACETYLSERINE SULFHYDRYLASE-B FROM *SALMONELLA TYPHIMURIUM*

A Dissertation APPROVED FOR THE
DEPARTMENT OF CHEMISTRY AND BIOCHEMISTRY

BY

Paul Cook, Ph.D.

Phillip Klebba, Ph.D.

Ann West, Ph.D.

George Richter-Addo, Ph.D.

David Nagle, Ph.D.

© Copyright by Wael Mhd-Rabeh Rabeh 2004
All Rights Reserved.

ACKNOWLEDGMENTS

I would like to thank all members of my graduate committee at the University of Oklahoma for their help, encouragement and advice that I received throughout my studies, and for allowing me to pursue a Ph.D. My committee members include the following professors: Dr. Ann West, Dr Phillip Klebba, Dr. George B Richter-Addo, Dr. David Nagel, Dr. Bruce Roe, Dr. David McCarthy, and Dr. Roland Lehr.

A special thanks to Dr. William Karsten, Dr. Lilian Chooback and Dr. Dali Liu who initially trained me and taught me the different lab techniques to be used. Also all the members of Dr. Cook's lab and staff; Dr. Corey Johnson, Andi Babak, Dr. Lei Zhang, Dr. Chia-Hui Tai, Mamar Baizid, Lei Li, Jean Keil and Hengyu “Carina” Xu for their help and support. Additional thanks goes to Dr. West’s lab members for their support and help, Hui "Toni" Tan, Jennifer Gray, Dr. Fabiola Janiak-Spens, Dr. Stace Porter and Daniel Copeland.

My sincerest thanks and gratitude goes to my research advisor Dr. Paul F. Cook for accepting me as a member in his lab. His continued support and help made my studies more enjoyable and successful. Cordial appreciations and thanks to Dr. Cook's family for inviting me to be part of them, and all the happy family gatherings we had together.

Thanks to all the members of the Islamic Society of Norman and its leader Shiekh Abo-Mustafa and all my family and friends in Oklahoma, Syria and Kuwait for all the support and advice they gave me. Lots of thanks go to Dr. Dea’a, Abear, Ayaha Abo

Shamh and the Jalabi family for their great company and all the good times we had together.

Lastly, I want to dedicate this dissertation to my wife, Inas Al-Baghdadi and her family, M. Abdul-Lattif, Wafa'a, Anas, Amany, Dana, Samar Zubaidy, to my beloved daughter Nadia, and son Muhammad, my brothers, Ayham, Muhannad, and Ahmad, my uncle Jamal and my parents Mohammad Rabeh and Nadia Haj-Ibrahim for their ultimate support, love, and help emotionally and financially throughout my stay in the United States and for bearing all the tough times they went through with me. They are the greatest gift I was blessed with.

Thanking you.

TABLE OF CONTENTS

Page

LIST OF TABLES ………………………………………………………..…….. viii

LIST OF ILLUSTRATIONS ……………………………………………….…… ix

LIST OF SCHEMES ……………………………………………………….. xi

LIST OF ABBREVIATIONS ……………………………………………......... xii

ABSTRACT ………………………………………………………………... xiv

Chapter

I. INTRODUCTION ……………………………………………………………. 1

Assimilation and Dissimilation of Sulfur ……………………..................... 2

Vitamin B_6 Dependent Enzymes …..……………………………………. 8

Tryptophan Synthase ……………..……………………………………….. 12

Cystathionine β-Synthase …………..…………………………………….. 19

Threonine Deaminase ……………….……………….…………................... 23

O-Acetylserine Sulfhydrylase-A ……………………………………...... 26

O-Acetylserine Sulfhydrylase-B …….……………………………….…... 49

Research Carried Out in This Dissertation and Publications ……………… 53

II. MECHANISM OF THE ADDITION HALF OF THE *O*-ACETYLSERINE SULFHYDRYLASE-A REACTION …………………………………………… 54

Materials and Methods……………………………………..……………. 56

Results ……………………………………………………………….. 62

Discussion ……………………………………………………………. 83

Chapter Page

III. SPECTRAL CHARACTERIZATION OF *O*-ACETYLSERINE SULFHYDRYLASE-B FROM *SALMONELLA TYPHIMURUM* …………….. 92

Materials and Methods…………………………………………..……………. 93

Results ……………………………………………………………………….. 100

Discussion ………………………………………………………………….. 119

Appendix A. A 3D Homology Model of the *O*-Acetylserine Sulfhydrylase-B …….. 130

References …………………………………………………………………….... 144

LIST OF TABLES

Table Page

1. Summary of the pK_a Values Obtained in Steady State for OASS-A ………....... 40

2. Summary of the pK_a Values Obtained in Steady State for OASS-B ……............ 51

3. Kinetic Data of the Second Half of OASS-A Reaction ………………………….. 63

LIST OF ILLUSTRATIONS

Figure Page

1. The 3D Structure of WT Tryptophan Synthase from *S. typhimurium*. ………….. 14

2. The 3D Structure of the WT OASS-A ……………………………….…………….. 29

3. The Active Site of the WT OASS-A ……………………………………......... 31

4. Overlay of a Monomer of the Open and Closed conformations of OASS-A …… 35

5. Overlay of the Active Sites of WT OASS-A and K41A mutant ………………... 37

6. (A) 3D Overlay of the Closed and Inhibited Forms of OASS-A
   (B) The Allosteric Site of the Inhibited Form of OASS-A …...………...……….. 47

7. RSSF spectra of the Second Half of the OASS-A Reaction ………………....….. 65

8. Plot of k_{obs} for the Second Half of the OASS-A Reaction …………………….… 67

9. ^{1}H NMR Spectra of the Second Half of the OASS-A by Cyanide …………….... 69

10. pH(D) Dependence of log($k_{max}/K_{mercaptoacetate}$) ……..……………………………. 73

11. pH(D) Dependence of log($k_{max}/K_{cyanide}$) …………………………………….... 75

12. Arrhenius Plots of the Second Half of the OASS-A Reaction ……………...….... 77

13. Spectra of the Second Half of the OASS-A in D_2O …………………….….…..... 80

14. pH-Dependence of the UV-Visible Spectrum of OASS-B ……………………… 102

15. Titration of OASS-B with L-Cysteine ……………………..………………….... 104

16. Titration of OASS-B with L-serine ……………………..……………….......... 107

17. OASS-B OAS/Acetate Lyase Activity …………………………………………. 110

18. OASS-B pH-Dependence of the Pre-Steady-State Spectra …………………...… 112

19. Emission Spectra of OASS-B in the Absence and Presence of OAS …………… 115

Figure Page

20. Emission Spectra of OASS-B in the Absence and Presence of Ligands ……….. 117

21. Fluorescence Excitation Spectra of OASS-B at 425 nm ……………………...… 120

22. Fluorescence Excitation Spectra of OASS-B at 500 nm ………………………... 122

A1. Multiple Amino Acid Sequence Alignment of OASS-B, OASS-A, CBS, and the β-Subunit of Tryptophan Synthase ……………………………………. 132

A2. Overlay of the Monomer of OASS-A and CBS ……………………………….. 134

A3. The Topology Diagram of OASS-A and OASS-B ……………………………. 137

A4. The Structure of the Monomer of OASS-B and OASS-A ……………………. 139

A5. Overlay of the Active Sites of OASS-A and OASS-B ……………………….. 141

LIST OF SCHEMES

Scheme Page

1. Reduction of Sulfate via Assimilation/Dissimilation ……………………………. 3
2. The Overall Reaction of Sulfate Chemical Activation ………………………..…. 5
3. The Last Two Reaction of the Cysteine Biosynthetic Pathway ……………...….. 7
4. General Chemical Mechanism for PLP-Dependent Enzymes for the β-Family 10
5. The Overall Reaction of Tryptophan Synthase ………………………………….. 12
6. The Overall Reaction of Cystathionine β-Synthase ……………………………... 20
7. The Overall Reaction of Threonine Deaminase …………………………………. 23
8. The Kinetic Mechanism of *O*-Acetylserine Sulfhydrylase Reaction …….……… 26
9. Minimal Chemical Mechanism of OASS ………..…………………………… 43
10. Proposed Chemical Mechanism for OASS-A ………………………………….. 85
11. Overall Reaction of the Second Half of the OASS-A Reaction ………………… 88
12. The Molecular Structures of the Enolimine and Ketoenamine Tautomers ……… 124

LIST OF ABBREVIATIONS

AA	α-aminoacrylate external Schiff base intermediate
APS	adenosine 5'-phosphosulfate
BCA	β-chloro-L-alanine
Caps	3-(*N*-cyclohexylamino)-1-propanesulfonic acid
CBS	cystathionine β-synthase
Ches	2-(*N*-cyclohexylamino)ethanesulfonic acid
DTNB	5,5'-dithiobis(2-nitrobenzoate)
DTT	dithiothreitol
E	internal Schiff base
ESB(I)	OAS external Schiff base
ESB(II)	cysteine external Schiff base
GD	*geminal*-diamine intermediate
Hepes	*N*-(2-hydroxyethyl)piperazine-*N*'-2-ethanesulfonic acid
IPTG	isopropylthio-β-*D*-galactoside
k_{obs}	observed first order rate constant
k_{obs}/K_s	second order rate constant
K_{ESB}	dissociation constant of the external Schiff base complex
Mes	2-(*N*-morpholino)ethanesulfonic acid
OAS	*O*-acetyl-L-serine
OASS-A	A-isozyme of *O*-acetylserine sulfhydrylase
OASS-B	B-isozyme of *O*-acetylserine sulfhydrylase

PAPS	3’-phosphoadenosine 5’-phosphosulfate
PLP	pyridoxal 5’-phosphate
RSSF	rapid-scanning-stopped-flow
SAT	serine acetyltransferase
SCRs	structurally conserved regions
SRB	sulfur reducing bacteria
Taps	3-[[tris (hydroxymethyl) amino] propanesulfonic acid
TD	threonine deaminase
TNB	5-thio-2-nitrobenzoate
VRs	variable regions
WT	wild type

ABSTRACT

O-acetylserine sulfhydrylase (OASS) catalyzes the last step in the cysteine biosynthetic pathway in enteric bacteria and plant, substitution of the β-acetoxy group of *O*-acetyl-L-serine with inorganic bisulfide. The first half of the OASS-A reaction, formation of the α-aminoacrylate intermediate, limits the overall reaction rate, while the second half-reaction is thought to be diffusion-limited. The second half-reaction of OASS-A starts with bisulfide adding to C_β of the α-aminoacrylate intermediate to form the external Schiff base with cysteine, which is then released after transimination. The second half-reaction is very fast with a pseudo-first-order rate constant >1000 s^{-1}; and as a result, limited information is available. Rapid-scanning-stopped-flow (RSSF) experiments were used in an attempt to detect intermediates along the reaction pathway. The pH(D) dependence of the second half-reaction has been determined using the natural substrate, bisulfide, and sulfide analogs. The pH-dependence of the first order rate constant for disappearance of the α-aminoacrylate intermediate was measured over the pH range (6.0-9.5) using the natural substrate bisulfide, and a number of nucleophile analogs. The rate is pH-dependent for substrates with a $pK_a > 7$, while the rate constant is pH-independent for substrates with a $pK_a < 7$ suggesting that the pK_as of the substrate and enzyme group are important in this half of the reaction. In D_2O, at low pD values, the amino acid external Schiff base is trapped, while in H_2O the reaction proceeds through release of the amino acid product, which is rate-limiting. A number of new β-substituted amino acids were produced and characterized by ^1H NMR spectroscopy. Data are discussed in terms of the overall mechanism of OASS-A.

The *O*-acetylserine sulfhydrylase-B (OASS-B) was recently overexpressed and purified to electrophoretic homogeneity (>98% pure). Both the quantity and purity of the enzyme permit more kinetic and structurally based studies to be conducted. Spectral studies were carried out to characterize the different enzyme forms of the B-isozyme and to compare it to those of the A-isozyme. UV-visible spectra of OASS-B were pH-dependent over the pH range (6-9) in the absence and presence of amino acid substrate, *O*-acetylserine (OAS). Titrating the free enzyme with the substrate analogs, L-serine, and the amino acid product, L-cysteine show behavior opposite to that observed with the A-isozyme. The pH-dependence of the pK_{ESB} for both amino acids yields one enzyme group on the acid side of the pH profile with a pK_a value 6.9-7.7. The pH-dependence of the OAS:acetate lyase activity of the α-aminoacrylate intermediate decreases from a constant value at high pH to a new constant values at low pH, giving a pK_a of about 8.9. The fluorescence spectra of the B-isozyme differ from those observed with the A-isozyme where the intensity of the tryptophan emission peak does not change in the A-isozyme but a significant change is observed in the B-isozyme. Also, the PLP emission peak is more intense in the A-isozyme than in the B-isozyme. More experimental evidence is needed to determine the kinetic mechanism and to characterize the B-isozyme.

CHAPTER I

INTRODUCTION

Assimilation and Dissimilation of Sulfur.

Unlike most of the elements required by living systems, which undergo extensive metabolic transformations, plant and enteric bacteria utilize sulfur in its most highly oxidized naturally occurring form, sulfate. The reduction of inorganic sulfate to sulfide and the oxidation of sulfide back to sulfate is known as the biological sulfur cycle, which contains assimilatory and dissimilatory reduction pathways (*1*). Assimilation and dissimilation pathways reduce sulfate to sulfide to be used in biological processes. The bulk of sulfur in living beings returns to the cycle in the form of sulfide due to death and decomposition by fungi and bacteria. The following section will briefly cover the assimilatory and dissimilatory pathways in the sulfur cycle.

Sulfate Dissimilatory Pathway

The assimilatory sulfate reduction pathway is largely restricted to plants and aerobic microorganisms where it provides reduced sulfur for the living system. Under anaerobic conditions, sulfur reducing bacteria (SRB) use a variety of electron donors and couple their oxidation to the reduction of sulfate, which is used as an oxidant in place of molecular oxygen to produce bisulfide and ATP through oxidative phosphorylation in a process known as dissimilatory sulfate reduction or methanogenesis (*1, 2*). The dissimilatory pathway uses APS as the activated form of sulfate and the pathway proceeds through the formation of free sulfite and sulfide (Scheme 1).

Scheme 1. Reduction of Sulfate via Assimilation/Dissimilation: Sulfate enters the cell and is then reduced to sulfide to be incorporated into the cell through the assimilation pathway or sulfate is used as oxidant in place of molecular oxygen in the dissimilation pathway. The following abbreviations are used: APS (adenosine 5’-phosphosulfate), PAPS (3’-phosphate 5’-phosphosulfate), (1) Sulfate permease, (2) ATP sulfurylase, (3) APS kinase, (4) PAPS reductase, (5) Sulfite reductase, (6) APS reductase, (7) Bisulfite reductase, (8) Trithionate reductase, (9) Thiosulfate reductase, (10) Serine acetyltransferase, (11) *O*-acetylserine sulfhydrylase.

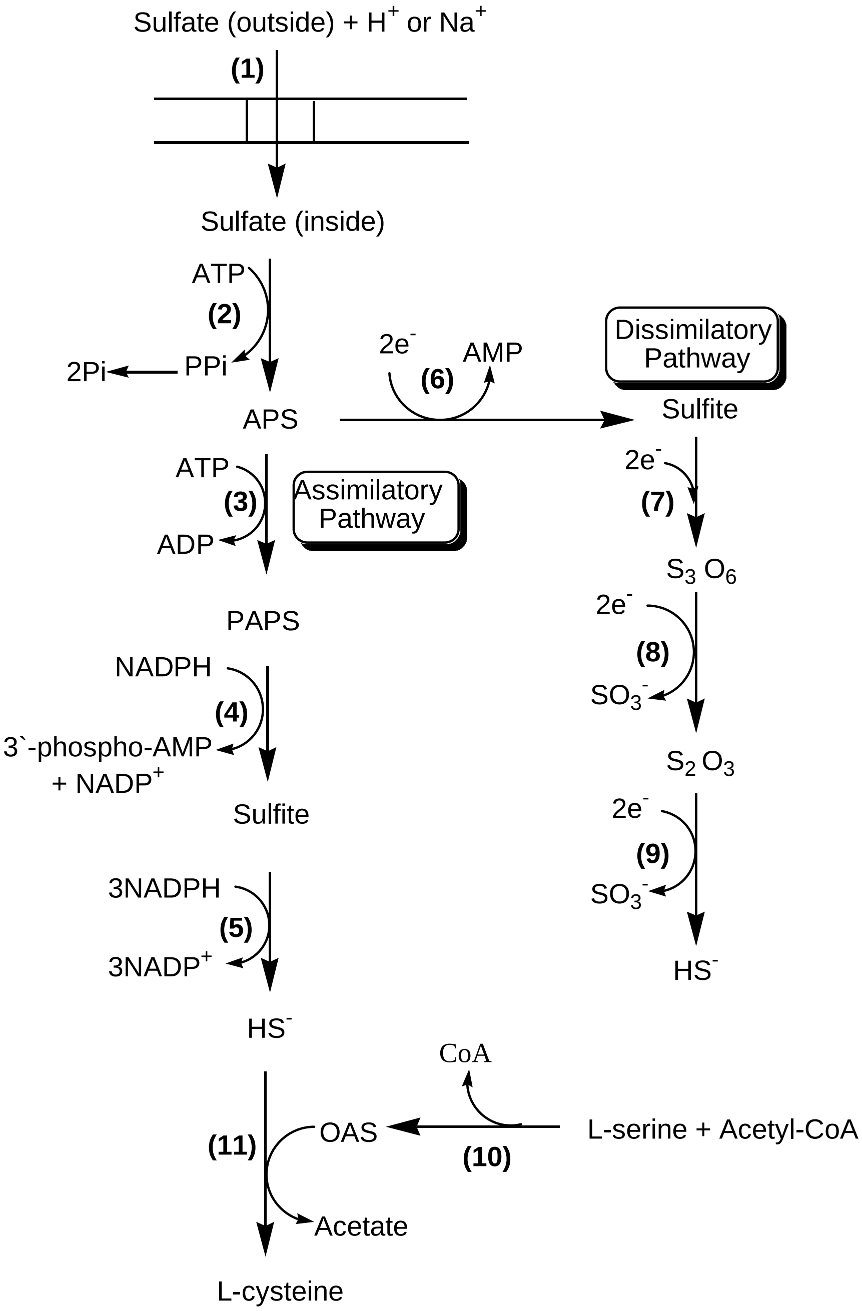
Sulfate (outside) + H⁺ or Na⁺
(1)
Sulfate (inside)
ATP
(2)
2Pi
PPi
APS
2e⁻
AMP
(6)
Dissimilatory Pathway
Sulfite
ATP
(3)
ADP
Assimilatory Pathway
2e⁻
(7)
S3 O6
PAPS
2e⁻
(8)
SO3⁻
NADPH
(4)
3`-phospho-AMP + NADP⁺
S2 O3
Sulfite
2e⁻
(9)
SO3⁻
3NADPH
(5)
3NADP⁺
HS⁻
HS⁻
CoA
(11)
OAS
(10)
L-serine + Acetyl-CoA
Acetate
L-cysteine

Sulfate Assimilation Pathway

The assimilation of sulfate begins with the transport of inorganic sulfate into the cell through active transport mediated by a carrier enzyme system, sulfate permease, encoded by *cys*A (*3*). The sulfate is then chemically activated by the following overall reaction (Scheme 2). Given a sufficient sulfate supply, sulfate uptake requires the symport of two protons, equivalent to two-thirds of an ATP, and under sulfate limitation it requires three protons, equivalent to one ATP (*2*).

Scheme 2.

$$2\ \mathrm{ATP} + \mathrm{SO_4^{2-}} \longrightarrow 2\mathrm{P_i} + \mathrm{ADP} + \mathrm{PAPS}$$

Sulfate activation starts with the synthesis of adenosine 5’-phosphosulfate (APS) from ATP and sulfate through the action of ATP sulfurylase (sulfate adenylyltransferase, EC 2.7.7.4) (Scheme 1) (*4*). Since this reaction is energetically unfavorable, the inorganic pyrophosphate produced by this reaction is hydrolyzed by inorganic pyrophosphatase to drive the reaction toward APS formation. APS kinase (adenylylsulfate kinase, EC 2.7.1.25) then phosphorylates the 3’-position of APS to give 3’-phosphoadenosine 5’-phosphosulfate (PAPS) using ATP as phosphoryl donor (*4*). Reductive elimination using NADPH as the reductant gives sulfite and 3’-phosphoadenosine 5’-phosphate. The resulting six electron reduction of sulfite to sulfide is carried out by the Mo-Fe containing sulfite reductase using reduced ferredoxin as the electron donor.

Sulfur is incorporated into the cell via the synthesis of the sulfur-containing amino acids (cysteine, cystine, and methionine) and the sulfur-containing growth factors (biotin, lipoic acid, and thiamin) (*2*). Cysteine is an important amino acid for all organisms due to the role it plays in protein folding. The formation of disulfide linkages between cysteine residues helps to stabilize the tertiary and quaternary structure of proteins. Disulfide linkages are most common in secreted proteins, where proteins are exposed to more oxidizing conditions than are found in the cellular interior. Most bacteria and plants can synthesize all 20 amino acids, and enteric bacteria and plants are able to synthesize cysteine and methionine using sulfate as the sole source of sulfur, which is reduced through the assimilation reduction pathway. On the other hand, mammals synthesize about half the amino acids (nonessential amino acids) and the remainder (essential amino acids) must be obtained from dietary sources in the form of methionine, which is used as the source of sulfur for homocysteine and cysteine synthesis (*5*). There are two pathways of L-cysteine biosynthesis: one is used by bacteria and plants and the other is used by mammals.

In mammals, L-cysteine is synthesized from homocysteine, a derivative of methionine (*5*). Methionine is an essential amino acid for mammals, making cysteine indirectly an essential amino acid as well. L-Methionine is converted to L-homocysteine by methionine adenosyltransferase (EC 2.5.1.6), various S-adenosylmethionine methyltransferases (EC 2.1.1.1) and S-adenosylhomocysteinase (EC 3.3.1.1). The last steps in cysteine synthesis in mammals includes the condensation of L-homocysteine and L-serine to form L-cystathionine through the action of cystathionine β-synthase (CBS; EC 4.2.1.22), a PLP-dependent enzyme. L-Cystathionine is then deaminated and hydrolyzed to form cysteine, α-ketobutyrate, and ammonia via cystathionine γ-lyase (EC; 4.4.1.1).

In enteric bacteria such as *Escherichia coli* and *Salmonella typhimurium* as well as in plants, the amino acid precursor of L-cysteine is L-serine, which undergoes a substitution of its β-hydroxyl group with a thiol in a two step reaction (*6, 7*). First, serine acetyltransferase (SAT; EC 2.3.1.30) activates serine by the addition of an acetyl moiety to its β-hydroxyl to form O-acetyl-L-serine (OAS) using acetyl-CoA as the acetyl donor (*8*). *O*-Acetylserine sulfhydrylase (OASS; EC 4.2.99.8) is the terminal enzyme in the cysteine biosyntheticpathway in plants and microorganisms, where it substitutes the acetyl group of OAS with sulfide and produce L-cysteine (Scheme 3).

Scheme 3.

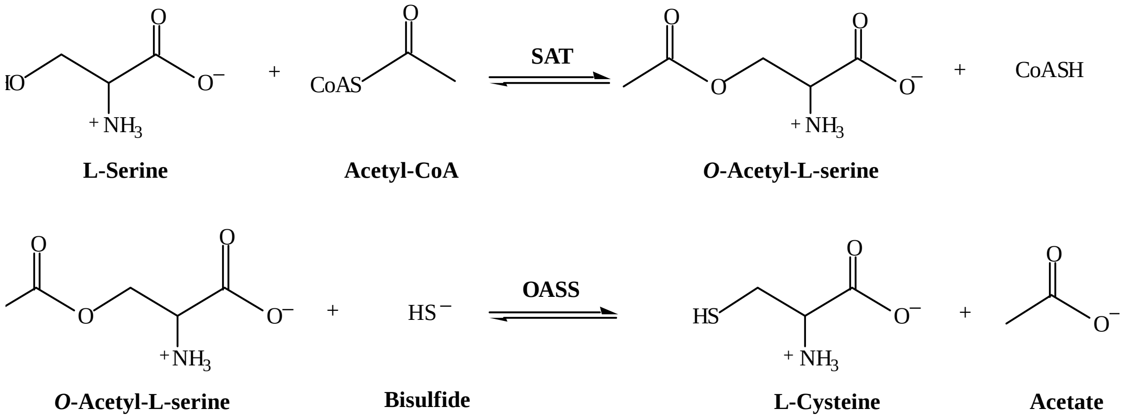

HO
O
O⁻
+NH3
+
CoAS
O
SAT
CoASH
L-Serine
Acetyl-CoA
***O*-Acetyl-L-serine**
HS⁻
OASS
HS
O-Acetyl-L-serine
Bisulfide
L-Cysteine
Acetate

SAT and OASS are found in a multienzyme complex, cysteine synthetase, which is composed of one homohexamer of SAT associated with two homodimers of OASS. The complex does not channel the intermediate substrate, OAS, between the two enzyme active sites, but it does result in stabilizing the acetyltransferase and might play a role in the metabolic regulation of the rate of cysteine formation (*9*, *10*). The complex can be resolved into free SAT and OASS upon incubation with OAS, and addition of sulfide counteracts the action of OAS (*10*, *11*). The binding of OASS to SAT results in a decrease in the turnover number of bound OASS by 50% and the K_m for OAS is increased. As a result, OASS in complex with SAT is considered unimportant as a catalyst while free OASS is active (*12*).

Vitamin B_6 Dependent Enzymes

Vitamin B6 in its biologically active phosphorylated derivatives, pyridoxal 5'-phosphate (PLP) and pyridoxamine 5'-phosphate (PMP), plays a major role in the metabolism of amino acids (racemization, transamination, β-elimination, β-replacement, decarboxylation, etc.). PLP-dependent enzymes are found in a variety of pathways ranging from the interconversion of β-amino acids to the biosynthesis of antibiotic compounds (*13*). PLP dependent enzymes are found in four out of the six EC classes of enzymes and they are part of , β and γ families (*13*). The α-family is the largest and was given the name because the substrate covalency changes occur at the C_α of the amino acid substrate. The α-family comprises all aminotransferases (with the possible exception of subgroup III) (*14*). The β and γ families catalyze covalency changes at the C_β and C_γ on the amino acid substrate, respectively. OASS is part of the β or fold II family.

PLP dependent enzymes, with the exception of phosphorylase, which uses the 5'-phosphate as a general base, catalyze their reaction via a number of covalent Schiff base intermediates with PLP. In almost all cases, PLP forms an internal Schiff base with the ε-amino group of an active site lysine residue (*15*). The internal Schiff base, protonated at the imine nitrogen, usually exhibits an absorption maximum at 400-430 nm attributed to the resonance stabilized ketoenamine in which electrons from O3' delocalize to the imine nitrogen (*15*). In some cases, the internal Schiff base absorbs in the near ultraviolet at 310-340 nm as a result of the enolimine form where the above resonance form is disallowed, and a proton resides on O3' of PLP. The first complex formed after the nucleophilic attack of the α-amine of the substrate on the internal Schiff base is the *geminal-diamine* intermediate, where the amine of the substrate and the lysine amine are both bonded at C4' of PLP, Scheme 4.

The lysine residue is displaced by the α-amino group of the amino acid substrate via transaldimination to generate the amino acid external Schiff-base (*13*), where a proton is transferred from the incoming α-amine of the amino acid substrate to the departing ε-amine of the enzyme lysine (*16*). These steps are common to all PLP-dependent enzymes involved in amino acid metabolism. A quinonoid intermediate is then formed after the abstraction of the α-proton of the external Schiff base and delocalization of electrons into the pyridine ring, where PLP acts as an electron sink to stabilize the developing negative charge. The quinonoid intermediate absorbs at wavelength higher than the external Schiff base (*17*). In order to form a quinonoid intermediate, N1 of the pyridinium ring must be protonated or ion-paired to an enzyme side chain as the intermediate forms (*16*). Formation of a quinonoid intermediate is not a must for many PLP-dependent enzymes, Scheme 4. General Chemical Mechanism for PLP-DependentE nzymes for the β-Family. The following are abbreviation for the enzyme forms used: E, internal Schiff base, GD, *geminal-diamine* intermediate; ESB, external Schiff base; Q, quinonoid intermediate; AA, α-aminoacrylate intermediate; X, functional group of the amino acid side chain; Nu, the nucleophilic substrate of the second half-reaction.

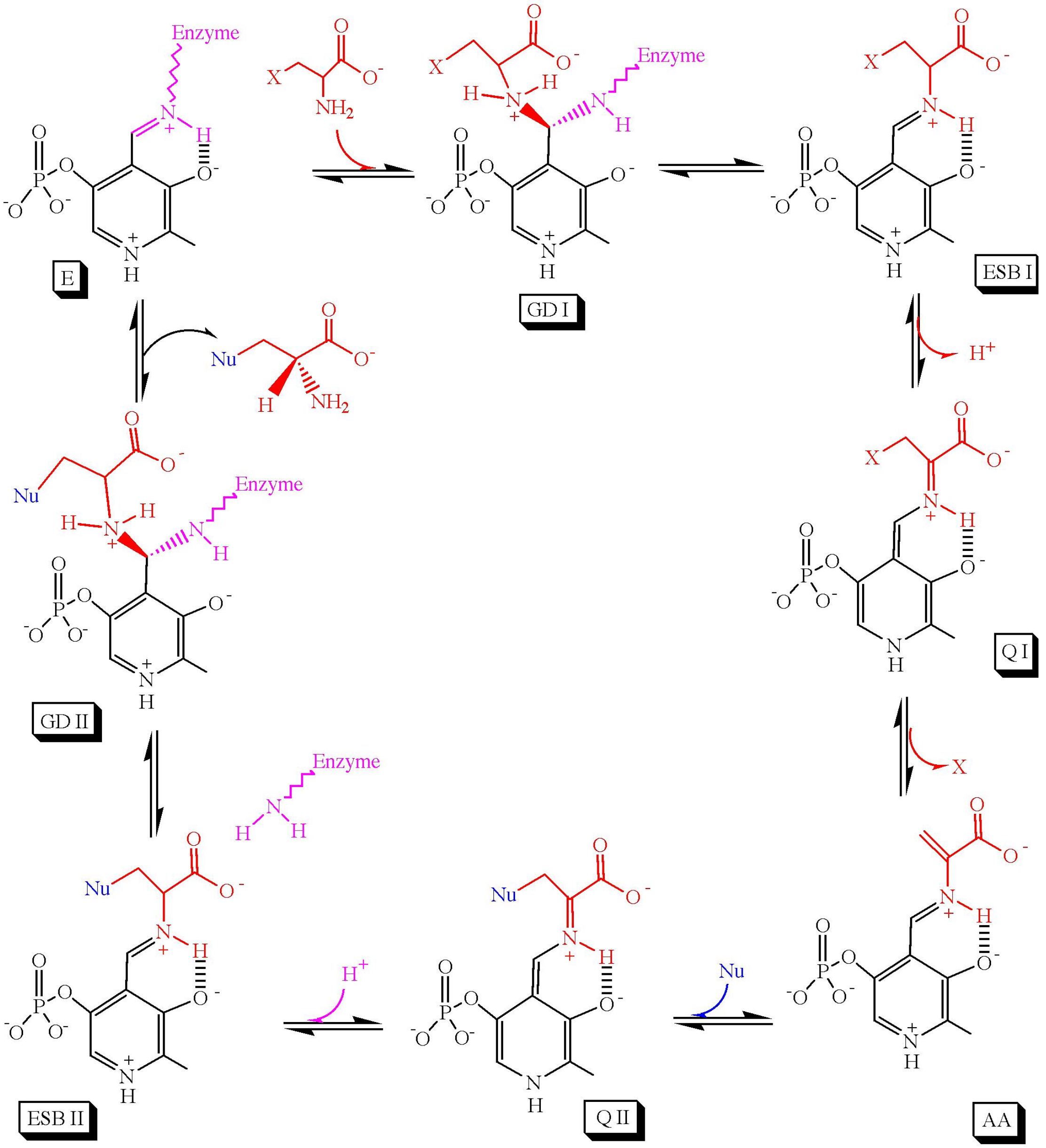
E
Enzyme
X
NH2
GD I
ESB I
H+
Q I
X
AA
Nu
Q II
H+
ESB II
Enzyme
GD II
Nu
H
NH2

and OASS-A does not form one under all experimental conditions tested. The α-aminoacrylate intermediate is formed upon elimination of the β-substituent of the amino acid substrate to mark the end of the first half-reaction. The α-aminoacrylate intermediate absorbs maximally between the wavelength of the substrate external Schiff base and the quinonoid intermediates. The following section will briefly cover some PLP enzymes, which are found to be similar to OASS, from the β-family.

Tryptophan Synthase

The bifunctional enzyme bacterial tryptophan synthase multienzyme complex catalyzes the last two steps in the biosynthesis of L-tryptophan. Tryptophan synthase is composed of 2 α- and 2 β-subunits. The α-subunit catalyzes the α-reaction, the reversible cleavage of indole glycerol 3-phosphate to give glyceraldyhyde 3-phosphate and indole. The β-subunit catalyzes, the PLP-dependent β-reaction, the irreversible formation of L-tryptophan from L-serine and indole (*18*, *19*) (Scheme 5).

Scheme 5.

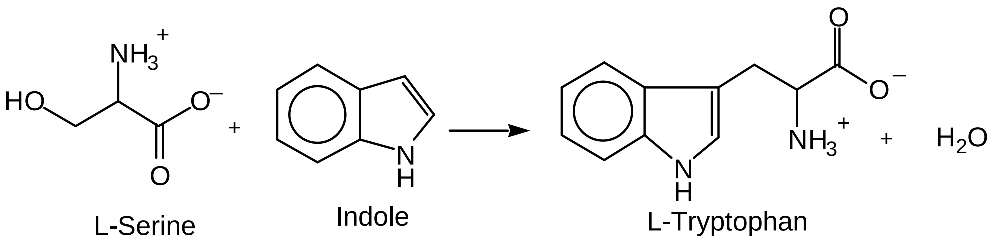

Three-Dimensional Structure. The 3D structure of the tryptophan synthase $\alpha_2\beta_2$ complex has an extended αββα arrangement with an overall length of about 150 Å (*20*) with a β_2 dimer located at the center of the complex and the two α-subunits at opposite ends of the complex (*19*). The α-subunit has an α/β barrel fold in which a substrate analog, indole 3-propanol phosphate, binds in the predominantly hydrophobic pit of the barrel Fig. 1 (*21*). The larger β-subunit (43 kDa) has two domains of equal sizes, the N- and C-domains, which have helix/sheet/helix structures Fig. 1. The PLP is sandwiched between the two domains and is shown on the surface of each domain at one end of the tunnel. The 3D-structure of the internal Schiff base form of the wild-type enzyme and the L-serine and L-tryptophan external Schiff bases of the K87T mutant enzyme (*20*) showed the binding environments of PLP are closely similar and the phosphate moiety of PLP is located at nearly identical positions in all the structures with some minor differences when tryptophan is bound to PLP. The conversion of the internal Schiff base to the external Schiff base results in a tilt of the planar pyridinium coenzyme ring by about 10°.

A 30 Å long hydrophobic tunnel, connects the α- and β-subunits, passes between the N- and C-domains of each β-subunit Fig. 1. It has been shown that indole, the product of the α-subunit, diffuses to the β-subunit active site through the tunnel to prevent the escape of indole into solution. The tunnel has a diameter and length sufficient to accommodate four molecules of indole (*19*). The $\alpha_2\beta_2$ complex serves to increase the rates of the α- and β-reactions up to 100-fold, increase substrate binding affinities, and alter reaction specificities. These changes are attributed to conformational changes occur upon assembly of the enzyme complex (*22*). Ligand binding to the active sites of the α- and β-subunits stabilize the αββα enzyme complex and reveals a large movement of part of the β-subunit termed the "mobile region" (residues 93–189) toward

Figure 1. Ribbon representation of the structure of WT tryptophan synthase from *S. typhimurium*. The structure shown is for the α-aminoacrylate intermediate of the β-reaction *(95)*, which was generated in the crystal under steady state conditions in the presence of serine and the α-site inhibitor 5-fluoroindole propanol phosphate (FIPP). A molecular two-fold axis of symmetry runs between αβ subunit pairs. The FIPP (green) and the PLP cofactor (pink), which are shown in space filling representation, are bonded to the active site of the α- and β-subunits, respectively. The smaller α-subunite (yellow) is connected to the β-subunite (aquamarine) through a 25Å tunnel. The following residues from both subunits align the tunnel are shown in space filling representation (yellow): $^{\alpha}$Phe-54, $^{\beta}$Phe-32, $^{\beta}$Cys-170, $^{\beta}$Ser-178, $^{\beta}$Phe-204, $^{\beta}$Phe-280, and $^{\beta}$Phe-306 The figure was prepared using DS Viewer 5.0 from Accelrys.

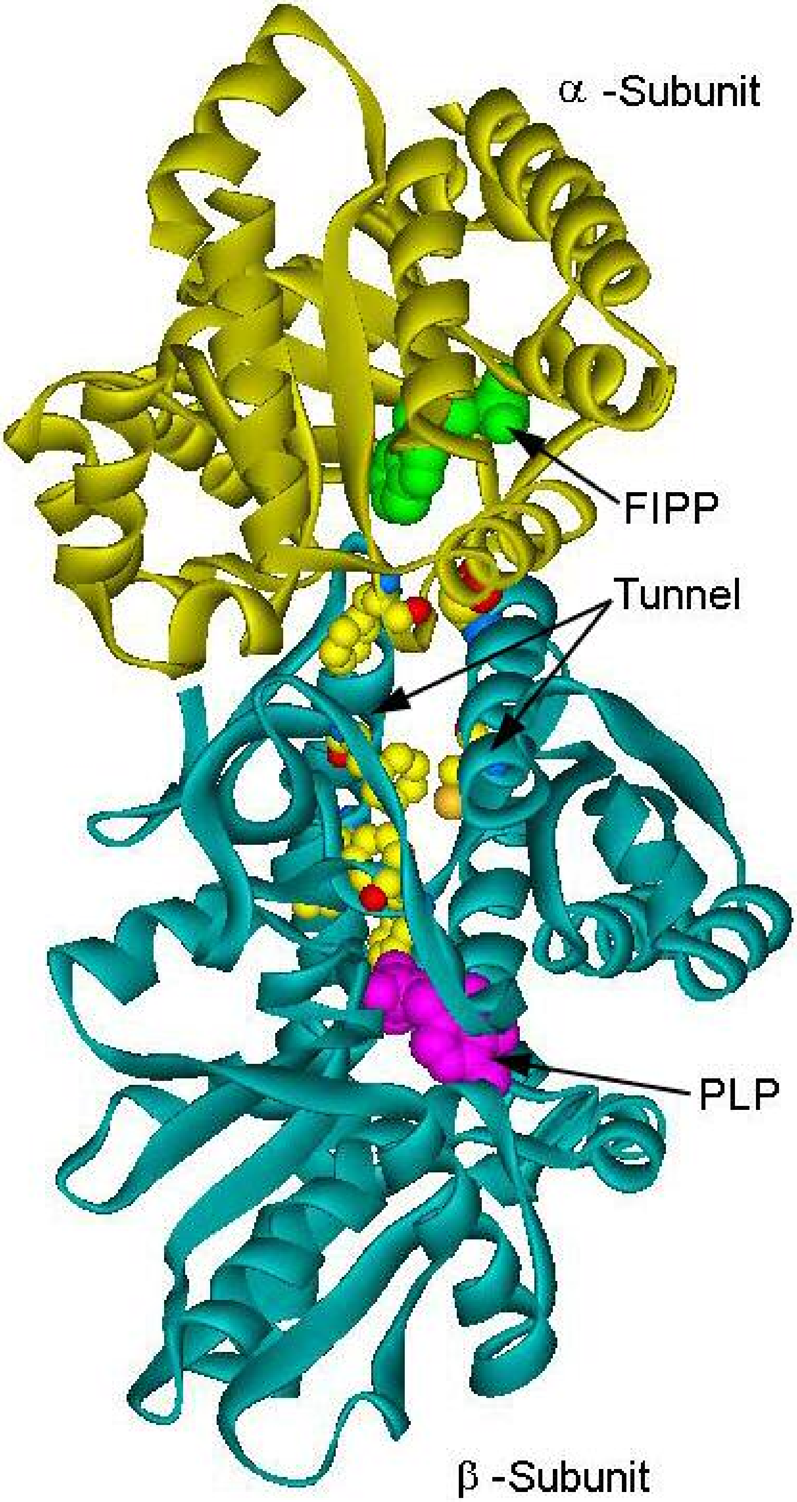
α -Subunit
FIPP
Tunnel
PLP
β -Subunit

the rest of the β-subunit (*21*). The conformational changes also decrease the volume of the tunnel and increase the buried surface area between the two domains of the β-subunit. Ligands that bind to the α-active site alter the reaction kinetics at the β-active site over a 30 Å distant. For example, the binding of glycerol 3-phosphate to the α-active site increases the affinity of the β-active site for the amino acid substrate, and the activity at the α-subunit is affected by the binding of the amino acid substrate, L-serine, to the β-subunit (*21, 23*).

The first monovalent cation site to be determined for a PLP-dependent enzyme in the β-family (*14*) or fold type II (*24*) was that of tryptophan synthase. The following are PLP-dependent enzymes that are activated by monovalent cation: dialkylglycine decarboxylase, pyruvate kinase, RNase T1, tyrosine phenol-lyase, tryptophanase, dialkylglycine decarboxylase, and tryptophan synthase (*25*). The monovalent cation in tryptophan synthase binds to a site in the C-terminal domain of the β-subunit about 8 Å from the phosphate of PLP and too distant from the active site to play a direct role in catalysis (*26*). The cation is stabilized by interaction with the carbonyl oxygens of three to six enzyme residues and with two water molecules. The interacting enzyme residues are located in a long loop (residues 259-310) that connects strand 8 with helix 10 and in a short loop (residues 231-234) between strand 7 and helix 9 (*20*). Residues in this region make several contacts with the α-subunit and contribute to the wall that lines the indole tunnel. Since the monovalent cation binding sites are not located in the active site, the bound cation should be classified as an allosteric effector (*25*). The allosteric effector may activate the enzyme by stabilizing the active conformation or may play a dynamic role. The presence of cations markedly improves the catalytic efficiency of the β-active site as revealed by the 20-40-fold increase of k_{cat}/K_m. Also, the apparent affinities of the α-aminoacrylate intermediate for indole in the Michaelis complex is increased in the presence of metal ions by about 2-3-fold. On the other hand, the activity of the $\alpha_2\beta_2$ complex is reduced in the absence of the monovalent cation, and the allosteric cross-talk between the α- and β-subunits is lost.

The Chemical Mechanism of the β-reaction. The β-subunit of tryptophan synthase catalyzes the β-replacement of the hydroxyl group of L-serine with an indole group to produce L-tryptophan in a PLP dependent reaction. The β-replacement reaction, involving indole, differs from most other PLP-dependent β-replacement reactions in that a C-C bond is cleaved. Furthermore, indole would be expected to be a very poor nucleophile for β-replacement reactions. The ε-amino group of βLys-87 forms an internal Schiff base (E; λ_{max} 410 and 330 nm) with the active site PLP. In the first-half of the β-reaction, the free enzyme is in an open conformation to allow binding and nucleophilic attack of the L-serine amino group on the C-4′ of PLP. The α-amine of L-serine displaces the ε-amine of βLys-87 via transaldimination and forms a serine external Schiff base (λ_{max} 424 nm) via geminal-diamine intermediates (λ_{max} 340 nm) (*27*). Serine external Schiff base accumulates as a stable intermediate before the slowest step in the first half-reaction, the removal of the C_α proton of L-serine external Schiff base (*27*). The α-aminoacrylate intermediate is formed after the elimination of the hydroxyl group of L-serine to end the first half of the β-reaction. The α-aminoacrylate intermediate yields a complicated final spectrum (λ_{max} 340 nm) with a broad envelope of absorbance extending out to 525 nm. The 340 nm band represents the enolimine tautomer (*19, 27*).

Direct evidence for the presence of the α-aminoacrylate intermediate comes from isolation of phosphopyridoxyl alanine from the $\alpha_2\beta_2$ enzyme complex treated with sodium borohydride in the presence of L-serine (*27*). Conversion of the L-serine external Schiff base to the α-aminoacrylate intermediate is accompanied by a change in the β-subunit conformation from an open to a closed conformation with access to solution blocked (*28*). Kinetic studies indicate that conversion of external Schiff base of L-serine to the α-aminoacrylate intermediate in the β-subunit activates the α-reaction significantly, and conformational changes in this step play a major role in allosteric interactions between the α- and β-subunits (*23, 29*).

The second half of the β-reaction is fast and is largely irreversible. It starts with the activation of the α-subunit product, indole, to facilitate the attack on the Schiff base of the α-aminoacrylate and forms quinonoid intermediate (λ_{max} at 420 nm) via indole tautomers (*19*). An external Schiff base of L-tryptophan is formed after the protonation of the C_α of the quinonoid intermediate followed by transimination with the ε-amino group of βLys-87 leading to the release of L-tryptophan and the conversion of the β-subunit back to its open free form, which is ready for a new cycle of catalysis (*27*). The reaction of L-serine at the β-active site activates indole 3-glycerol phosphate cleavage at the α-active site by 25-fold such that indole is not produced until L-serine has reacted to form the α-aminoacrylate intermediate in the β-subunit, over a distance of 30 Å (*21*). The rate of indole diffusion from the α- to the β-active site is very fast (> 1,000 s^{-1}), and this explains why indole does not accumulate during a single turnover in the α- and β-reactions. The removal of the C_α proton of L-serine in the first half of the β-reaction is rate limiting with the β-subunit alone but not when it is found in the $\alpha_2\beta_2$ enzyme complex. Association of the α- and β-subunit shifts the rate-limiting step from the removal of the C_α proton of L-serine external Schiff base to a much later step, protonation of the quinonoid of L-tryptophan (*19*). The major effect of the α-subunit on the catalytic power of the β-subunit is to accelerate the rate of abstraction of the C_α proton of L-serine (*19*). Therefore, the L-serine external Schiff base accumulates in the first half of the β-reaction under steady-state conditions with the β-subunit but not with the $\alpha_2\beta_2$ complex (*27*). A quinonoid intermediate has not been detected in the first half of the β-reaction but was detected in the second half of the β-reaction upon addition of L-tryptophan to the internal Schiff base with λ_{max} at 474 nm (*27*). A quinonoid with absorbance at 474 nm is not common among PLP enzymes, which usually give quinonoid intermediates with bands >500 nm (*30, 31*).

The replacement of the hydroxyl group of serine by indole in the tryptophan synthetase reaction proceeds with retention of configuration at C-3 of the amino acid substrate (*32, 33*). Tryptophan synthase mediates group transfer only on one face of the coenzyme-substrate complex, the *si* face, where the *pro-S* proton at C-4' of the PLP is removed and added back to the *si* face of the quinonoid intermediate, to yield the L-amino acid external Schiff base, and the reaction proceed with retention of the stereochemistry of the L-amino acid (*32-34*).

Cystathionine β-Synthase

Cystathionine β-synthase (CBS; EC 4.2.1.22) is the first enzyme of the transsulfuration pathway in higher eukaryotes where the potentially toxic homocysteine is converted to cysteine via two PLP-dependent enzymes. First, CBS condenses homocysteine and serine to give cystathionine, which undergo a γ-elimination reaction catalyzed by cystathionine γ-lyase in which cystathionine is cleaved to L-cysteine, α-ketobutyrate and ammonia (*35, 36*) (Scheme 6).

Scheme 6.

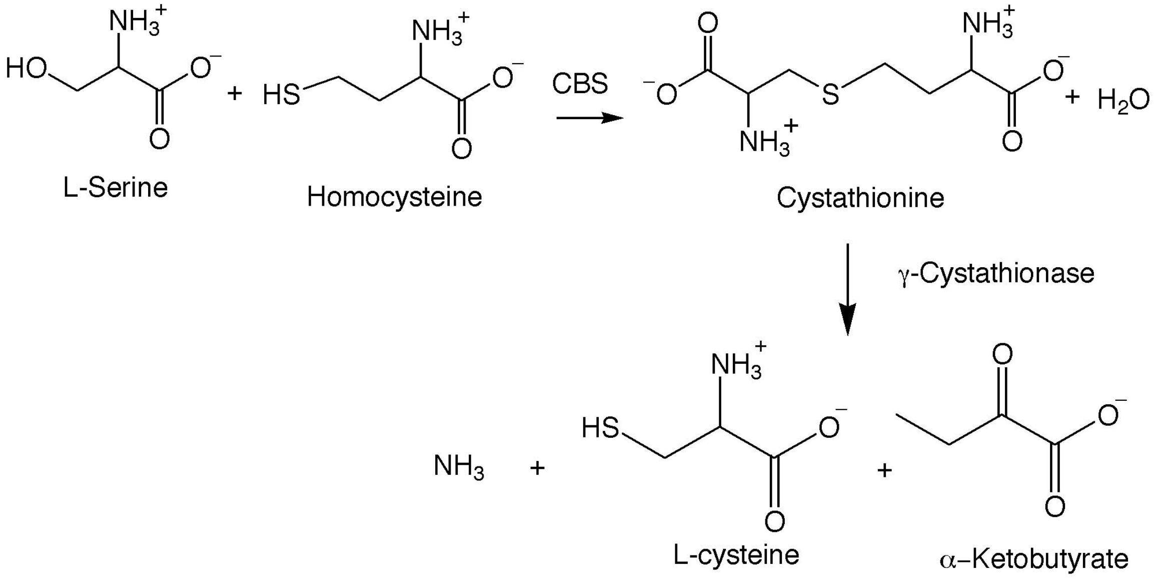

In microbes, the transsulfuration pathway operates in the forward direction, that is, in the degradation of methionine. In mammals, methionine is an essential amino acid, which can be converted via homocysteine to cysteine by the transsulfuration pathway, where elevated blood levels of homocysteine are a risk factor for the development of cardiovascular disease. One of the causes of elevated homocysteine is a genetic lack of CBS and excess methionine intake may be another explanation. Control of methionine intake and supplementing the diet with folic acid and vitamin B_{12} in the diet are used to lower homocysteine levels.

Three-Dimensional Structure. The human CBS is a homotetramer with 63 kDa subunits in which each subunit binds two cofactors, PLP and heme (*37*). Recent studies have shown that the heme moiety does not play a direct role in catalysis; rather, it plays a regulatory role. Each subunit is composed of two domains, N- and C-terminal domains, where the isolated N-terminal domain of CBS is more active than the full-length enzyme suggesting that the C-terminal domain regulates enzyme activity. The coenzyme PLP is deeply buried in a cleft between the two domains, where the active site is accessible only via a narrow channel. The dimer interface in human CBS is mainly hydrophobic in character (*37*). The C-terminal regulatory domain includes the so-called 'CBS domain', which gets displaced from the active site upon binding of the allosteric activator *S*-adenosyl-L-methionine. The CBS domain is named after cystathionine β-synthase with a highly conserved 53 amino acid motif found in a wide variety of proteins of diverse biological function including inosine monophosphate dehydrogenase, 5' AMP-activated protein kinase, chloride channels and a variety of other proteins (*38*). In all proteins, with the exception of CBS, this motif is present in multiple copies but no function has yet been attributed.

The nitrogen of the pyridine ring of PLP forms a H-bond to the hydroxyl of Ser-349 similar to the other PLP-enzymes of the β-family (*37*). Another H-bond is formed between the 3' hydroxyl group of PLP and the N^{ε} of Asn-149. The phosphate binding loop is located between β-strand 7 and α-helix 7. Residues Gly256-Thr260 form an extended H-bonding network with the phosphate moiety of PLP, thus anchoring the PLP to the protein matrix. In addition, the positive pole of α-helix 7 dipole compensates for the negative charge of the PLP phosphate group (*37*). The conformation of the residues surrounding the cofactor is highly conserved between CBS and OASS-A in which an asparagine loop adopts two slightly different conformations, indicating its flexibility and ability to bind the carboxylate group of the amino acid substrate by local conformational changes. In OASS-A, this conformational change includes atom movements of >7 Å upon substrate binding.

Chemical Mechanism. CBS catalyzes a ping-pong kinetic mechanism with the first half of its reaction identical to that of the tryptophan synthase β-reaction that is, the conversion of L-serine to the α-aminoacrylate Schiff base (*39*, *40*). The first half-reaction results in the removal of the α-proton of L-serine and the β-elimination of its hydroxyl group form the α- aminoacrylate intermediate. The β-elimination of the poor leaving group (OH^-) of L-serine requires enzyme assisted protonation. Addition of L-serine to the CBS internal Schiff base (λ_{max} 412 nm) results in the formation of an external Schiff base (λ_{max} 416 nm) via a *geminal-diamine* intermediate (λ_{max} 320 nm), where an α-aminoacrylate intermediate (λ_{max} 460 nm) is formed at the end of the first half of CBS reaction (*38*). The formation of the external Schiff base of L-serine is faster than the formation of the α-aminoacrylate intermediate, and the rate constant for the α-aminoacrylate intermediate formation is about 20-fold greater than the overall reaction rate. Thus, formation of the α-aminoacrylate intermediate is not the rate-limiting step as it the case with OASS-A.

The second half of CBS reaction involves the nucleophilic attack of the γ–thiol of L-homocysteine on the α-aminoacrylate intermediate to give the L-cystathionine external Schiff base. The enzyme lysine group (initial found in Schiff base linkage to PLP) then displaces L-cystathionine by transimination to regenerate the free enzyme form. The accumulation of cystathionine external Schiff base in the second half-reaction indicates that the product release is the rate limiting, and the rate of the overall reaction is rate-limited by the conversion of the α-aminoacrylate to L-cystathionine external Schiff base (*41*). In contrast, formation of the α-aminoacrylate intermediate is limiting in the OASS-A reaction, whereas product release is thought to be the rate-limiting step with tryptophan synthase (*40*). Quinonoid intermediates were not observed in either half of the CBS reactions (*41*).

Threonine Deaminase

Control of branched-chain amino acid biosynthesis in plants and microorganisms is achieved in part by the biosynthetic threonine deaminase (TD) pathway in which TD catalyzes the PLP-dependent dehydration/deamination of L-threonine (or L-serine) to 2-ketobutyrate (or pyruvate) (scheme 7) (*42*).

Scheme 7.

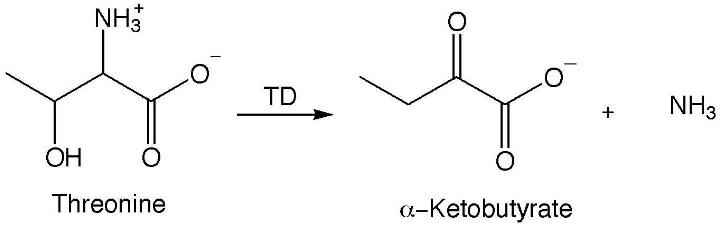

The end-products of the threonine deaminase pathway, isoleucine or valine, control carbon flow through the pathway in order to maintain a proper balance of metabolites for efficient protein synthesis (*42*). Neither isoleucine nor valine show appreciable affinity for the active site of TD, rather they bind to the allosteric site (*43*). Binding experiments with [^{3}H]isoleucine clearly confirmed the existence of two structurally different allosteric effector-binding sites per TD monomer (*44*). Isoleucine binds preferentially to a low activity T state of TD as an allosteric inhibitor, resulting in an increase in the sigmoidicity of the rate profile. Valine, on the other hand, activates the enzyme by preferentially binding to the high activity R state of TD, thereby giving rise to virtually hyperbolic kinetics. Isoleucine binding to a high-affinity site induces a modification of the conformation at the level of the regulatory domain, allowing the second effector-binding site with lower affinity to interact with a second isoleucine. The binding of the second isoleucine leads to a second modification of the conformation in the catalytic domain, leading to the observed inhibition (*44*). Also, the high-affinity binding site interacts with both regulators, isoleucine and valine. However, valine interaction induces different conformational modifications leading to reversal of isoleucine binding and reversal of inhibition. TD, like some PLP-dependent enzymes, has been shown to be stimulated by monovalent cations (*45*).

Three-Dimensional Structure. TD is a homotetramer (M_r 224 kDa) of identical 514-residue chains in which each polypeptide chain adopts two roughly equal-sized N- and C-terminal domains (*46*). Each subunit folds into a larger N-terminal domain, which contains the active site with one PLP bound per subunit (*46*). The N-terminal domain is composed of two α/β fold units, where each unit consists of four parallel β-strands, with helices on either side of the sheet. The PLP site is between the two α/β folds (*42*). The N-domain shows a striking similarity to the β-subunit of the tryptophan synthase. The C-terminal domain, also called the regulatory domain, is only slightly smaller in size and has an α/β organization, with three helices flanking eight antiparallel β-strands. The N- and C-terminal domains constitute two globular domains connected by a helix and there are no contacts between the domains within each subunit (*46*). The four N-terminal catalytic domains form the core of the TD tetramer, whereas the C-terminal regulatory domains form the ends and project out from a core of catalytic N-terminal domains. The subunits, and especially the regulatory domains, associate extensively to form dimers, and the dimers associate less extensively to form the tetramer. The tetramer can be considered a “dimer of dimers”, where interactions are weak, and involve contacts between catalytic domains. Thus, most of the interactions involved in the quaternary structure take place between the regulatory domains of each "dimer" (*46*).

TD is part of the β-family or type II fold family utilizing the same overall fold, with many of the catalytic active site residues conserved. The following residues are important in catalyzing the TD reaction, Ser-315 interacts with the pyridinium nitrogen of PLP, Phe-61 and Gly-241 provides van der Waals interaction with the aromatic pyridine ring, a tetraglycine loop (Gly188–Gly191) forms H-bonds with the 3’-hydroxyl and the amino acid substrates, and the N-terminus of helix 7 neutralize the negative charge of the phosphate group of PLP (*46*). Out of the several hundred PLP-dependent enzymes of known sequences, threonine deaminase is one of the few cooperative, feedback-regulated allosteric enzymes that utilize PLP as a cofactor (*47*).

O-Acetylserine Sulfhydrylase

Sulfur-containing amino acids play an important role in a variety of cellular functions such as protein synthesis, methylation, and polyamine and glutathione synthesis. Sulfur containing compounds, and especially cysteine and methionine, are essential for the growth and activities of all cells (*48*). Methionine initiates the synthesis of proteins, whereas cysteine plays a critical role in the structure, stability, and catalytic function of many proteins. In addition, cysteine is a precursor to glutathione, which is an important antioxidant. In enteric bacteria, two isozymes of OASS, -A and -B, are produced under aerobic and anaerobic growth conditions, respectively (*49-51*). The A- and B-isozymes are both homodimeric with MWs of about 68.9 and 70.8 kDa, respectively, and each has one tightly bound PLP per subunit.

O-Acetylserine Sulfhydrylase-A (OASS-A)

Kinetic Mechanism. The kinetic mechanism of OASS-A is Bi Bi ping pong as shown by initial velocity studies in the absence and presence of products and dead end inhibitors, isotope exchange at equilibrium, and equilibrium spectral studies (*52, 53*) (scheme 8).

Scheme 8.

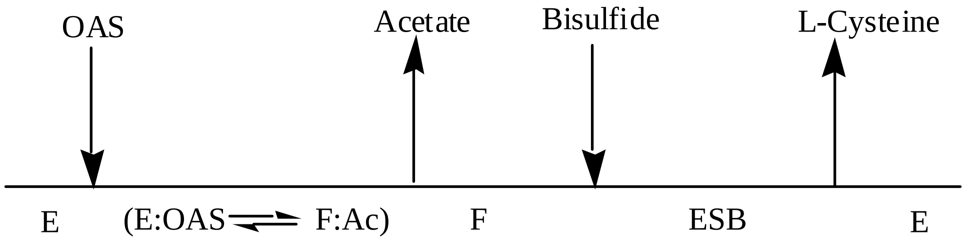

OAS binds to the internal Schiff base form of the enzyme (E), and acetate is released as the first product to yield the α-aminoacrylate (F) form of the enzyme. Bisulfide then adds as the second substrate to (F) to produce the cysteine external Schiff base (ESB). L-cysteine is released as the final product upon transimination. The initial velocity pattern obtained in the absence of added inhibitors exhibits competitive inhibition by both substrates, which is normally diagnostic for a ping pong mechanism, resulting from substrates binding to the incorrect enzyme form, OAS to F and bisulfide to E. In the present case, however, the inhibition results from the binding of substrates to an inhibitory allosteric site (*vide infra*, (*54*)). Substrates binding to the allosteric site affect substrate occupancy and reaction at the active site, and the end result is apparent competitive substrate inhibition.

The turnover number of the enzyme is 280 s^{-1}, and the first half-reaction limits the overall reaction. The second half-reaction is very fast and likely diffusion limited with a first-order rate constant >1000 s^{-1} measured at 5 μM bisulfide at pH 6.5 (*55*). In a classical one-site ping pong mechanism, the individual half-reactions are independent of the concentration of the other substrate. This is not the case forO ASS-A, and the V/K_{OAS} values were not identical when bisulfide (10^5 $M^{-1}s^{-1}$) or 5-thio-2-nitrobenzoate (TNB; 37 $M^{-1}s^{-1}$) was the nucleophilic substrate (*53*). The V/K values for the second-half reaction were within a factor of two of one another when different amino acid substrates were used. These data are reconciled as a result of a decrease in activity of the enzyme dependent on occupancy of the allosteric anion-binding site (*vide infra*). The rate with TNB is 10^4-fold lower than that obtained with bisulfide. With TNB as the nucleophilic substrate, only one third of the α-aminoacrylate intermediate is converted to the amino acid product, S-(3-carboxy-4-nitrophenyl)-L-cysteine, while the remaining two thirds is converted to pyruvate and ammonia.

Three-Dimensional Structure of OASS-A. OASS-A is an example of a fold type II enzyme, containing two domains of mixed α/β structure with one PLP moiety bound between the two domains (*24*). Other PLP enzymes with known structure share the same fold type as OASS-A are: tryptophan synthase (*20*), threonine deaminase (*56*), cystathionine β-synthase (*37*) and aminocyclopropane deaminase (*57*). The CBS structure is very similar to that of OASS-A that when a superposition between CBS and OASS-A yields a root mean square deviation (r.m.s.d.) of only 1.32 Å, while the differences between the structures are mainly located in the loop regions (residues 95–104, 282–298 and 359–369) (*37*).

The 3D structure of OASS-A without ligands bound has been solved to 2.2 Å resolution (*46*). The enzyme is a homodimer of 315 amino acid residues per subunit. The dimer is arranged such that entry to the two active sites is on the same side, Fig. 2. The subunits interact with one another only at the dimer interface and each of the active sites is made up of amino acids from a single subunit. The recently identified allosteric anion-binding site, located at the dimer interface, provides a reason for the overall dimeric structure other than stability (*58*). Each subunit is composed of two domains, an N-terminal domain, comprised predominantly of residues 1-145, and a C-terminal domain, comprised predominantly of residues 146-315. A portion of the N-terminal domain sequence, residues 13-34, crosses over into the C-terminal domain, forming the first two strands of its central β–sheet. Each domain is composed of an α/β fold with a central twisted β-sheet surrounded by α-helices, Fig. 2. The active site is located at the interface of the two domains, deep within the protein. The PLP cofactor is in Schiff base linkage with the ε-amino group of Lys-41, Fig. 3. The pyridine ring fits into a shallow

Figure 2. Ribbon representation of the structure of OASS-A. Left. The dimer of OASS-A with PLP in space-filling representation. A molecular two-fold axis runs from the lower left to the upper right of the molecule. Right. A monomer of OASS-A is shown. The two-domain nature of the structure is shown with the central, twisted β-sheet in both domains surrounded by helices (*24*). The entry to the active site is on the left of the monomer. The figure was prepared using DS Viewer 5.0 from Accelrys.

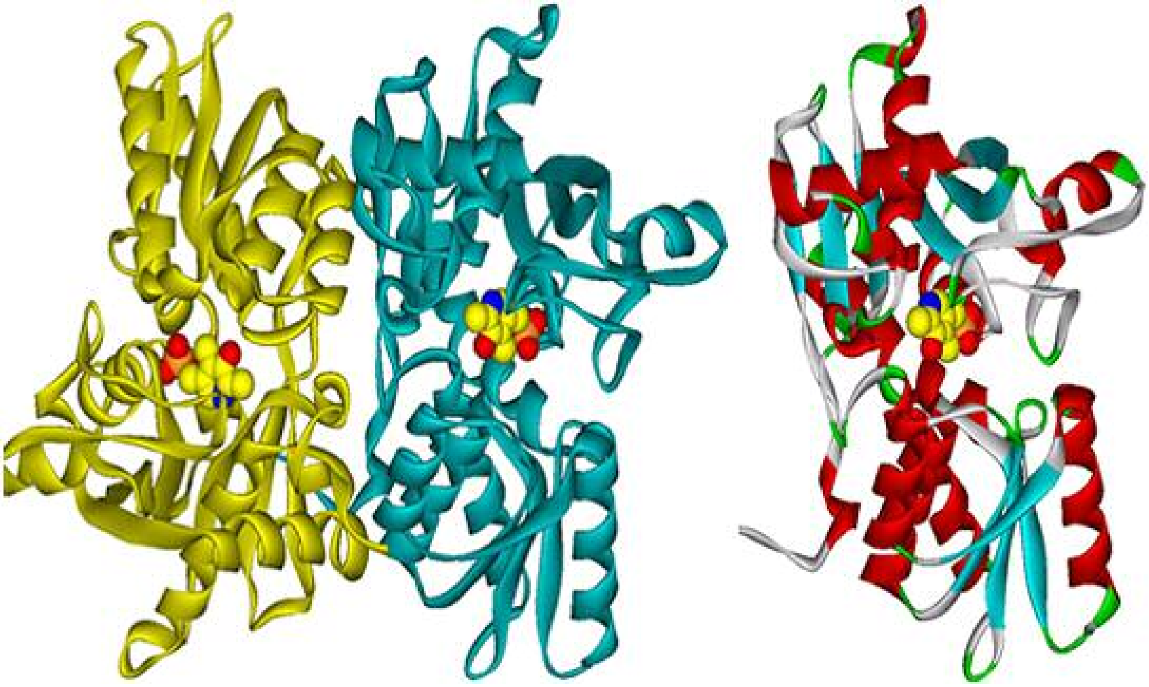

Figure 3. Stereo view looking into the active site of OASS-A (*24*). The *re* face of the cofactor is visible at the bottom of the active site cleft. The Schiff base linkage is shown between C4’ of PLP and Lys-41. Serine 272 is within H-bonding distance to N1 of the pyridine ring. The asparagines loop, which interacts with the α-carboxylate group of the amino acid substrate, is shown on the right and the threonine loop, which interacts with the 5’-phosphate is on the left. The side chain of N71 interacts with O3’ of the cofactor. The figure was prepared using DS Viewer 5.0 from Accelrys.

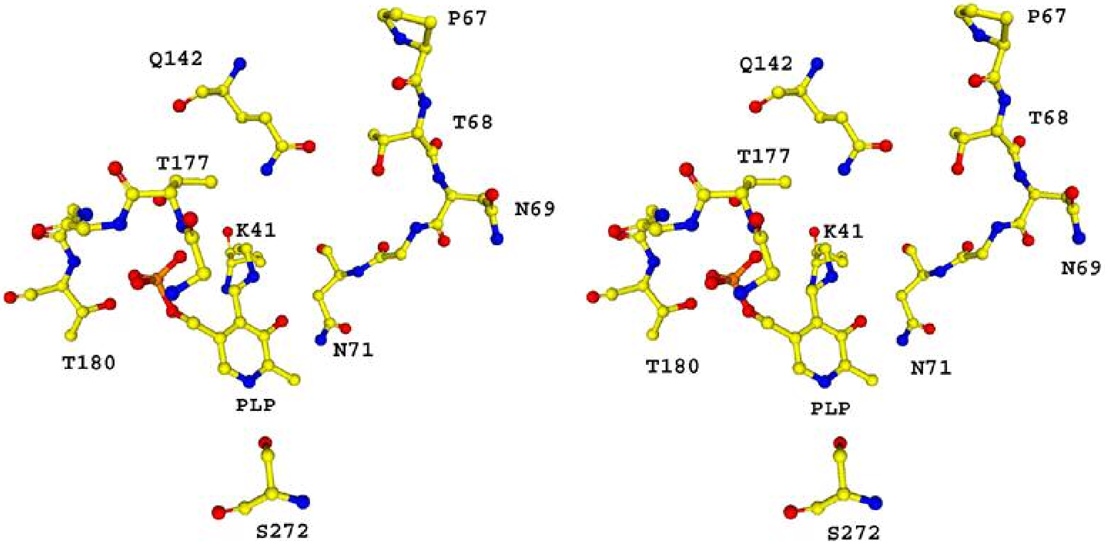
P67
Q142
T68
T177
N69
K41
T180
N71
PLP
S272
P67
Q142
T68
T177
K41
N69
T180
N71
PLP
S272

crevice and is supported at the back by Val-40. The 5'-phosphate of PLP is anchored by 8 H-bonds contributed by main chain and side chain functional groups in the G176-T180 loop, Fig. 3 (*59*).

The 5'-phosphate is dianionic, as suggested by ^{31}P NMR (*60, 61*), and its charge is partially neutralized by the dipole of helix 7, in the C-terminal domain, one of three helix dipoles directed toward the active site. The phenolic O3' of the cofactor is within H-bonding distance of the amide nitrogen of the Asn-71 side chain and the Schiff base nitrogen. Asn-71 is part of a loop structure (68-72) called the asparagines loop, and along with Glu-142, binds the substrate carboxylate group in the external Schiff base and subsequent intermediates along the reaction pathway, Fig. 3. A second helix dipole, contributed by helix 2, is directed at the asparagines loop and likely contributes to charge neutralization when substrate is bound. Finally, the pyridine nitrogen of the cofactor is within H-bonding distance to S272, and the dipole of helix 10. On the basis of the proximity of the helix dipole, it is unlikely that N1 of the PLP is protonated. A view looking into the active site indicates the *re* face of the PLP imine is exposed to the incoming amino acid.

Replacement of the Schiff base lysine, Lys-41, with alanine, resulted in isolation of a yellow enzyme suggesting PLP was bound in Schiff base linkage with a free amino acid, and this was shown to be methionine (*62*). Unlike the free enzyme, which is instantaneously reduced by $NaBH_4$, the Lys-41A mutant enzyme was resistant to reduction, suggesting the enzyme was in a closed conformation. The structure of the Lys-41A mutant enzyme of OASS-A revealed an external Schiff base between the enzyme and L-methionine (*59*). An overlay of the overall structure of the free enzyme and that of the Lys-41A mutant enzyme shows a large conformational change in a sub-domain of the N-terminal domain in which the central β-sheet has relaxed, closing the active site, Fig. 4. The closed form has the methionine substrate analog buried within the protein, and the active site cleft is no longer accessible to bulk solvent with only a narrow channel remaining to allow the passage of small molecules such as acetate (the first product) or bisulfide (the second substrate). In the open form, the C-terminal is less ordered than the N-terminal with higher thermal factor in the open conformation, but it becomes more ordered in the closed form of the enzyme.

Formation of the external Schiff base with methionine results in a rotation of the cofactor and subsequent movements of the pyridine nitrogen toward the protein interior and the external Schiff base linkage closer to the active site entrance, Fig. 5. The α-carboxylate group of the amino acid substrate is in a strong H-bonding network with residues of the asparagines loop (residues 68-72). Asn-69 moves 7Å compared to its position in the open conformation to make two new H-bonds, one with the α-carboxylate of amino acid substrate and the other with O3’ of PLP. The interaction between the asparagines loop and the α-carboxylate is the trigger that causes the movement of the sub-domain consisting of β-strands 4 and 5 and α-helices 3 and 4, reducing the twist of the central β-sheet and closing the site. Active site closure serves to expel bulk solvent and to properly position functional groups for catalysis. The cofactor pyridine ring, the Schiff base linkage, and the α-carboxylate group are all co-planar, while C_α of the amino acid substrate lies outside this plane. Modeling in the Schiff base lysine, Lys-41, shows superposition of its β-methylene with Ala-41 of the mutant enzyme and the lysine directed toward the *si* face of the external Schiff base. The side chain of methionine is

Figure 4. Overlay of a monomer of the open and closed conformations of OASS-A in ribbon representation (*24*, *62*). The open form is in yellow and the closed form is in aquamarine. PLP is shown as a space-filling model in the active site. The change in position of one of the loops in the two structures is shown to illustrate the large conformation change that occurs upon formation of the external Schiff base. The figure was prepared using DS Viewer 5.0 from Accelrys.

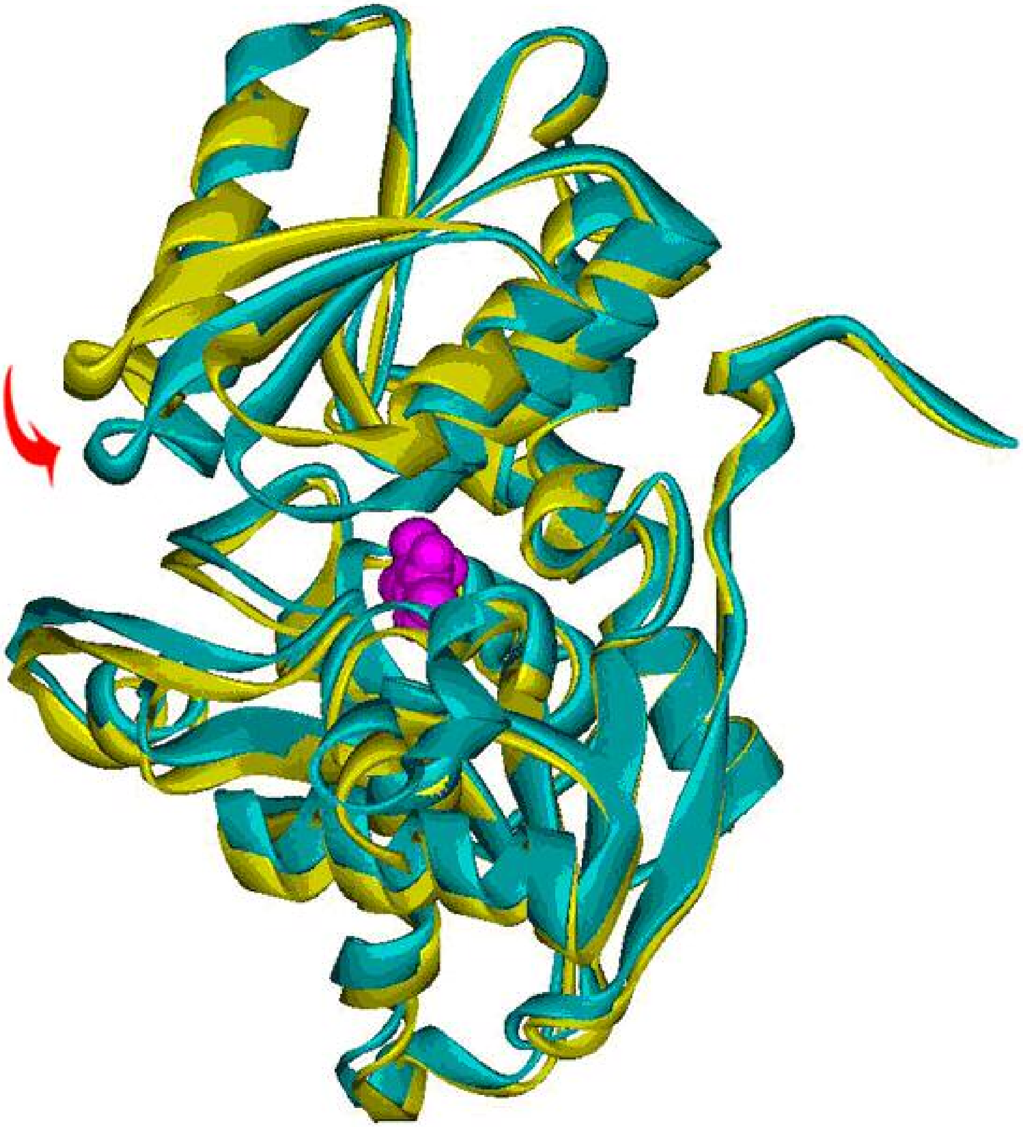

Figure 5. Overlay of the active sites of the wild type free enzyme (aquamarine) and the methionine external Schiff base of the Lys-41A mutant enzyme (yellow) (*24, 62*). Note the change in position of N69 of the asparagines loop as it moves to interact with the substrate carboxylate and O3’ of the coenzyme. The side chain of methionine is directed out of the figure toward the entrance to the active site. The ` indicates the open form of the enzyme. The figure was prepared using DS Viewer 5.0 from Accelrys.

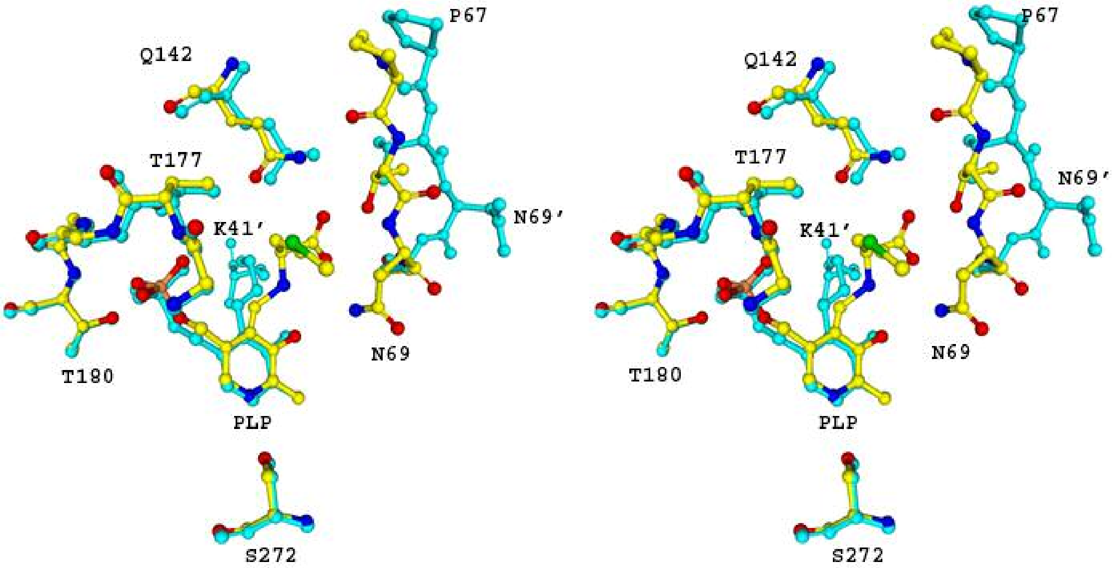
P67
Q142
T177
N69′
K41′
T180
N69
PLP
S272
P67
Q142
T177
N69′
K41′
T180
N69
PLP
S272

directed toward the entrance of the active site and away from the *re* face of the imine, i.e. the amino acid's α-proton and its side chain are *anti*.

Chemical Mechanism. The ping pong kinetic mechanism elucidated for the OASS-A indicates its reaction is catalyzed in two steps as an elimination-addition reaction to give the overall β-substitution reaction. Ultraviolet-visible spectral studies are consistent with an internal Schiff base (λ_{max} = 412 nm) present as the resting form of the enzyme and the α-aminoacrylate external Schiff base (λ_{max} = 330, 470 nm) present after elimination of the β-acetoxy group (*52, 60, 61, 63*). The pH dependence of V/K_{OAS}, which reflects free enzyme and the free amino acid substrate, exhibits a pK_a of 7.0 on the acidic side, while values of 6.7 on the acid side and 8.3 on the base side were measured with β-chloro-L-alanine (BCA) as the amino acid substrate (*64*). The pH dependence of V/K_{TNB}, which reflects the α-aminoacrylate external Schiff base and free TNB, shows pK_a values of 6.9-7.1 on the acidic side and 8.3 on the basic side. There are no ionizable groups in the active site of OASS-A that could be responsible for the pK_a of 7.0, Fig. 3, and there is no need for a general base in the elimination of acetate (when OAS was used as substrate) or chloride (when BCA was used as substrate), in which both are stable leaving groups. All pK_a values are summarized in Table 1 (*64*).

The basic pK_a observed in the V/K_{BCA} profile is that of the α-amine of the amino acid substrate, required to be unprotonated for nucleophilic attack on C4' of the PLP Schiff base. The basic pK_a observed in the V/K_{TNB} profile is attributed to the ε-amino group of Lys-41, which act as a general acid to protonate C_α as the product external Schiff base is formed. The enzyme also exhibits a β-elimination reaction in the absence of the nucleophilic substrate, in which transimination of the α-aminoacrylate external

Table 1: Summary of the pK_a Values for OASS-A (*64*).

	pK_a Acidic Side	pK_a Basic Side
OAS/Sulfide		
V/E_t	7.1	ND
V/K_{OAS}	7.0	ND
$V/K_{sulfide}$	7.3	ND
OAS/TNB		
V/E_t		9.0
V/K_{OAS}	7.45	ND
V/K_{TNB}	7.1	8.2
BCA/TNB		
V/E_t		9.0
V/K_{BCA}	6.7	7.4
V/K_{TNB}	6.9	8.3

Schiff base occurs giving free enzyme and free α-aminoacrylate, which decomposes in solution to pyruvate and ammonia (*60*). The pH dependence of the first order rate constant for disappearance of the α-aminoacrylate external Schiff base gives a pK_a of 8.2, which reflects the ε-amino group of Lys-41. The value agrees very well with the basic side pK_a in the V/K_{TNB} profile for the overall β-replacement reaction (*vide supra*).

The group with a pK_a of about 7.0 observed in both half-reactions reflects the same enzyme group that must be unprotonated for optimum activity. The lack of a need for additional acid-base or nucleophilic catalysis and the absence of ionizable group in the active site suggest the group is required unprotonated to stabilize the optimum catalytic conformation of the enzyme. In agreement with this suggestion a pK_a of about 7.0 is observed in the following processes. Excitation of OASS-A at 280 nm gives two emission maxima, one at 340 nm due to Trp emission, and a second at 500 nm resulting from triplet-singlet energy transfer between Trp 51 and the PLP, and the latter thus reflects the relative orientation of the two fluorophores. The pH dependence of the enhancement of long wavelength fluorescence by acetate gives a pK_a of 7.0. Phosphorescence (*65*) and time-resolved fluorescence (*66, 67*) studies have identified two conformers, and their interconversion exhibits a pK_a of 7.0. The proposed pH-dependent conformational change may be the one required to close the active site prior to chemistry.

On the basis of the above information, the following general mechanism is proposed for OASS-A using the natural substrates OAS and bisulfide, Scheme 9. The resting enzyme is in the open conformation and above pH 7.0, is component to undergo the conformational change to the closed conformation. The amino acid substrate, OAS, binds as the monoanion with its α-amine unprotonated to carry out a nucleophilic attack on C4’ of the internal Schiff base (E). As the external Schiff base (ESB, observed transiently in the pre-steady state with OAS as the substrate (*68*)) is formed via *geminal*-diamine intermediates (GD) the active site closes triggered by the interaction of substrate α-carboxylate with the asparagines loop. Lys-41, initially in internal Schiff base linkage with PLP, serves as a general base to deprotonate C_α (ESB) in the β-elimination reaction responsible for the release of acetate to end the first half-reaction. Acetate diffuses away from the active site as it opens partially to release product and allow entry of bisulfide. The difference in conformation of the external Schiff base (ESB) and the α-aminoacrylate external Schiff base (AA) forms of the enzyme is clearly shown by differences in their ^{31}P NMR chemical shifts (*69*). At the beginning of the second half reaction (AA), Lys-41 is protonated and bisulfide diffuses into the active site and attacks C_β of α-aminoacrylate to give the cysteine external Schiff base. The active site then opens to expel the cysteine product upon transamination using Lys-41.

On the basis of the external Schiff base structure, Fig. 5, the α-proton is directed away from the *si* face of the cofactor, while the methionine side chain is directed away from the *re* face toward the entrance of the active site in anticipation of its expulsion. The structure is consistent with *anti*-elimination, and an E2 reaction is preferred compared to an E1 reaction in the case where no protonation of the leaving group is required as is the case for the OASS-A reaction (*70*). In an E1 reaction, a quinonoid intermediate should be produced as the α-proton is abstracted by Lys-41 acting as a general base. Since α-proton abstraction is rate-limiting in the direction of formation of the α-aminoacrylate intermediate (vide infra), the quinonoid intermediate would not be observed in the direction of its formation, but should be in the direction of formation of the OAS external Schiff base from the α-aminoacrylate intermediate and acetate. Consistent with an E2 reaction, no quinonoid intermediate is observed under these conditions, even in the presence of D_2O, which slows down protonation at C_α (*70, 71*).

Scheme 9. Minimal Chemical Mechanism of OASS.

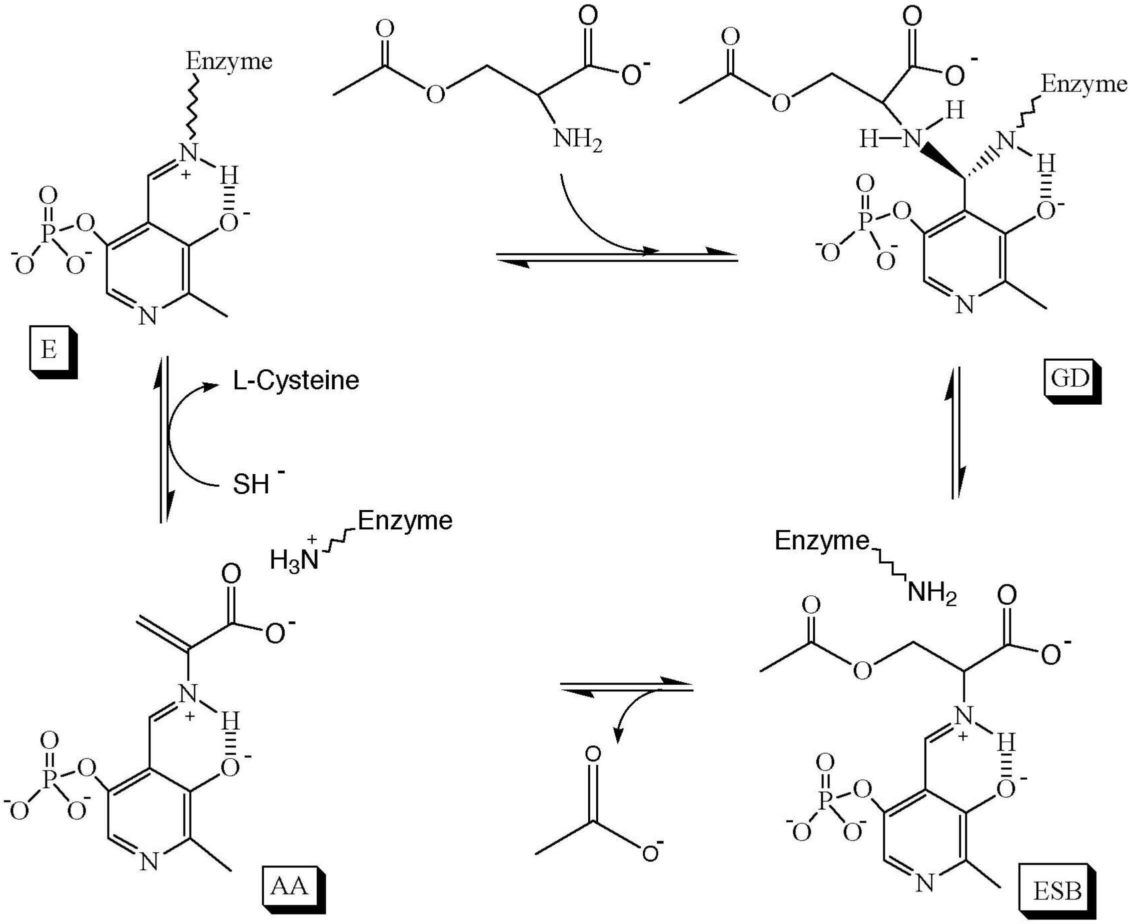

In addition, as suggested above, the dipole of helix 10 is in close proximity to and directed toward the pyridine nitrogen of the cofactor making it unlikely that N1 is protonated. Finally, changing Ser-272 to alanine, which eliminates any possibility of H-bonding to N1, or aspartate, which should stabilize a quinonoid intermediate, has no effect on V/K_{OAS} (*72*). Taken together, data are consistent with an *anti*-E2 reaction, or concerted elimination of the α-proton and the acetoxy group. Measurement of the primary ^{18}O kinetic isotope effect on acetoxy elimination in the absence and presence of deuterium at C_α is planned. If the ^{18}O kinetic isotope effect measured with OAS remains the same or increases when measured with OAS-2D, results will support a concerted elimination, while a decrease in the ^{18}O kinetic isotope effect with OAS-2-D would be consistent with a stepwise, or E1, reaction.

The primary deuterium isotope effect measured using OAS-2-D in the steady state is pH dependent, increasing from a value of 1.7 at neutral pH to a limiting value of 2.8 at low pH (*55*). Data indicate that OAS is a sticky substrate with a stickiness factor of 1.5, that is once OAS binds to enzyme it goes on to product, the α-aminoacrylate intermediate, 1.5 times faster than it dissociates from enzyme. An isotope effect within error identical to the value of 2.8 obtained in the steady state is also measured monitoring the appearance of the α-aminoacrylate intermediate at 470 nm in the pre-steady state. The value of 2.8 is thus the intrinsic isotope effect on α-proton abstraction. The frame of reference for primary kinetic deuterium isotope effects on the basis of semiclassical considerations is 6-8 for a symmetric transition state, and the value of 2.8 thus suggests an early or late transition state (*73*).

Substitution of deuterium at C2 of OAS allows measurement of a secondary kinetic deuterium isotope effect. The frame of reference for secondary kinetic isotope effects in the OASS-A reaction is the secondary isotope effect on the equilibrium constant for formation of the α-aminoacrylate intermediate (*74*). This secondary equilibrium isotope effect is 1.8 as measured experimentally, while the value for the secondary kinetic isotope effect is quite modest with a measured value of 1.1, suggesting very little hybridization change at C_β in the transition state. Assuming an anti-E2 reaction data are consistent with an asynchronous transition state in which little bond formation has occurred between the ε-amino of Lys-41 and the α-proton of the OAS external Schiff base and even less bond cleavage has occurred between C_β and the acetoxy oxygen.

Regulation of OASS-A. Cysteine is a reducing agent and thus is potentially toxic to the cell and its regulation is critical for the survival of the cell. Cysteine biosynthesis is regulated at two levels, at the gene level and by direct modulation of enzyme activity by metabolites (*75*). The cysteine regulon of *Salmonella typhimurium* consists of 14 or more genes necessary for the synthesis of OAS, the uptake and reduction of sulfate to sulfide, and the reaction of sulfide with OAS to form L-cysteine. Derepression of the cysteine regulon requires a combination of sulfur starvation, L-cysteine precursor and coinducer OAS (*76, 77*). OAS is not only a direct precursor of L-cysteine but also serves as an internal inducer, which required for derepression of all the enzymes in the cysteine biosynthesis pathway except for serine acetyltransferase (SAT), whose expression is not subject to this form of regulation. On the other hand, OASS is regulated directly by its substrate. Sulfide gives partial competitive substrate inhibitor of OASS-A to prevent an uncontrolled increase in cysteine biosynthesis and SAT is feedback inhibited by L-cysteine with apparent K_i of $1x10^{-6}$ M (*49*).

A new structure was reported recently, shows a chloride ion is bound at the dimer interface (*46*). The structure of the enzyme differs from that of the open, or resting form, and the closed, or external Schiff base form, in that the asparagines loop is moved up and away from a position where it could interact with the substrate β-carboxylate group. Fig. 6A shows an overlay of the structures of the closed and inhibited forms of the enzyme.

The asparagines (substrate-binding) loop is labeled to illustrate the change in its position in the two structures. A close up of the structure of the inhibitor-binding site with chloride bound is also shown in Fig. 6B. The chloride ion participates in five H-bonding interactions, three with protein residues (the amide nitrogen of N7, the guanidinium group of Arg-34, and the peptide nitrogen of Leu-268 of the other monomer), and two with water molecules that contribute to the H-bonding network around the chloride binding site. As chloride binds, it collides with the carbonyl oxygen of Pro-36 causing conformational changes in which the peptide bond of Pro-36 flips and a cascade of side chain reorientations then take place resulting in the movement of the asparagines loop to a new location. The new conformation of the asparagines loop prevents any H-bonding interaction with the α-carboxylate of the amino acid substrate. One of the largest movements within the asparagines substrate-binding loop is that of Asn-69. The new position of Asn-69 is away from the α-carboxylate of the amino acid substrate, and H-bonding interactions are not allowed. The inhibited form thus would produce a destabilization of the external Schiff base, and lead to the release of OAS.

The physiologic inhibitor is likely bisulfide, which is a substrate inhibitor (*52*, *53*), and is similar in diameter (1.7 Å) to chloride (1.67 Å) that was observed in 3D structure of the inhibited conformation. A number of small anions, including divalent ions such as sulfate, also inhibit by binding to the allosteric site (*54*). Inhibitors can apparently bind to all enzyme forms, i.e. free enzyme, the external Schiff base and the α-aminoacrylate intermediate, to give an enzyme with reduced activity. The allosteric

Figure 6. (A) Overlay of the structures of the closed and inhibited forms of the enzyme in ribbon representation *(46, 62)*. The asparagines loop is in aquamarine in the inhibited form (yellow is used for the open form). Note the position of N69 in the inhibited structure. (B) A close up of the structure of the inhibitor-binding site with chloride bound in the dimmer interface. N69’ is in the inhibited form of the enzyme. The figure was prepared using DS Viewer 5.0 from Accelrys.

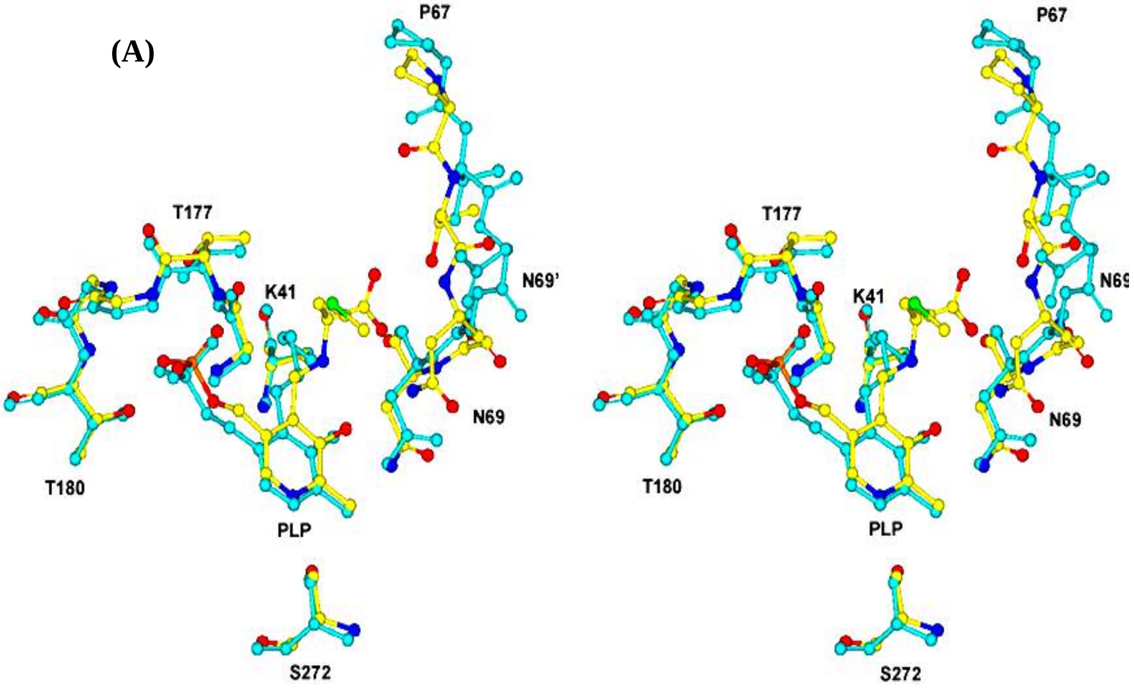
(A)
P67
T177
K41
N69'
N69
T180
PLP
S272
P67
T177
K41
N69
N69
T180
PLP
S272

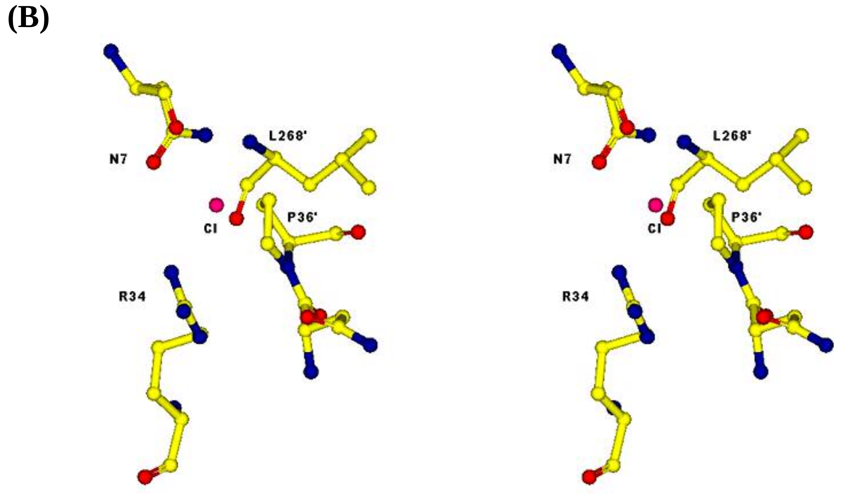
(B)
N7
L268'
Cl
P36'
R34
N7
L268'
Cl
P36'
R34

inhibition is thought to regulate runaway cysteine synthesis, which is possible when the concentration of OAS and sulfide are high.

O-Acetylserine Sulfhydrylase-B (OASS-B)

The OASS-B isozyme is thought to be expressed under anaerobic growth conditions, and it appears to be less substrate selective than the OASS-A isozyme to both the amino acid and nucleophilic substrates (*78*). OASS-B can utilize more reduced forms of sulfur, for example, it can utilize thiosulfate as a physiological substrate, and its uptake provides an alternative means for cysteine biosynthesis and eliminates the need for sulfate reduction (*79*). The kinetic and chemical mechanisms of the two isozymes of OASS are similar but not identical (*64, 80*).

Kinetic Mechanism. OASS-B has a ping-pong kinetic mechanism on the basisof initial velocity patterns obtained in the absence of inhibitors. Both substrates exhibit competitive inhibition, which is normally diagnostic for a ping pong mechanism, resulting from substrates binding to the incorrect enzyme form, OAS to F and bisulfide to E (*64*). In a classical one-site ping pong mechanism, the individual half-reactions are independent of the concentration of the other substrate. This is not the case for the OASS-A reaction, with V/K_{OAS} 4000-fold higher when sulfide is the nucleophile compared to that measured with TNB; the V/K for the nucleophiles are in agreement regardless of the amino acid substrate used (*78*). In the case of the B-isozyme, the V/K_{OAS} is only 3-fold higher when sulfide is the nucleophile compared to that of TNB, and the $V/K_{sulfide}$ is only 6-fold higher when OAS is the substrate compared to that of BCA (*78*). The substrate inhibition observed with the A-isozyme is a result of binding of substrates to an inhibitory allosteric site (*vide infra,* (*54*)). On the other hand, the absence of inhibition with the B-isozyme may suggest the absence of the allosteric anion-binding site present in the A-isozyme.

The kinetic mechanism of OASS-B appears qualitatively identical to that of OASS-A (*78*). OAS binds to the internal Schiff base form of the enzyme (E), and acetate is released as the first product to yield the α-aminoacrylate (F) form of the enzyme, Scheme 8. Bisulfide then adds as the second substrate to (F) to produce the cysteine external Schiff base (ESB). Cysteine is released as the final product upon transimination by the active site lysine (Scheme 8, chapter I).

Chemical Mechanism. The OASS-B reaction is catalyzed in two half-reactions as an elimination-addition reaction to give an overall β-substitution reaction. The pH dependence of V/K_{OAS}, which reflects free enzyme and the free amino acid substrate, exhibits pK_a values of 6.0 and 7.0 on the acidic side, while V/K_{BCA} profile exhibit pK_a values of 7.6 on the acid side and 9.0 on the base side (*64*). All pK_a values are summarized in Table 2. The basic pK_a observed in the V/K_{BCA} profile is that of the α-amine of the amino acid substrate, required to be unprotonated for nucleophilic attack on C4’ of the PLP Schiff base. The pH dependence of V/K_{TNB}, which reflects the α-aminoacrylate external Schiff base and free TNB, shows pK_a values of 7.6 on the acidic side and 8.7-8.9 on the basic side. The group with a pK_a of about 7.6 observed in both half-reactions reflects the same enzyme group that must be unprotonated, likely to stabilize the optimum catalytic conformation of the enzyme, where its participation is important in opening and closing the active site. The pK_a of 8.7-8.9 in the V/K_{TNB} pH

Table 2: Summary of the pK_a Values for OASS-B (*64*).

	pK_a Acidic Side	pK_a Basic Side
OAS/Sulfide		
V/E_t		
V/K_{OAS}	6	
	7	
$V/K_{sulfide}$		
OAS/TNB		
V/E_t	6.7	8.2
V/K_{OAS}	5.9	
V/K_{TNB}		8.7
BCA/TNB		
V/E_t	6.5	
V/K_{BCA}	7.6	9.0
V/K_{TNB}	7.6	8.9

profile reflects the protonation state of the ε-amino group of Lys-42 that is originally in Schiff base linkage with PLP. A pK_a of 7, reflecting the protonation of HS^- to H_2S, is not observed probably as a result of the slow transaldimination of the final amino acid product. Therefore, the pK_a of sulfide is perturbed to a lower pH value. The V profiles reflect pK_as of groups on enzyme in the rate-limiting steps in both half-reactions when reactants are saturating. The V profiles for the OAS/TNB and BCA/TNB substrate pairs yield pK_a values of 6.5-6.7 on the acidic side and 8.2-9.0 on the basic side. Both pK_as observed are likely for Lys-42 that is required to be unprotonated in the first half-reaction to accept a proton from C_α of the OAS external Schiff base complex to form the α-aminoacrylate intermediate (IV) (Scheme 9, chapter I). Lys-42 is required to be protonated at the beginning of the second half of the OASS-B reaction to donate a proton to the C_α of the α-aminoacrylate intermediate to form the amino acid product external Schiff base.

OASS-B has a chemical mechanism that is similar to that observed with the A-isozyme. The amino acid substrate, OAS, binds in the monoanionic form with its α-amine unprotonated to carry out a nucleophilic attack on C4' of the internal Schiff base. In the OASS-B isozyme, an enzyme group is required to be protonated and likely interacts with the α-carboxyl group. The OAS external Schiff base is formed via *geminal*-diamine intermediates, and Lys-42, initially in internal Schiff base linkage with PLP, serves as a general base to deprotonate C_α in the β-elimination reaction responsible for the release of acetate to end the first half-reaction. The preliminary data for OASS-B are consistent with a mechanism in which a general acid is not needed to eliminate acetate (when OAS was used as substrate) or chloride (when BCA was used as substrate);

both are stable leaving groups. Acetate diffuses away from the active site as it opens partially, and allow entry of the second substrate, bisulfide. At the beginning of the second half reaction, Lys-42 is protonated and bisulfide diffuses into the active site and attacks C_β of the α-aminoacrylate intermediate to give the cysteine external Schiff base. The active site then opens to expel the cysteine product upon transimination via Lys-42 and the free enzyme is produced for new cycle of catalysis.

Research Carried Out in This Dissertation and Publications.

In this dissertation studies are directed toward elucidation of the mechanism of the second half of the OASS-A reaction. In addition, OASS-B has been cloned, over-expressed and characterized. Most of the introduction and background on OASS-A has been published.

Rabeh, W. M. and Cook, P. F. (2004). “Structure and Mechanism of *O*-Acetylserine Sulfhydrylase.” *J. Biol. Chem.* 279, 26803-26806.

CHAPTER II

MECHANISM OF THE ADDITION HALF OF THE *O*-ACETYLSERINE SULFHYDRYLASE-A REACTION

The first half of the OASS-A reaction, formation of the α-aminoacrylate intermediate, limits the overall reaction rate, while the second half-reaction is thought to be diffusion-limited. The second half-reaction of OASS-A is, formally, the reversal of the first half-reaction with the nucleophilic substrate, bisulfide, adding to C_β of the α-aminoacrylate intermediate to form the external Schiff base with cysteine. The amino acid product is then released after transimination. The second half-reaction is very fast and, the nucleophilic substrate is thought to diffuse into the active site and form the product upon collision. The pH dependence of the V/K for TNB (an alternative substrate) when BCA is used as the amino acid substrate shows pK_a values of 6.9 and 8.3 with these pK_a reflecting the pH-dependent conformational change and the Schiff base lysine (Lys-41) that must protonate C_α of the α-aminoacrylate intermediate to form the product external Schiff base (*64*). The rate of the second half-reaction is at or very near the diffusion limit, and as a result, limited information is available on the second half-reaction of OASS-A.

In order to characterize the second half-reaction, the pH dependence of the pseudo-first order rate constant for disappearance of the α-aminoacrylate intermediate was measured over the pH range (6.0-9.5) using the natural substrate bisulfide, and a number of nucleophile analogs. In this study, rapid-scanning-stopped-flow (RSSF) experiments are used in an attempt to detect intermediates along the reaction pathway. The pH(D) dependence of the second half-reaction has been determined using the natural substrate, bisulfide, and sulfide analogs. The rate is pH-dependent for substrates with a $pK_a > 7$, while the rate constant is pH-independent for substrates with a $pK_a < 7$ suggesting that the pK_as of the substrate and enzyme group are important in this half of the reaction. In D_2O, at low pD values, the amino acid external Schiff base is trapped, while in H_2O the reaction proceeds through release of the amino acid product, which is rate-limiting. A number of new β-substituted amino acid were produced and characterized by ^{1}H NMR spectroscopy. Data are discussed in terms of the overall mechanism of OASS-A.

MATERIALS AND METHODS

Chemicals and Enzyme. 2-Mercaptoethanol, mercaptosuccinic acid, 2-mercaptopyridine, thiosalicylic acid, mercaptoacetic acid, and cyanide were obtained from Aldrich Chemicals, while 1,2,4-triazole, *O*-acetyl-L-serine, 5,5'-dithiobis(2-nitrobenzoic acid), and formic acid were obtained from Sigma. Phenol was from Fisher scientific, and buffers (Ches, Hepes, Tris, and Taps) were from Research Organics. All other chemicals and reagents were obtained from commercial sources and were of the highest purity available. *O*-Acetylserine sulfhydrylase-A (OASS-A) was purified from a plasmid-containing overproducing strain using the method of Hara et al. (*81*) adapted to HPLC (*53*).

Enzyme Assay. The activity of OASS-A was monitored using 5-thio-2-nitrobenzate (TNB) as the nucleophilic substrate (*53*). TNB was prepared fresh daily by the reduction of 5,5'-dithiobis(2-nitrobenzoate) (DTNB) with dithiothreitol (DTT). The disappearance of TNB was monitored continually at 412 nm (ε412, 13,600 M^{-1} cm^{-1}) using a Beckman DU 640 spectrophotometer and a circulating water bath to maintain the temperature of the cell compartment at 25˚C. All assays were carried out in 100 mM

Hepes, pH 7.0, at 25°C with an OAS concentration of 1 mM and a TNB concentration of 50 µM.

Rapid-Scanning-Stopped-Flow. Pre-steady state kinetic measurements were carried out using an OLIS-RSM 1000 stopped-flow spectrophotometer in the multiple wavelength mode. Sample solutions were prepared in two syringes at the same pH with a final buffer concentration of 100 mM. The first syringe contained enzyme at a final concentration no lower than 15 µM and enough OAS was added to convert the free enzyme to the α-aminoacrylate intermediate. The second syringe contained sulfide or a sulfide analog at twice the final desired concentration. Data were collected with a repetitive scan rate of 15 ms for the wavelength range 300-600 nm and the number of scans collected was dependent on the rate of the reaction. The disappearance of the α-aminoacrylate external Schiff base was monitored at 470 and 330 nm, and the appearance of the internal Schiff base was monitored at 412 nm. The reaction temperature was maintained at 25˚C using a circular water bath. At 25˚C, the pH was varied from 5.0 to 6.5 for sulfide, fixed at 7.0 for the following nucleophilic substrate, 2-mercaptoethanol, mercaptosuccinic acid, 2-mercaptopyridine, phenol, hydroxylamine, and formate, and varied from 5.5 to 9.5 for the following nucleophilic substrates, thiosalicylate, mercaptoacetate, 1,2,4-triazole, and cyanide. The pH of the reaction was measured at the beginning and end of the reaction, and the following buffers were used for the pH ranges indicated: Mes (pH 5.0-6.5), Hepes (pH 7.0-8.0), and Taps (pH 8.5-9.5). Experiments were also carried out at 8, 15, and 35˚C.

The rapid-scanning-stopped-flow (RSSF) spectral data were fitted using the software provided by OLIS. To obtain the first order rate constant (k_{obs}) for the conversion of the α–aminoacrylate intermediate to free enzyme, eq. 1 was used.

$$A_t = A_0 e^{(-k_{obs}t)} + B_0 \qquad [1]$$

In eq. 1, A_t is the absorbance at any time t, A_0 is the absorbance at time zero, and B_0 corrects for the background absorbance. The first-order rate constant (k_{obs}) obtained at different nucleophile concentrations were fitted to a linear function to obtain the second order rate constant (k_{max}/K_{ESB}):

$$\mathrm{k}_{\mathrm{obs}} = \frac{\mathrm{k}_{\mathrm{max}}}{\mathrm{K}_{\mathrm{ESB}}}[\mathrm{Nucleophile}] \qquad [2]$$

In eq. 2, k_{max}/K_S is the second order rate constant for the conversion of the α-aminoacrylate external Schiff base and sulfide (or sulfide analog) to free enzyme and amino acid product. The second order rate constant was measured at different pH values and the resulting data were fitted to eq. 3 with a Basic version of a FORTRAN program developed by Cleland (*82*):

$$\log y = \log \frac{C}{1 + K/H} \qquad (3)$$

In eq. 3, y is the observed value of k_{max}/K_S at any pH, C is the pH-independent value of y, H is the hydrogen ion concentration, and K is the acid dissociation constant of a group on enzyme. The second order-rate constant was plotted vs. reciprocal temperature at pH 7.0 and the enthalpy of activation was estimated graphically according to the (eq. 4).

$$\log(k_{\max} / K_s) = -\frac{E_{act}}{2.303R}\left(\frac{1}{T}\right) \qquad [4]$$

In eq. 4, E_{act} is the energy of activation of the reaction and T is absolute temperature in K.

Stopped-Flow Solvent Isotope Effect Studies. The pD dependence for the second half of the OASS-A reaction was measured using cyanide, 1,2,4-triazole, and mercaptoacetate as nucleophilic substrates. All buffers and substrates were prepared in D_2O and the pD value was adjusted with DCl or KOD as needed. The pD value was measured using a pH meter, which was previously equilibrated in D_2O for 30 minutes. The pD value was calculated by adding 0.4 to the pH meter reading to correct for the isotope effect on the pH electrode (*83*). The OASS-A stock solution was exchanged into D_2O by concentrating the enzyme to about 0.1 mL using an Amicon ultrafiltration cell. The enzyme was diluted with 5 mL of buffer in D_2O, concentrated to 0.1 mL, and diluted with 1 mL of buffer in D_2O. Sample solutions were prepared in two syringes at the same pD value with a final buffer concentration of 100 mM as described above. Experiments were then carried out at 25˚C and 8˚C. The pD value for each reaction mixture was obtained before and after each run in which the pD change during the reaction was not significant. The RSSF spectra were collected and data at 412 nm and 470 nm were fitted using eqs. 1 and 2 as described above. The pD profile was obtained by plotting the second order rate constant vs. pD.

Ultraviolet-Visible Spectral Studies. Absorbance spectra of the *O*-thioacetyl-L-serine external Schiff base of OASS-A were recorded utilizing a Hewlett Packard 8452A photodiode array spectrophotometer over the wavelength range 300-600 nm. The temperature was maintained at 25°C in a reaction cuvette of 1cm path length and 1 mL volume at pD 6.0 using 100 mM Mes. The blank contains all components minus enzyme. The α-aminoacrylate intermediate was generated by adding OAS equal to the enzyme concentration. Mercaptoacetate was added to a final concentration of 10 mM to yield the *O*-thioacetyl-L-serine external Schiff base.

NMR Spectroscopy. A number of amino acids were prepared using 10 mM OAS, 10 mM nucleophile, and 0.5 mg OASS-A. All substrates and enzyme were prepared in D_2O as described above and the pD value of the reaction was maintained at 6.5 using 100 mM phosphate buffer. The enzyme was added last to initiate the reaction, and the reaction was incubated at room temperature overnight. The structural identity of the products was confirmed using NMR and spectra were collected on a Varian Mercury VX-300 MHz NMR. The spectra were referenced to the residual HDO peak at 4.69 ppm. The proton spectra were collected using a presaturation pulse sequence to minimize the water peak with an acquisition time of 2 seconds and 16 scans. The carbon spectra were collected in 10,000 scans with a delay of 1 second. Assignment of NMR resonances employed atom numbering system starting with C_α of the amino acid substrate. Assignments of ^1H and ^{13}C NMR resonances were confirmed by two-dimensional spectroscopy (COSY). The gCOSY sequence supplied by Varian was employed with 128 increments and 1 transient. Data for the amino acids studied are as follow:

***O*-acetyl-L-serine**, ^{1}H NMR (D_2O, 300 MHz) gave δ 4.34 (m, 2H, C(β)-H2), 3.92 (M, 1H, C(α)-H1) 1.97 (CH_3). ^{13}C NMR (D_2O, 75 MHz) gave δ 171.5, 171.6 (C=0), 63.1 (C(β)), 53.5 (C(α)), 19.5 (CH_3).

***S*-2-pyridyl-L-cysteine**, ^{1}H NMR (D_2O, 300 MHz) gave δ 8.22 (ddd, 1H, *J* = 5.1, 1.5, 1.0 Hz C(6)-H), 7.50 (m, 1H, C(4)-H), 7.24 (dt, 1H, *J* = 8.3, 1, 1, C(β)-H), 7.04 (ddd, 1H, *J* = 8.0, 5.0, 1.0 Hz, C(5)-H), 3.58 (d, 1H, *J* = 15 Hz, C(β)-H2), 3.33 (d, 1H, *J* = 15 Hz, C(β)-H2).

***S*-2-hydroxyethyl-L-cysteine**, ^{1}H NMR (D_2O, 300 MHz) gave δ 3.6 (td, 2H, *J* = 6.0, 1.1 Hz, C(ε)-H2), 2.96 (m, 2H, C(β)-H2), 2.61 (t, 2H, *J* = 6.0 Hz, C(δ)-H2).

β-1,2,4-triazole-L-alanine, ^{1}H NMR (D_2O, 300 MHz) gave δ 8.32, 7.93 (s,2H, C(3)-H, C(5)-H), 4.5 (m, 2H, C(β)-H).

β-cyano-L-alanine, ^{1}H NMR (D_2O, 300 MHz) gave δ 2.86 (d, 2H, *J* = 6.0 Hz, C(β)-H).^{13}C NMR (D_2O, 75 MHz) gave δ 173.6 (C=O), 117.6 (CN), 50.3 (C(α)), 20.41 (C(β)).

A time course was obtained for the cyanide reaction using the presaturation pulse sequence with a variable preacquisition delay time and eight scans averaged per data point. Forty-one data points were collected over a period of sixteen hours. These points were collected every 250 seconds in the first hour, every 900 seconds for the next three hours, and one point each hour for the last twelve hours. It was possible to monitor the reaction using both the increase of the β-cyano-L-alanine product C(β)-H2 (2.86 ppm) and the appearance of acetate (1.77 ppm) versus time. The rate of the appearance of the first product acetate was fitted to (eq. 5).

$$[Acetate] = ae^{-kt} \tag{5}$$

RESULTS

Rapid-Scanning-Stopped-Flow Studies. RSSF measurements were carried out to obtain information on the identity and the rate of appearance and disappearance of intermediates in the pre-steady state for the second half of the OASS-A reaction. The α-aminoacrylate intermediate exhibits maximum absorbance at 330 and 470 nm (*68*). The intermediate was pre-formed in one syringe and reacted with different concentrations of sulfide or sulfide analogs in the second syringe. Reaction with sulfide gives a rapid disappearance of the α-aminoacrylate intermediate and appearance of free enzyme (λ_{max}, 412 nm) within the RSSF instrument dead time of about 4 ms, (data not shown). Only at pH 5.0 with a total sulfide concentration of 1.5 μM was the last portion of the time course for disappearance at 470 nm observed, with a pseudo-first-order rate constant of about 100 s^{-1} estimated.

Since the rate of the second half-reaction was too fast with the natural substrate, bisulfide, attempts were made to monitor the reaction using nucleophilic analogs of sulfide. Different nucleophiles containing sulfur, nitrogen, carbon or oxygen were tested as possible substrates, Table 3. Reaction of all nucleophiles show in Table 3 was conducted at pH 7.0 and the nucleophiles are split into classes depending on the

Table 3: Kinetic Data for Nucleophilic Substrate-Analogs.

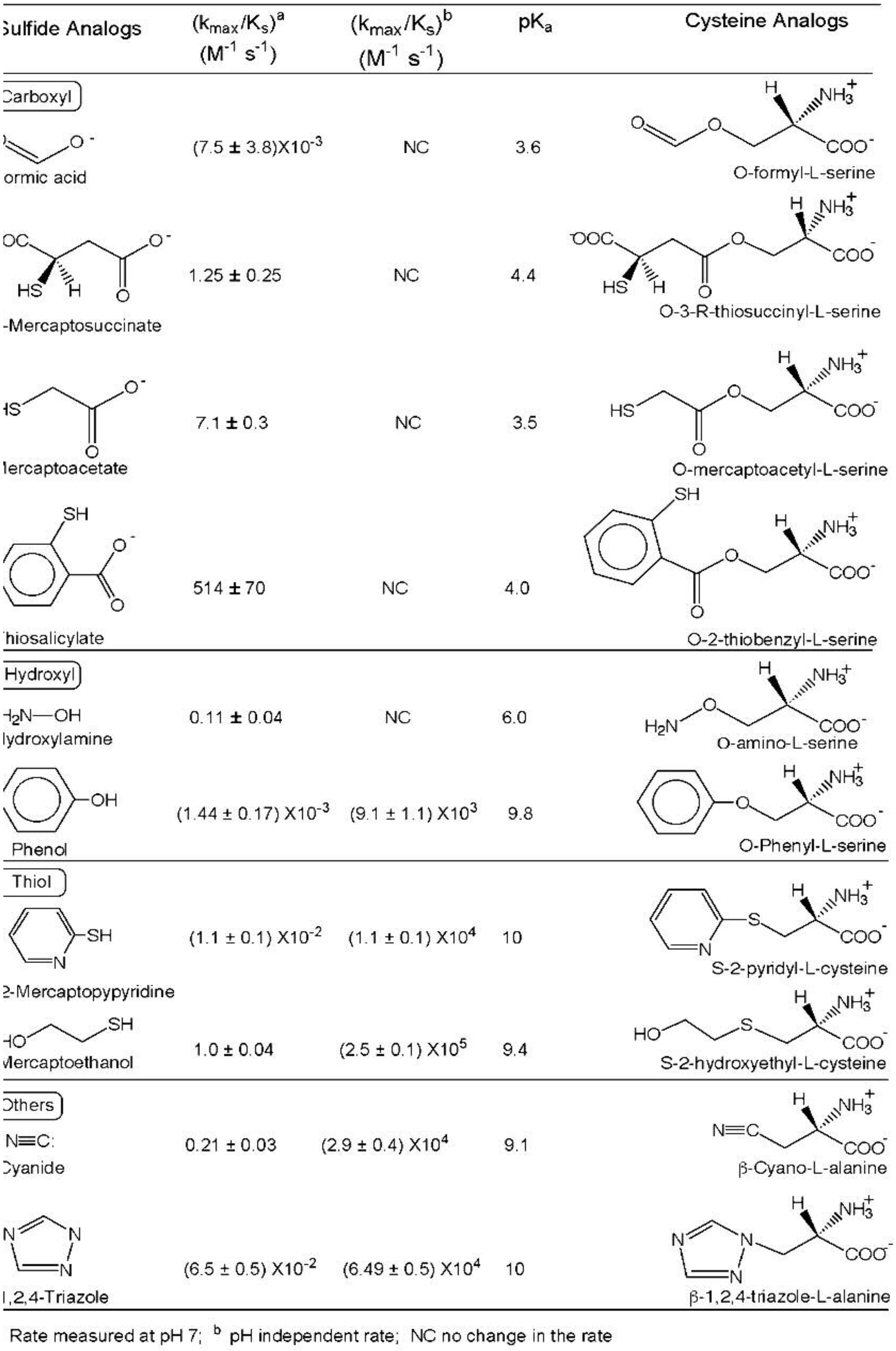

Sulfide Analogs	$(k_{max}/K_s)^a$ $(M^{-1}\ s^{-1})$	$(k_{max}/K_s)^b$ $(M^{-1}\ s^{-1})$	pK_a	Cysteine Analogs
Carboxyl				
ormic acid	$(7.5 \pm 3.8)X10^{-3}$	NC	3.6	O-formyl-L-serine
-Mercaptosuccinate	1.25 ± 0.25	NC	4.4	O-3-R-thiosuccinyl-L-serine
Mercaptoacetate	7.1 ± 0.3	NC	3.5	O-mercaptoacetyl-L-serine
Thiosalicylate	514 ± 70	NC	4.0	O-2-thiobenzyl-L-serine
Hydroxyl				
H_2N—OH Hydroxylamine	0.11 ± 0.04	NC	6.0	O-amino-L-serine
Phenol	$(1.44 \pm 0.17)\ X10^{-3}$	$(9.1 \pm 1.1)\ X10^{3}$	9.8	O-Phenyl-L-serine
Thiol				
2-Mercaptopypyridine	$(1.1 \pm 0.1)\ X10^{-2}$	$(1.1 \pm 0.1)\ X10^{4}$	10	S-2-pyridyl-L-cysteine
Mercaptoethanol	1.0 ± 0.04	$(2.5 \pm 0.1)\ X10^{5}$	9.4	S-2-hydroxyethyl-L-cysteine
Others				
N≡C: Cyanide	0.21 ± 0.03	$(2.9 \pm 0.4)\ X10^{4}$	9.1	β-Cyano-L-alanine
1,2,4-Triazole	$(6.5 \pm 0.5)\ X10^{-2}$	$(6.49 \pm 0.5)\ X10^{4}$	10	β-1,2,4-triazole-L-alanine

Rate measured at pH 7; ^{b} pH independent rate; NC no change in the rate nucleophile functional group. The rate of disappearance of the α-aminoacrylate intermediate was measured as a function of nucleophile concentration using the stopped-flow method by monitoring the reaction at 412 and 470 nm. As an example, data obtained with 1,2,4-triazole are shown in Fig. 7. The spectral time course exhibits two clear isosbestic points, which suggests that the two tautomeric forms of the α-aminoacrylate intermediate, λ_{max} at 470 and 330 nm, are converted to the internal Schiff base, λ_{max} at 412 nm, with no detectable accumulation of additional intermediates. The time courses for the increase in absorbance at 412 nm and the decrease in absorbance at 470 nm give identical rate constants, Fig. 7B, as expected for interconversion of two species. The first order rate constant (k_{obs}) obtained using the RSSF method at different nucleophile concentrations is a linear function of analog concentration, and its slope represents the second order rate constant (k_{max}/K_s), Fig. 8. A summary of data obtained for a variety of nucleophilic substrates is given in Table 3. In addition to the nucleophiles listed, others that gave no detectable reaction rate are thiophenol, 2-mercaptoimidazole, 2-mercaptobenzoxazole, pyridine, m-bromophenol, benzoin, benzimidazole, benzoate, 4-nitrothiophenol, 4-chloro-2-phenol, 2-mercaptobenzimidazole, and 2-chloroaniline.

^{1}H NMR Spectroscopy. To confirm the structure of the amino acid product obtained from the reaction of OASS-A with different sulfide analogs, time courses were measured using ^{1}H NMR. Fig. 9A shows an example of NMR spectra for the reaction of OASS-A with 10 mM OAS and 10 mM cyanide at pD 6.5 as a function of time. Spectra were obtained at time zero before any enzyme was added, and then as a function of time. The time course for production of acetate was fitted to eq. 5 to yield a first order rate of 0.0076 min^{-1}. From Fig. 9B, the following assignments are made: the 1.77 ppm resonance is due

Figure 7. Rapid-scanning-stopped-flow spectra of the conversion of the α–aminoacrylate intermediate of OASS-A to free enzyme using 1,2,4-triazole as the nucleophilic substrate. (A) Spectrum 1 represent the α–aminoacrylate intermediate with λ_{max} at 470 and 330 nm, and spectrum 9 represent free enzyme (internal Schiff base) with λ_{max} at 412 nm. The time interval between spectra is about 13 s. The enzyme concentration was 80 µM and 1,2,4-triazole was 1 mM. Data were measured at pH 6.0, 100 mM Mes, and 25˚C. (B) Time courses obtained from data in 1A at 412 and 470 nm. The rate constant calculated from both wavelengths is identical. No other intermediates are detected under these conditions.

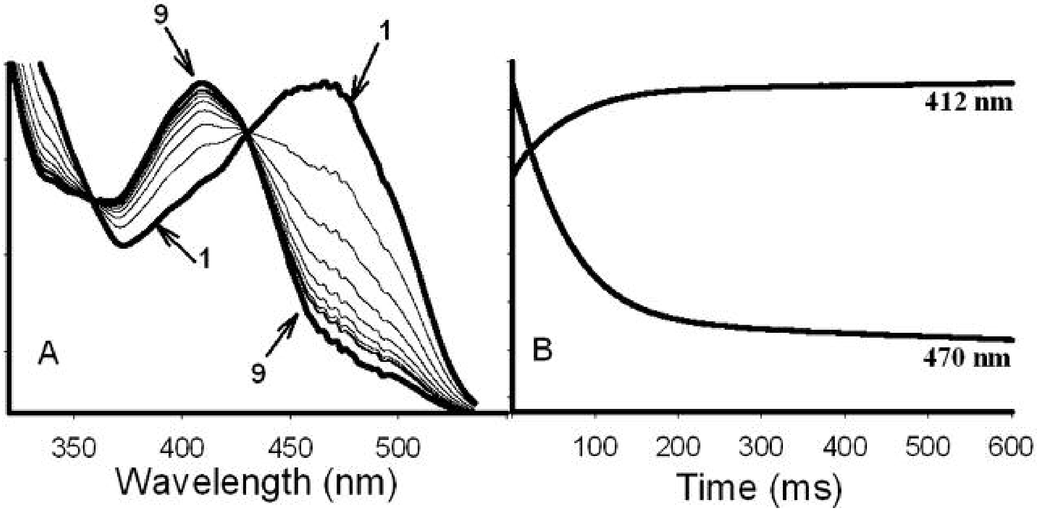
9
1
1
9
A
350
400
450
500
Wavelength (nm)
B
412 nm
470 nm
100
200
300
400
500
600
Time (ms)

Figure 8. Plot of the observed first order rate constant for the second half of the OASS-A reaction (measured as in Fig. 7) against the concentration of 1,2,4-triazole. All data were collected at 25˚C, and pH values of 6.0, 6.5, 7.0, 7.5, and 8.0 represent lines 1-5, respectively. The second order rate constant (k_{max}/K_s) is the slope of the line, and was calculated using eq. 2.

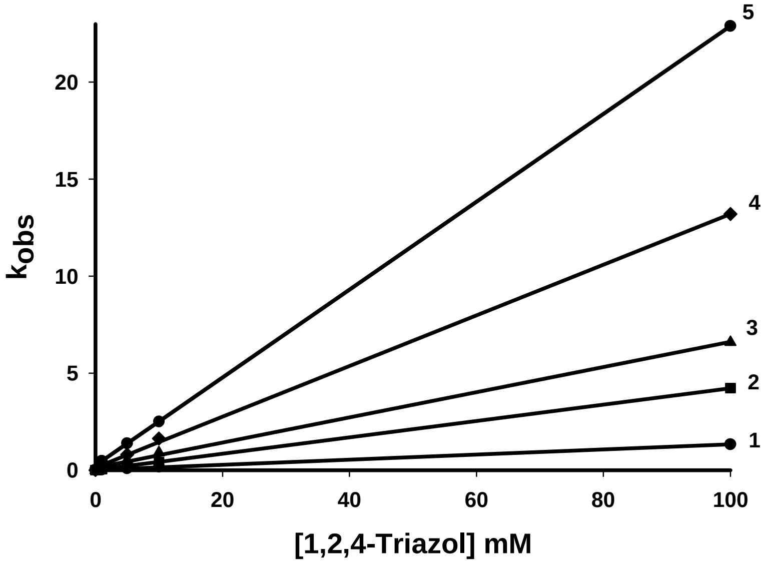
k_obs
0
5
10
15
20
0
20
40
60
80
100
[1,2,4-Triazol] mM
1
2
3
4
5

Figure 9. ^{1}H NMR spectra of the OASS-A catalyzed reaction using 10 mM OAS and 10 mM cyanide at pD 6.5, 100 mM phosphate buffer as described in Methods. All spectra were referenced to the residual HDO peak at 4.69 ppm. (A) Time course obtained using cyanide as the nucleophilic substrate. A presaturation pulse sequence was used with a variable preacquisition delay time and eight scans per data point. Forty-one data points were collected over a period of sixteen hours. These points were collected every 250 seconds in the first hour, every 900 seconds for the next three hours, and one point each hour for the last twelve hours. It was possible to monitor the reaction using the appearance of acetate (1.77 ppm) versus time with a first order rate constant of 0.0076 min^{-1}. (B) NMR spectra collected at the beginning of the reaction (t= 0) before adding any enzyme and at different time intervals as labeled on the spectra. At t= 0, the ^{1}H NMR spectrum is identical to the OAS spectrum in which its ^{1}H NMR (D_2O, 300 MHz) gave δ 4.34 (m, 2H, C(β)-H2), 3.92 (M, 1H, C(α)-H1), and 1.97 (CH_3). The final spectrum of the reaction mixture is identical to that of β-cyano-L-alanine in which its ^{1}H NMR (D_2O, 300 MHz) gave δ 2.86 (d, 2H, J = 6.0 Hz, C(β)-H). The α-proton is not observed since the position is deuterated as a result of running the reaction in D_2O.

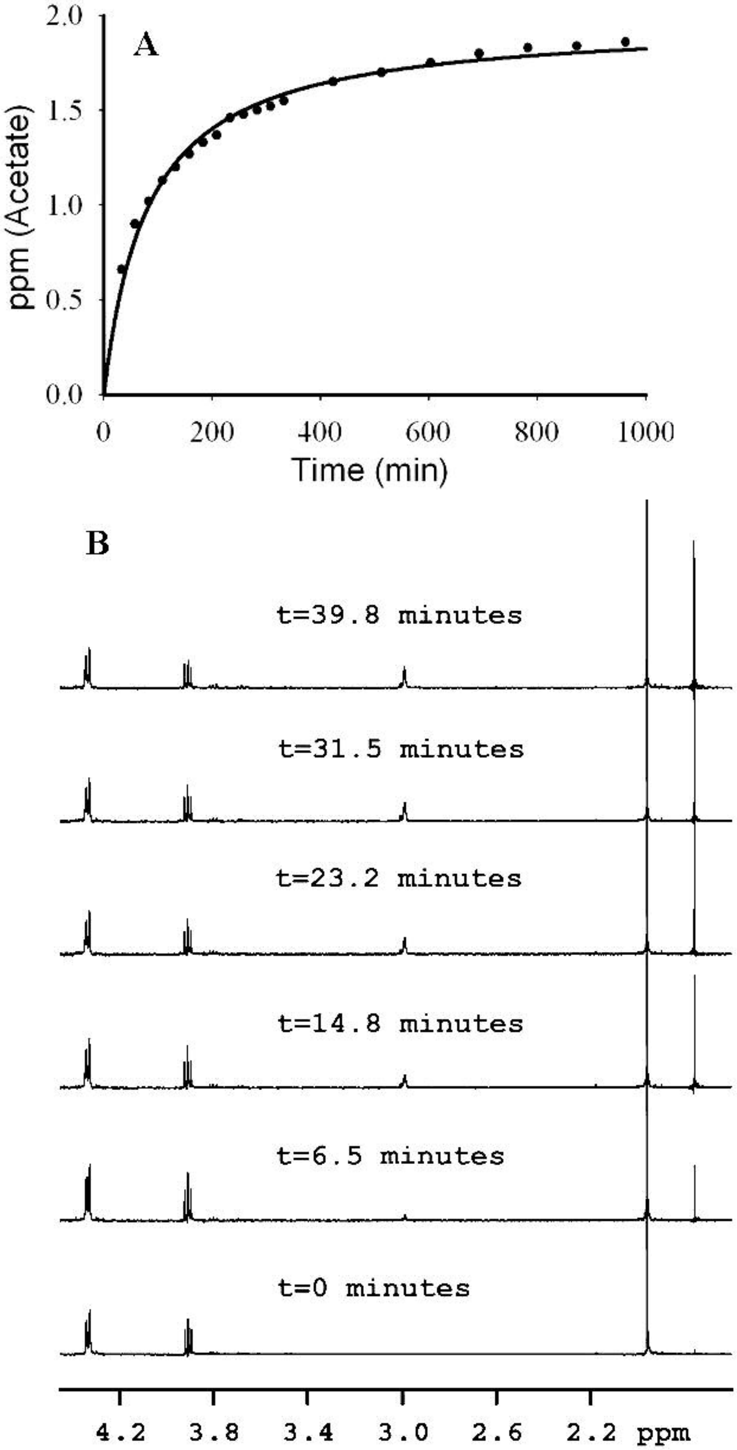
A
ppm (Acetate)
0.0
0.5
1.0
1.5
2.0
0
200
400
600
800
1000
Time (min)
B
t=39.8 minutes
t=31.5 minutes
t=23.2 minutes
t=14.8 minutes
t=6.5 minutes
t=0 minutes
4.2
3.8
3.4
3.0
2.6
2.2
ppm

to the CH_3 of the product acetate, the 1.97 ppm resonance is due to the CH_3 of the acetoxy group of OAS, the 2.86 ppm resonance is due to C_β of β-cyano-L-alanine (the amino acid product), the 3.92 ppm resonance is due to C_α of OAS, and the 4.34 ppm resonance is due to C_β of OAS. β-cyano-L-alanine would also have a resonance at 3.78 ppm due to C_α, but this position is deuterated in the product as a result of carrying out the reaction in D_2O. The 4.34 ppm resonance of the C_β of OAS is shifted to 2.86 ppm as a result of replacement of the acetoxy group of OAS by a cyanide group in the β-cyano-L-alanine product. The 1.97 ppm resonance of the CH_3 of OAS is shifted to 1.91 ppm as it is released as the first product, acetate. The spectrum of the final product of this reaction agrees with the spectrum obtained with the commercially available β-cyano-L-alanine.

The structure identity of the different amino acid products was identified using NMR spectroscopy. The proton chemical shifts for the amino acid substrate, OAS, were significantly different than those of the amino acid product, as a result of the electron deshielding effects of the surrounding nuclei (*84*). An example is the reaction of the α-aminoacrylate intermediate with mercaptoethanol, where the nucleophilic group could be either its oxygen or thiol group. The NMR spectrum of the amino acid product, *S*-2-hydroxyethyl-L-cysteine, shows the β-protons (2.96 ppm) are shifted upfield (toward 0.0 ppm) from its position of 4.34 ppm in the OAS spectrum. This allowed the distinction between O and S attack, indicating that sulfur was the attacking group. Oxygen is more electronegative than sulfur and pulls electrons away from the β-protons causing a significantly larger chemical shift value than in the amino acid products, where C_β is bonded to sulfur, which has an electronegativity identical to that of carbon. In comparison, if the oxygen had been the attacking group, the β-protons of the amino acid product would have been located between 3.6 and 4.5 ppm (*84*).

pH Dependence of the Second Order Rate Constant. To further investigate, whether functional groups on enzyme and/or nucleophilic substrate are involved in catalysis, the second order rate constant (k_{max}/K_S) was measured as a function of pH using several of the nucleophiles including cyanide, 1,2,4-triazole, mercaptoacetate and thiosalicylate. The second order rate constant was measured at 25˚C over the pH range 5.5-8.0. Data were not collected above pH 8.0 because of the high rate of decomposition of the α-aminoacrylate intermediate to free enzyme, ammonia, and pyruvate (*60*). In the case of mercaptoacetate (Fig. 10) and thiosalicylate (data not shown), the second order rate constant is pH-independent. On the other hand, the pH-dependence of the second order rate constants at 25˚C measured with cyanide (Fig. 11B) and 1,2,4-triazole (not shown) were qualitatively very similar with a limiting slope of +1 and an apparent pK_a of about 7.2 ± 0.2 for both substrates. To decrease the rate of decomposition of the α-aminoacrylate intermediate, the second order rate constant for cyanide and 1,2,4-triazole were measured at 8˚C. Thus, data could be collected at pH values higher than 7.5. The pH-dependence of the second order rate constant for cyanide (Fig. 11C) and 1,2,4-triazole (not shown) at 8˚C are similar with a limiting slope of +1. A pK_a value of 8.1 ± 0.7 was observed in both pH profiles at 8˚C.

The pH dependence of the second order rate constant for the second half of the OASS-A reaction was further measured with cyanide at 15 and 35˚C (Fig. 11A), and gave a limiting slope of +1 with pK_a values of 7.2 ± 0.2 and 7.6 ± 0.7, respectively. An Arrhenius plot, Fig. 12, is nonlinear with a transition at around 18°C. Heat of activation

Figure 10. pH (●) and pD (○) dependence of the second order rate constant measured with mercaptoacetate at 25˚C as described in Methods. Points are experimental values, and the line is the average value. Inverse solvent deuterium isotope effect is observed with ${}^{D2O}(k_{max}/K_s)$ value of about 0.2.

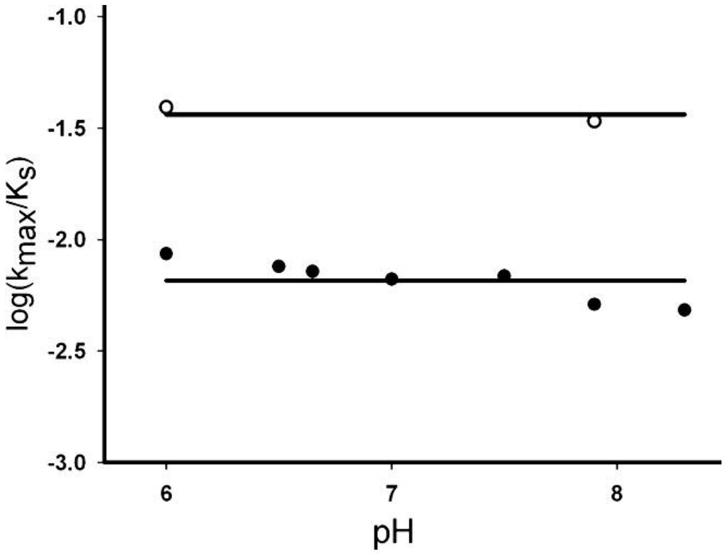
-1.0
-1.5
-2.0
-2.5
-3.0
log(k_max/K_S)
6
7
8
pH

Figure 11. pH(D) dependence of the second order rate constant measured with cyanide. (A) The pH dependence of the second order rate constant collected at (●) 15˚C, and (▲) 35˚C, gave pK_a values of 7.2 ± 0.2 and 7.6 ± 0.7, respectively. (B) The pH(D) dependence of the second order rate constant collected at 25˚C in (●) H_2O, and (○) D_2O, gave pK_a values of 7.2 ± 0.2 and 7.9 ± 0.7, respectively. (C) The pH(D) dependence of the second order rate constant collected at 8˚C in (●) H_2O, and (○) D_2O, gave pK_a values of 8.1 ± 0.7 and 8.9 ± 0.7, respectively. An inverse solvent isotope effect was observed at all temperatures tested with a calculated $^{D2O}(k_{max}/K_s)$ value of about 0.45 at 8˚C. The rate data were fitted using eq. 3. Points are experimental values, and the curve is theoretical based on the fit to eq. 3.

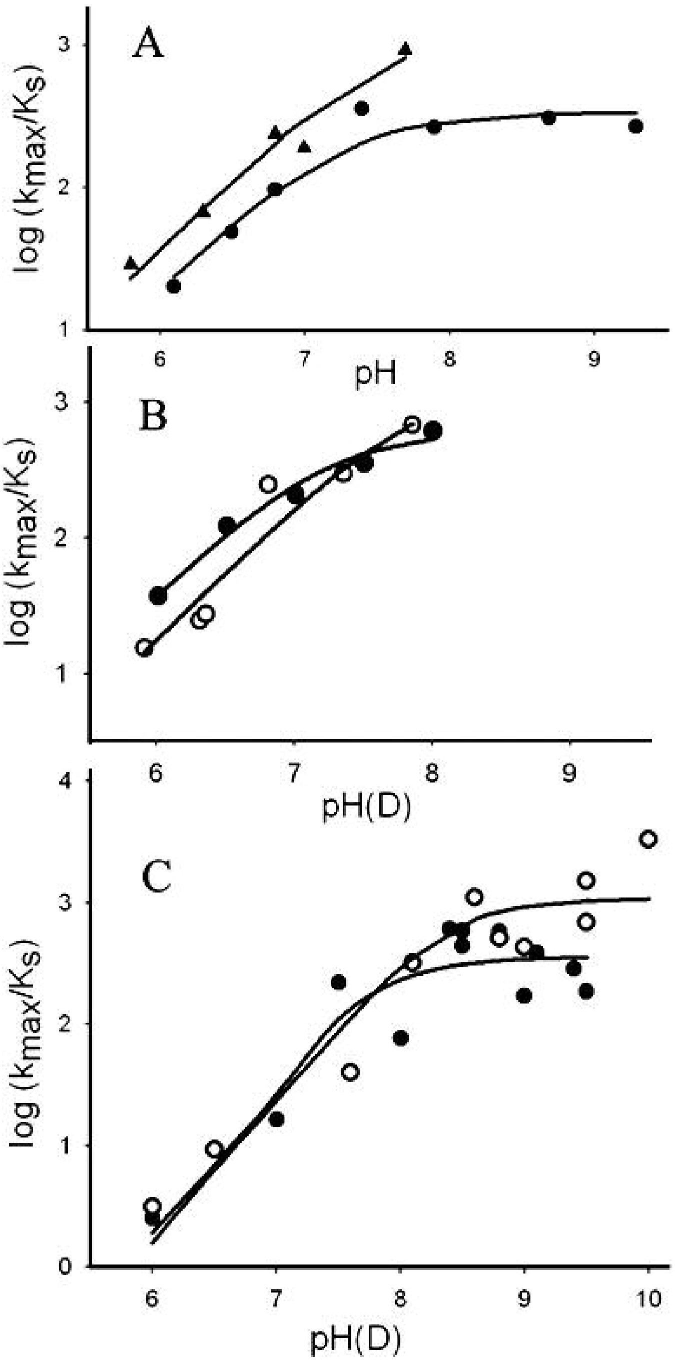
A
log (kmax/Ks)
3
2
1
6
7
8
9
pH
B
log (kmax/Ks)
3
2
1
6
7
8
9
pH(D)
C
log (kmax/Ks)
4
3
2
1
0
6
7
8
9
10
pH(D)

Figure 12. Arrhenius plots of the second order rate-constant of the second half-reaction of OASS-A at pH 7. Arrhenius plot obtained shows a biphasic pattern, with a transition at around 18°C. The E_{act} value was calculated from the graph giving values at temperature >18°C of10.2 kJ/mol and 170 kJ /mol at temperatures <18 °C.

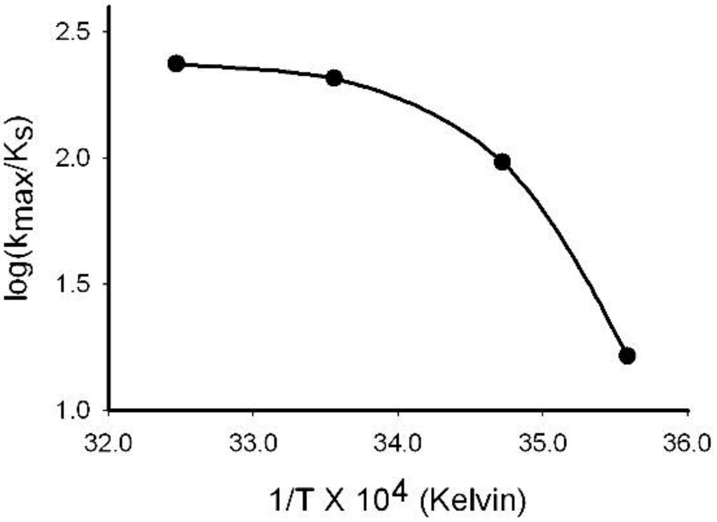

log(kmax/Ks)
2.5
2.0
1.5
1.0
32.0
33.0
34.0
35.0
36.0
1/T X 10⁴ (Kelvin)

was calculated using the slope of the line at low and high temperature according to eq. 4. The energy of activation at temperatures >18°C is about 10.2 kJ/mol but increases approximately 17-fold at temperatures <18°C (ΔEact = 170 kJ /mol).

Spectral Studies in D_2O. If protonation of C_α in the second half of the OASS-A reaction to give the external Schiff base, ESB(II), is rate-limiting, a solvent kinetic deuterium isotope effect is predicted. All RSSF spectra obtained in D_2O exhibit two clear isosbestic points, similar to those shown in water, Fig. 7. However, the enzyme spectrum obtained after the reaction of the nucleophilic substrate with the α-aminoacrylate intermediate in D_2O has λ_{max} at 418 nm compared to that of the free enzyme in D_2O, λ_{max} at 412 nm. The reaction of mercaptoacetate with the α-aminoacrylate intermediate in D_2O yields the *O*-mercaptoacetyl-L-serine external Schiff base form of the enzyme, Fig. 13A, where spectrum 1 is the absorbance spectrum of the α-aminoacrylate intermediate obtained in D_2O, spectrum 2 and 3 are the absorbance spectra of the *O*-mercaptoacetyl-L-serine external Schiff base at pD 6.0 (λ_{max} at 418 nm) and 7.9 (λ_{max} at 412 and 418 nm), respectively. At pD 7.9, the *O*-mercaptoacetyl-L-serine external Schiff base spectrum suggests an equilibrium between the free and the external Schiff base form of the enzyme. Addition of 1 mM OAS to the enzyme with a λ_{max} at 418 nm gives the α-aminoacrylate intermediate, which was detected at λ_{max} 470 nm. On the basis of the above, the final enzyme form obtained upon the reaction of different nucleophiles with the α-aminoacrylate intermediate in D_2O is the product external Schiff base, as opposed to that of the internal Schiff base in H_2O. To determine whether the external Schiff base formed in D_2O is stable; its spectrum was recorder using a photodiode array spectrophotometer as described in the methods section. In Fig. 13B, Figure 13. (A) RSSF spectra for the reaction of the α-aminoacrylate intermediate with 10 mM mercaptoacetate in D_2O. Plot 1 is the absorbance spectrum of the starting complex, the α-aminoacrylate intermediate; plot 2 and 3 are the absorbance spectrum of the *O*-mercaptoacetyl-L-serine external Schiff base at pD 6.0 (λ_{max} at 418 nm) and 7.9 (λ_{max} at 412 and 418 nm), respectively. (B) UV-visible spectra collected using photodiode array spectrophotometer at pD 6.0. Plot 1 is the absorbance spectrum of free OASS-A, and plot 2 is the *O*-mercaptoacetyl-L-serine external Schiff base measured in D_2O.

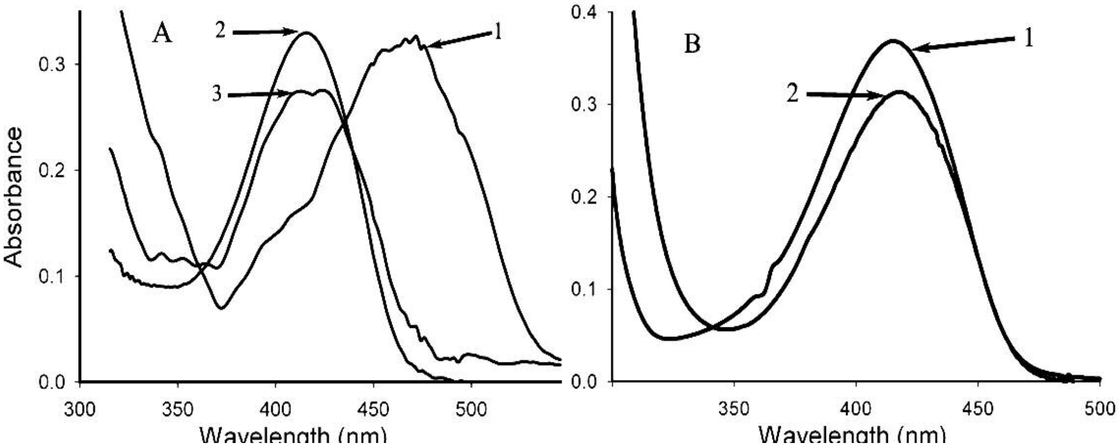
A
2
3
1
Absorbance
0.0
0.1
0.2
0.3
300
350
400
450
500
Wavelength (nm)
B
1
2
0.0
0.1
0.2
0.3
0.4
350
400
450
500
Wavelength (nm)

spectrum 1 is the absorbance spectrum for free enzyme measured at pD 6.0, and spectrum 2 is the absorbance spectrum for *O*-mercaptoacetyl-L-serine external Schiff base at pD 6.0. There is no shift in the λ_{max} of free enzyme in D_2O compared to H_2O.

Stopped-Flow Solvent Isotope Effect Studies. In order to determine whether a solvent deuterium isotope effect is observed, the pD dependence of the second order rate constant was measured as above using cyanide, 1,2,4-triazole, and mercaptoacetate. The second order rate constant at 25˚C, using mercaptoacetate is pD-independent (Fig. 10) and yields an inverse solvent isotope effect with $^{D2O}(k_{max}/K_S)$ of about 0.2. The second order rate constant is pD-dependent over the pD range 6.0-8.5 measured at 25˚C with cyanide (Fig. 11B) and 1,2,4-triazole (not shown), which exhibit a slope of +1 with a pK_a value of 7.9 ± 0.7. The data in D_2O nearly superimpose on the data obtained in H_2O, even though a shift to a higher pD value is expected as a result of the equilibrium isotope effect on the pK_a of the group titrated (*83*). The pD profile obtained for both substrates has large errors at pD higher than 8.0. As a result, the value of the solvent isotope effect was not calculated but is inverse and near 0.4, on the basis of the expected shift in the pK_a. The pD dependence of the second order rate constant for cyanide and 1,2,4-triazole were also measured at 8˚C to lower the rate of the α-aminoacrylate intermediate decomposition. The pD profile obtained at 8˚C for cyanide (Fig. 11C) and 1,2,4-triazole (not shown) are similar with a limiting slope of +1, and superimpose on the data obtained in H_2O. A pK_a value of 8.9 ± 0.7 was obtained from the pD profile of cyanide. An inverse solvent isotope effect with $^{D2O}(k_{max}/K_s)$ of about 0.45 was calculated from the pH(D) cyanide profile.

DISCUSSION

Rapid-Scanning-Stopped-Flow-Studies (RSSF). Very little is know about the second half of the OASS-A reaction in which the α-aminoacrylate intermediate and bisulfide are converted to L-cysteine and free enzyme. Previous studies indicated the second half-reaction to be very rapid and the only species observed upon reacting enzyme with OAS and sulfide are the α-aminoacrylate intermediate and free enzyme (*68*). It was thus proposed that the second half-reaction is diffusion limited. In agreement, the $V/K_{SH}E_t$ is 8×10^7 $M^{-1}s^{-1}$ (*11*). In the present studies, the only condition that allowed a measurable pre-steady-state rate of disappearance of the α-aminoacrylate intermediate, 100 s^{-1}, was obtained with a total sulfide concentration of 1.5 μM at pH 5.0. Sulfide has two pK_a values, 6.8 and 13.8, so that at pH 5.0 most of the sulfide is H_2S, and bisulfide, the true substrate for OASS-A, is only 24 nM.

In an attempt to slow down the second half-reaction, a number of nucleophiles were used as analogs of the second substrate, bisulfide. For all the nucleophiles tested, no nucleophile was found to have a second order rate constant equal to that obtained with bisulfide. On the other hand, one can relate nucleophilicity of the analogs to their pK_a values, Table 3. Nucleophiles with low pK_a values have a lower second order rate-constant (k_{max}/K_S) when compared to those with high pK_a values, in agreement with the proposed direct nucleophilic attack of the nucleophile on the α-aminoacrylate intermediate. In Table 3, nucleophiles from the carboxyl class show that size does not play a major role in determining the rate of the second half-reaction. However, nucleophiles from the carboxyl class have a lower second order rate constant than all other classes because they have a lower nucleophilicity. Nonetheless, as demonstrated in Table 3, the high turnover number for OASS-A, along with its acceptance of a wide variety of nucleophilic substrates, makes it a good tool for the preparation of a number of new β-substituted α-amino acids, even when the rate constant is low.

pH Dependence of the Second Order Rate Constant. Enzyme kinetic parameters and/or microscopic rate constants are a function of pH because of ionization of protic positions on the enzyme and/or substrate. In a ping-pong kinetic mechanism, the V/K pH profile for the substrates reflects the individual half-reactions (*85*). The V/K_{TNB} pH profile obtained with BCA as the amino acid substrate yields pK_a values of about 7 on the acid side and 8.2 on the basic side (*64*). The enzyme group with a pK_a of 7 must be unprotonated to stabilize the optimum catalytic conformation of the enzyme, while the enzyme group with pK_a of 8.2 is attributed to the ε-amino group of Lys-41, which must be protonated to donate a proton to C_α of the α-aminoacrylate intermediate as the amino acid external Schiff base, ESB(II), is formed, Scheme 10.

In the pre-steady state, k_{max}/K_s for the sulfide analogs reflects the slow step(s) in the conversion of the α-aminoacrylate intermediate and sulfide analog to free enzyme and amino acid product. In this study, the pH profiles for thiosalicylate and mercaptoacetate at 25˚C are pH-independent. Both nucleophiles have low pK_a values of 4.0 and 3.5, respectively. The pH-independence of k_{max}/K_s indicates neither enzyme nor substrate functional groups are titrated over the pH range 5.5-8.0. In both cases, the pK_a of the nucleophile is not observed because it is lower than pH 5.5.

The behavior of nucleophiles with high pK_a values is different. The pH-rate profiles at 25˚ for cyanide (Fig. 11B) and 1,2,4-trizole (not shown) are pH-dependent

Scheme 10. Proposed Chemical Mechanism for OASS-A. E, the internal Schiff base; GD(I), *geminal*-diamine intermediate; ESB(I), OAS external Schiff base; AA, the α-aminoacrylate intermediate; ESB(II), cysteine external Schiff base; GD(II), *geminal*-diamine intermediate with cysteine.

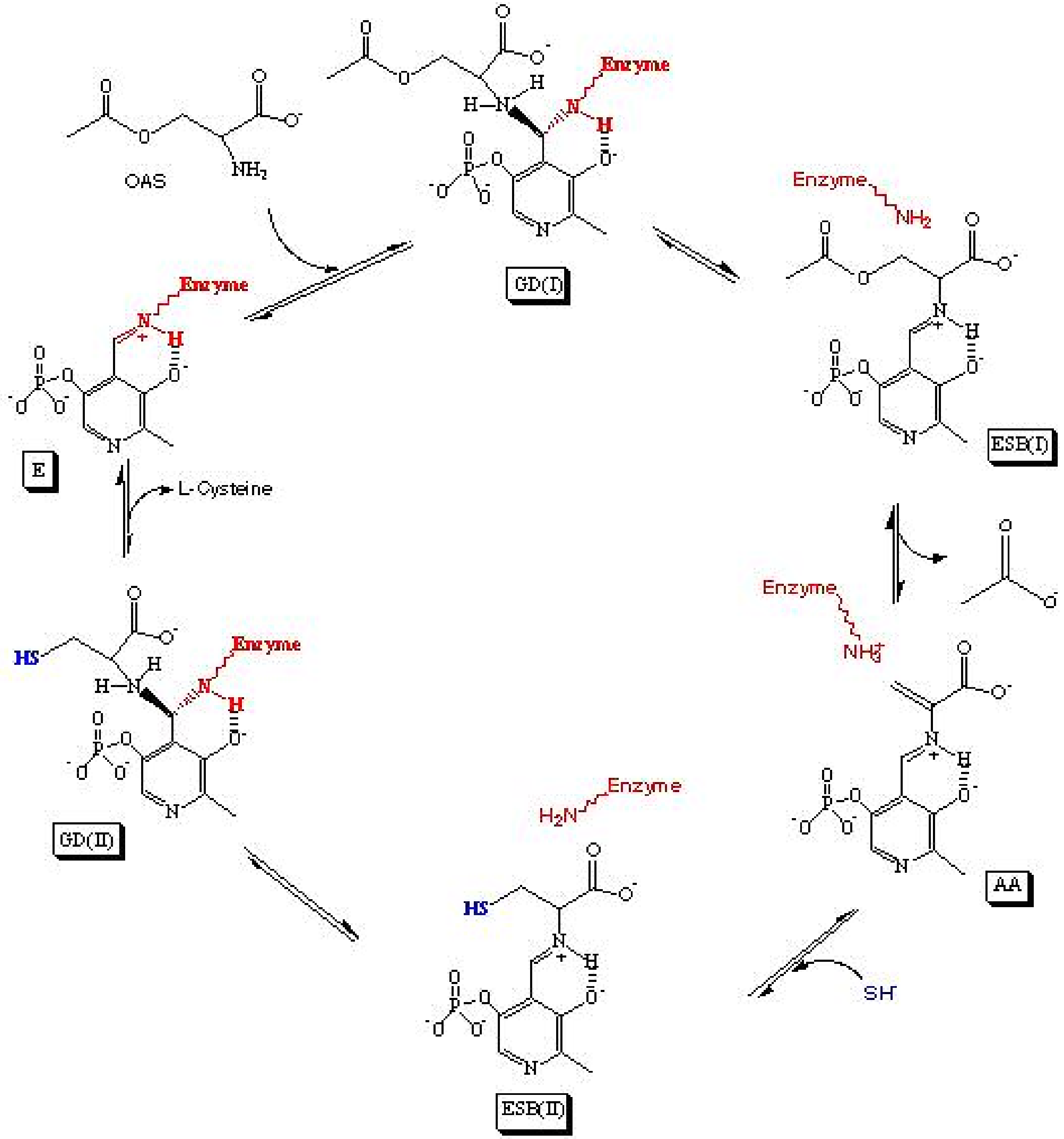
OAS
Enzyme
GD(I)
E
L-Cysteine
ESB(I)
AA
SH-
ESB(II)
GD(II)
HS

with the requirement for a group on the acid side with a pK_a of about 7, while cyanide and 1,2,4-triazole have pK_a values of 9.1 and 10, respectively. If the pH-rate profiles could be extended to high enough pH one would expect k_{max}/K_S to decrease above the pK_a of the nucleophile. Data suggest that reverse protonation states exist between the nucleophile and the enzyme group with a pK_a of 7. The group with a pK_a of 7 is required protonated, while the nucleophile is required unprotonated. At 35°C, Fig. 11A, although the pH range is again limited, data are similar to those obtained at 25°C. Data at 15°C, Fig. 11A, however, indicate a pH independent region above 7.5 to about 9, in agreement with the above explanation; a pK_a of about 7.6 is now observed on the acid side of the profile. As discussed above the group with a pK_a of 7 must be protonated, opposite to the interpretation on the basis of the pH dependence of the steady state parameter V/K_{TNB}. In the steady state the starting point is the α-aminoacrylate external Schiff base and free TNB, and the group with a pK_a of 7 must be unprotonated to stabilize the closed conformation *(64)*. In the pre-steady state the slow step is the conformational change to open the active site and release product, and the group with a pK_a of 7 must be protonated to stabilize the open conformation.

At 8˚C, a condition that exhibits a large E_a at pH 7, a higher pK_a is observed in the $\log(k_{max}/K_{CN})$ vs. pH profile. The pKa is near 8, 0.5 pH units higher than that observed at the higher temperatures. In addition, the rate appears to be decreasing above pH 9, consistent with the pKa of cyanide. The plot of $\log(k_{max}/K_{CN})$ at pH 7 vs. 1/T is biphasic, suggesting a change in rate limiting step with a break at about 18˚C. Data support a rate-limiting conformational change accompanying product release requiring an enzyme group with a pK_a of 7 protonated, as suggested above. At lower temperature, however, the conformational is very slow.

pD dependence of the Absorbance Spectra. In H_2O, the enzyme form present after reaction of the α-aminoacrylate intermediate with nucleophile is the internal Schiff base (free enzyme, E). In D_2O using cyanide, 1,2,4-triazole, or mercaptoacetate as the nucleophilic substrate the amino acid external Schiff base (ESB(II), λ_{max} 418 nm) is the final form of the enzyme at pD 6.0, Fig. 13. Reaction of the α-aminoacrylate intermediate (AA) with different concentrations of the nucleophilic substrate in D_2O gave the ESB(II) without releasing the amino acid product, while free enzyme (λ_{max} 412 nm) is present at the end of the reaction in H_2O. Data indicate the conformational change to open the active site is very slow in D_2O. At pD 7.9, the second half-reaction in D_2O yields an equilibrium between the ESB(II) and the free enzyme forms, Scheme 10. Thus the pH and pD profiles cannot be directly compared to give a solvent deuterium isotope effect. In H_2O, chemistry limits only at low temperature while product release limits at high temperature. In D_2O, product release does not occur in the time scale of the assay and thus a large solvent deuterium isotope effect is observed, suggesting the involvement of a group on protein to open the active site, consistent with the above discussion. The observed pD independent rate is faster in D_2O than the pH independent rate in H_2O as a result of the very slow conformational change in D_2O, k_2 in Scheme 11.

Scheme 11.

$$\text{AA} + \text{SH}^- \xrightarrow{k_1} \text{ESB} \xrightarrow{k_2} \text{E} + \text{L-Cys}$$

The Chemical Mechanism of the OASS-A Reaction. The amino acid substrate, OAS, binds as the monoanionic form with its α-amine unprotonated to carry out a nucleophilic attack on C4' of the internal Schiff base (E). As the OAS external Schiff base (ESB(I), observed transiently in the pre-steady state with OAS as the substrate (*68*)) is formed via *geminal*-diamine intermediates, GD(I), the active site closes triggered by the interaction of the substrate α-carboxylate with the asparagines loop (*59*). Lys-41, initially in internal Schiff base linkage with PLP, serves as a general base to deprotonate C_α in the α,β-elimination reaction responsible for the release of acetate and the formation of the α-aminoacrylate intermediate (AA) to end the first half of the OASS-A reaction. The active site opens partially to release the first product, acetate, and allow entry of bisulfide, the second nucleophilic substrate. The difference in conformation of the external Schiff base and the α-aminoacrylate external Schiff base forms of the enzyme is clearly shown by differences in their ^{31}P NMR chemical shifts (*69*).

At the beginning of the second half-reaction, Lys-41 is protonated and the nucleophilic substrate diffuses into the active site and attacks C_β of the AA to give ESB(II). The nucleophile has no binding site as a substrate and likely adds to the AA directly upon diffusion into the active site (*68*). The ESB(II) is formed upon addition of the nucleophile to the AA as was indicated by the shift in the λ_{max} from 412 to 418 nm upon adding cysteine to OASS-A in the reverse direction of the second half-reaction (*63*). The ESB(II) is rapidly formed and does not accumulates in the pre-steady state but is seen transiently when cysteine adds to free enzyme to form the cysteine external Schiff base (*68*). A *geminal*-diamine intermediate, GD(II), is expected to precede ESB(II), where the ε-amino group of Lys-41 and the amino acid product are bonded to C4' of

PLP. No *geminal*-diamine intermediate was visualized under the experimental conditions used in this study and the addition of cysteine to free enzyme in the pre-steady state also does not show the presence of a *geminal*-diamine intermediate (*68*). The presence of one or more *geminal*-diamine intermediate is important to release the amino acid products, thus the formation and decay of GD(II) must be very rapid, and the equilibrium between this intermediate and the free enzyme must be far toward the latter. The active site then opens to expel the cysteine product upon transimination by Lys-41. This step requires an enzyme group with a pK_a of 7.0 to be protonated to open the active site as was observed in the $k_{max/}K_S$ pH profile for cyanide and 1,2,4-triazole. No quinonoid intermediate was detected in the second half of the OASS-A reaction under the experimental conditions used. Data are in agreement with the absence of a quinonoid intermediate in the first half of the OASS-A reaction under all the experimental conditions used (*63*, *68*). The chemical step, represented by the proton transfer step, is not rate limiting; rather, the enzyme conformational changes to open the active site and release the amino acid substrate is the rate limiting step in the second half-reaction. The second half-reaction in D_2O yields the ESB(II) form of the enzyme, which is the locked conformation as a result of the requirement for a proton transfer step to open the active site and release the amino acid product. On the other hand, at pD 7.9, the enzyme ESB(II) complex was found in equilibrium with the free enzyme form (E) as a result of having the enzyme group that is important to open the active, unprotonated.

In conclusion, the second half of the OASS-A reaction is limited by the conformational change needed to open the active site and release the amino acid product. No quinonoid or *geminal*-diamine intermediates were detected; rather, the amino acid external Schiff base of the enzyme was found to be very stable when the reaction was run in D_2O.

Chapter III

Spectral Characterization of *O*-Acetylserine Sulfhydrylase-B from *Salmonella typhimurium*

The OASS-B isozyme is thought to be expressed under anaerobic growth conditions, and it appears to be less substrate selective than the A-isozyme to both the amino acid and nucleophilic substrates (78). OASS-B has a ping-pong kinetic mechanism on the basis of initial velocity patterns obtained in the absence of inhibitors. Both substrate exhibit competitive inhibition, and the kinetic mechanism of OASS-B appears qualitatively identical to that of OASS-A (78). The OASS-B reaction substitutes the acetyl group of OAS with a thiol group to yield cysteine in a β-substitution reaction. The B-isozyme has chemical mechanism that is similar to that observed with the A-isozyme in which OAS binds wih its α-amine unprotonated to carry out a nucleophilic attack on C4' of the internal Schiff base.

Little data were collected on the B-isozyme as a result of the poor expression system. A new expression system is developed and yields high amounts of enzyme with purity 98%. Both the quantity and purity of the B-isozyme now permit more kinetic and structurally based studies to be conducted.

MATERIALS AND METHODS

Chemicals. *O*-Acetyl-L-serine, DTNB, L-cysteine and chloramphenicol were obtained from Sigma. The buffers Ches, Hepes, Mes, Caps, Taps, and imidazole were obtained from Research Organics. Ampicillin was obtained from Midwest Scientific. IPTG was obtained from Research Product International, and L-serine was obtained from Aldrich. All other chemicals and reagents were obtained from commercial sources and were of the highest purity available.

Enzyme. The OASS-B gene, *cys*M, was subcloned into the pET16B vector by PCR using the pRSM17 vector (*86*), which contains the *cys*M gene as the template. Conditions for PCR cycling were as follow: denaturation at 94°C for 40 s, primer annealing at 45°C for 45 s, and primer elongation at 68°C for 90 s. The cycle was repeated 35 times, and the reaction was incubated for 10 min at 68°C to complete any immature PCR products. The primers used in the PCR have up stream *Nde* I and down stream *Xho* I restriction sites and the primers sequences in which the bold letters represent the restriction site, are as follow:

Forward primer: 5’-GGCTTTTTTACGAGCTGAA**CATATG**AATACATTAGAAC-3’
Reverse primer: 5’-GGCCG**CTCGAG**CGGTTAAATCCCTGCCCCCTGG-3’

The new plasmid, pWR, adds a 10-His tag to the N-terminus of OASS-B. The pWR vector was then transformed into the BL21-Star (DE3)-RIL *E. coli* strain, which uses a T7 promoter-based expression system. The *E. coli* strain contains the RIL plasmid (pACYS) that confers chloramphenicol resistance and contains genes for rare tRNAs. The pWR plasmid confers ampicillin resistance for selection. A chloramphenicol concentration of 50 µg/mL was used in the overnight culture. The induction culture was grown at 30°C in LB medium containing ampicillin (100 µg/mL) and chloramphenicol (35µg/mL). When the induction culture reached an OD_{600} of 0.7 – 0.9, it was induced by the addition of 0.5 mM IPTG and allowed to grow for 5 h. The pH was maintained at 7.0 during growth using 10 N KOH and 20 N HCl. After centrifugation at 8,000 *g* for 30 min, the cell pellet was resuspended in sonication buffer that contains 50 mM phosphate, pH 7.8 and 300 mM NaCl. The cells were sonicated for 3 min with a 30 s rest time between each minute of pulse. 0.05 g of PLP was added to the supernatant, which was stirred for 1 h at 4°C. The supernatant was loaded onto a Ni^{2+}-NTA agarose affinity column, 15 mL bed volume, that was pre-equilibrated with sonication buffer, and the column was washed with 10 bed volumes of 50 mM imidazole. The chromatogram was then developed in steps of 50 mM imidazole using 10 bed volumes, and OASS-B eluted between 0.15 and 0.2 M imidazole. The enzyme was dialyzed against 4 L of 5 mM Hepes, pH 8 and stored at 4°C. SDS-PAGE showed the enzyme to be more than 98% pure.

Molecular Mass of OASS-B. Mass spectra of OASS-B were recorded on a Micromass Q-TOF quadrupole time-of flight mass spectrometer equipped with a Z-spray electrospray ionization (ESI) source. The software controlling the instrument was MassLynx version 3.5. A Harvard syringe pump (Harvard Apparatus, South Natick, MA, USA) was used to deliver the sample solution to the electrospray source at a flow rate of 5 µL/min. A 5 µL solution of 0.1 mg/mL OASS-B was injected and eluted with 0.1% formic acid in 50% aqueous methanol. The electrospray capillary voltage was set at 3000 V, the cone voltage was set at 30 V and the source temperature was 80°C. The mass spectrometer was calibrated over the mass range 50-1500 amu using a 0.05 µg/µL CsI and 2 µg/µL NaI in methanol. The molecular weight is calculated using the Transform tool in MassLynx 3.5 (Waters) software.

Enzyme Assay. OASS-B activity was monitored using 5-thio-2-nitrobenzate (TNB) as a substrate analog of bisulfide (*87*). The TNB was prepared fresh daily by reduction of DTNB by the disulfide reducing agent DTT. The disappearance of TNB was monitored continually at 412 nm (ε412, 13,600 M^{-1} cm^{-1}) using a Beckman DU 640 spectrophotometer. All assays were performed in 100 mM Hepes, pH 7, at 25°C with an OAS concentration of 10 μM and a TNB concentration of 15 μM.

Ultraviolet-Visible Spectral Studies. Absorption spectra were measured utilizing a Hewlett Packard 8452A photodiode array spectrophotometer. The absorbance spectra of OASS-B were recorded over the wavelength range 300-600 nm at 25°C in reaction cuvettes of 1cm path length and 1 mL volume; in all cases the blank consisted of all components minus OASS-B. Spectra were measured as a function of pH from 5.5-11 using the following buffers at a final concentration of 200 mM: Mes (pH 5.5-6.5), Hepes (pH 7-8), Taps (pH 8.5-9), Ches (pH 9.5-10), and Caps (pH 10.5-11). The pH of the solutions was confirmed by measuring the pH before and after spectral measurements. To determine the pH dependence of the spectra of the free enzyme and the α-aminoacrylate intermediate, absorbance spectra were recorded in the absence and presence of 2 mM OAS as function of pH. The OASS-B concentration was maintained at 20-30 μM for all spectra.

The absorbance spectra of OASS-B in the presence of different concentration of L-cysteine or L-serine were obtained as described previously (*63*). Amino acid substrates were added in a stepwise manner giving final concentrations of L-cysteine of 1-100 mM, and L-serine of 10-200 mM. The pH was varied from 5.5 to 11 utilizing the same buffers listed above. Absorption spectra were measured at zero substrate concentration and after each substrate addition. To find λ_{max} for the reaction, a difference spectrum at saturating cysteine (or serine) and free enzyme was obtained giving a maximum absorbance at 457 nm. All spectra were corrected for dilution and changes in the baseline absorbance (using the difference in absorbance at 550 nm). The ΔA457 was then plotted vs. the amino acid concentration to generate an estimate of K_{ESB}, where ESB represents the amino acid external Schiff base. A plot of pK_{ESB} vs pH was fitted to eq. 8 to obtain the pK_a values of enzyme and/or substrate functional groups that are involved in formation of the ESB form of the enzyme.

OAS:acetate Lyase Activity. The first-order rate of degradation of the α-aminoacrylate intermediate was measured utilizing a Hewlett Packard 8452A photodiode array spectrophotometer as described previously (*60*). OASS-B was maintained at a final concentration of 20 µM and it was converted to the α-aminoacrylate intermediate by adding a concentration of OAS $\leq$ OASS-B. The first order rate constant for disappearance of the α-aminoacrylate intermediate was calculated at 472 and 325 nm and the rate constant for the appearance of free enzyme was calculated at 414 nm. A fit of the data to a first order rate law gave the first order rate constant (k_{obs}). The experiment was carried out over the pH range 6.5-9.8 utilizing 200 mM buffer, as described above. A plot of log k_{obs} vs. pH provided an estimate of the pK_a of the group involved in the deacetylase activity.

Rapid-Scanning-Stopped-Flow Studies. Pre-steady-state kinetic measurements were carried out using an OLIS-RSM 1000 stopped-flow spectrophotometer. Sample solutions were prepared in two syringes at the same pH with a final buffer concentration of 100 mM; the pH was varied from 5.5-7.5 utilizing the buffers listed above. The first syringe contained OASS-B at a concentration no lower than 30 µM, while the second syringe contained different concentrations of OAS at final concentrations ranging from 0.1 to 10 mM, L-serine at final concentrations of 10-200 mM, or L-cysteine at final concentrations of 5-100 mM. Data were collected with a repetitive scan rate of 15 ms from 300-600 nm and the number of scans collected depended on the rate of the reaction. The disappearance of free enzyme was monitored at 414 nm, the appearance of the α-aminoacrylate intermediate was monitored at 472 and 325 nm, and the external Schiff base was monitored at 414 nm. The rate data were fitted to eq. 10 to obtain the first order rate constant (k_{obs}). k_{obs} was plotted vs. substrate concentration and fitted to Michaelis-Menten equation to obtain the second order rate constant (k_{max}/K_{ESB}). k_{max}/K_{ESB} was plotted vs. pH to obtain the pH profile in the pre-steady-state.

Fluorescence Studies. Fluorescence spectra were recorded on a Shimadzu RF-5301 PC spectrofluorometer. The reaction temperature was maintained at 25˚C using a circular water bath. Quartz cuvettes with a 3 mL volume and 1 cm path length were used to measure the spectrum for sample and blank. The blank contains all the sample components except OASS-B, which was fixed at a final concentration of 0.25 mg/mL. The spectra of free enzyme and α-aminoacrylate intermediate were measured at pH 6.5 utilizing a final concentration of 100 mM Hepes. On the other hand, spectra for free enzyme, and enzyme in complex with 50 mM cysteine, 100 mM acetate, or 100 mM serine were measured at pH 9 utilizing a final concentration of 100 mM Taps. The excitation and emission slit widths were set to 1.5 and 5 nm, respectively. The emission spectra were scanned from 300-600 nm with the excitation monochromator fixed at 298 nm. The excitation spectra were measured from 250-550 nm with the emission monochromator fixed at 425, 500 and 550 nm.

Data Processing. Data were fitted using the appropriate rate equation and the EnzFitter program software (Elsevier Science, Amsterdam, The Netherlands). Initial rate data were fitted to eq. 6, which describes double competitive substrate inhibition in a ping pong mechanism. The K_{ESB} values for cysteine and serine were obtained using the equation for a rectangular hyperbola, eq. 7.

$$v = \frac{V\mathbf{AB}}{K_a\mathbf{B}\left(1+\frac{\mathbf{B}}{K_{Ib}}\right)+K_b\mathbf{A}\left(1+\frac{\mathbf{A}}{K_{Ia}}\right)+\mathbf{AB}} \qquad [6]$$

$$\Delta\mathbf{A}_{457}^{obs} = \frac{\left(\Delta\mathbf{A}_{457}^{max}\right)\mathbf{L}}{K_{ESB}+\mathbf{L}} \qquad [7]$$

In eq. 6, v and V are initial and maximum rates, respectively, **A** and **B** are reactant concentrations, K_a and K_b are K_m values for A and B, respectively, and K_{Ia} and K_{Ib} are substrate inhibition constants for A and B, respectively. In eq. 7, **L** is ligand concentration (cysteine or serine), K_{ESB} is the dissociation constant for the external Schiff base, and ΔA_{457}^{obs} and ΔA_{457}^{max} are observed and maximum changes at 457 nm as a result of formation of the external Schiff base.

Data for K_{ESB} vs. pH were fitted to eqs. 8 and 9, when the pK_{ESB} vs. pH exhibited a slope of +1 at low pH or decreased from a constant value at one pH to another constant value, respectively.

$$\log y = \log\frac{\mathbf{C}}{\left(1+\mathbf{H}/K\right)} \qquad [8]$$

$$\log y = \frac{Y_L + Y_H\left(\mathbf{H}/K\right)}{1+\mathbf{H}/K} \qquad [9]$$

In eqs. 8 and 9 y is the kinetic parameter obtained at any pH, **H** is the hydrogen ion concentration, C is a pH independent value of Y, Y_L and Y_H are pH independent values at high and low pH, respectively, and K is the acid dissociation constant of the group whose ionization or protonation decreases the amount of the ESB formed.

Global fitting of the RSSF spectral data was carried out using the fitting program provided by OLIS and fitted to eq. 10 to obtain first order rate constants (k_{obs}) for the conversion of the free enzyme to the α-aminoacrylate intermediate.

$$A_t = A_0 e^{(-k_{obs} \cdot t)} + B_0 \qquad [10]$$

In eq. 10, A_t is the absorbance at time t, A_0 is the absorbance at time zero, and B_0 corrects for background absorbance. The rate constant, k_{obs}, was then plotted against pH and fitted to eq. 8 to estimate the pK_a of the enzyme group involved in the titration.

RESULTS

Enzyme. OASS-B was tagged with an additional ten histidine residues at the N-terminal of the protein and purified using Ni^{2+}-NTA agarose affinity chromatography. A large quantity (50-75 mg/L) of purified OASS-B was obtained, and according to SDS-PAGE, the recombinant enzyme was purified to electrophoretic homogeneity (>98% pure) and had a molecular weight of 35.4 kDa, which was confirmed by ESI mass spectrophotometry. Both the quantity and purity of this enzyme now permit more kinetic and structurally based studies to be conducted.

Ultraviolet-Visible Spectral Studies. UV-vis spectra for native enzyme were collected for OASS-B in the absence and presence of OAS over the wavelength range 300-600 nm as a function of pH from 6 - 10, Fig. 14. The free enzyme is bright yellow in color and exhibits a typical PLP enzyme spectrum with λ_{max} for the internal Schiff base at 414 nm (ε_{414} of 11.5 M^{-1} cm^{-1}) and A_{280}/A_{414} of 3.5. The absorbance spectra of the free enzyme were pH-dependent over the pH range tested, Fig. 14. At pH 7.0, the free enzyme spectrum (Fig 14, plot 1) has λ_{max} values of 325 and 414 nm. At pH 10 Fig 14, plot 3 a slight enhancement in absorbance at 414 nm is observed at the expense of the 325 nm absorbance. Addition of OAS to free enzyme results in a decrease in absorbance at 414 nm concomitant with an increase in absorbance at 325 and 472 nm (ε_{472} of 15.6 mM^{-1} cm^{-1}), which reflects the formation of the α-aminoacrylate intermediate (*88*). The absorbance spectrum for the α-aminoacrylate intermediate is also pH-dependent. At pH 7.0, the α-aminoacrylate intermediate spectrum (Fig 14, plot 2) has λ_{max} value of 325 and 472 nm, and at pH 10 Fig 14, plot 4 an increase in the absorbance at 325 nm and a decrease at 472 nm is observed. The α-aminoacrylate intermediate is unstable throughout the pH range tested as result of decomposition to give free enzyme, pyruvate, and ammonia (*60*).

UV-vis absorbance spectra for the reaction of L-cysteine with OASS-B at pH 9.4 are shown in Fig. 15A. Equilibrium measurements for the second half-reaction consisted of the addition of L-cysteine to OASS-B in an attempt to drive the second half-reaction in the reverse direction, forming the α-aminoacrylate intermediate. Titration of OASS-B

Figure 14. pH dependence of the UV-visible spectrum of OASS-B. Absorbance spectra were measured on Hewlett Packard 8452A photodiode array spectrophotometer as described under Material and Methods. The spectra for free enzyme were measured in the absence and presence of 2 mM OAS at different pH 7 and 10. 1) free enzyme at pH 7.0 (──); 2) the α-aminoacrylate intermediate at pH 7.0 (──); 3) free enzyme at pH 10 (----); 4) the α-aminoacrylate intermediate at pH 10 (----). OASS-B concentration was 1 mg/mL.

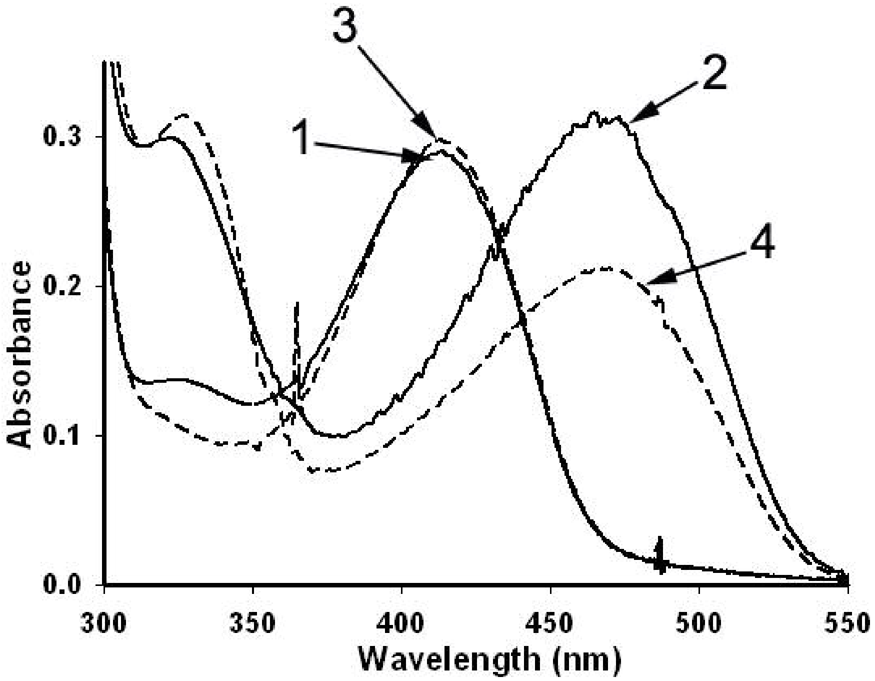

3
2
1
4
Absorbance
0.0
0.1
0.2
0.3
300
350
400
450
500
550
Wavelength (nm)

Figure 15. Spectral Titration of OASS-B with L-Cysteine. A) Titration of the enzyme with L-cysteine. Absorbance spectra were measured with 16 µM of OASS-B at pH 9.4 and 25°C using the concentrations indicated. Inset. Difference for free enzyme and enzyme with 100 mM cysteine spectra. B) A plot of ΔAbs_{325} vs. cysteine concentration: the concentration of cysteine at half the maximum ΔAbs_{325} is K_{ESB}. C) A plot of pK_{ESB} vs. pH. The curve has limiting slope of +1 on the acid side with pK_a value of 6.9 ± 0.3. Points are experimental values, while the curve istheoretical based on the fit to eq. 8.

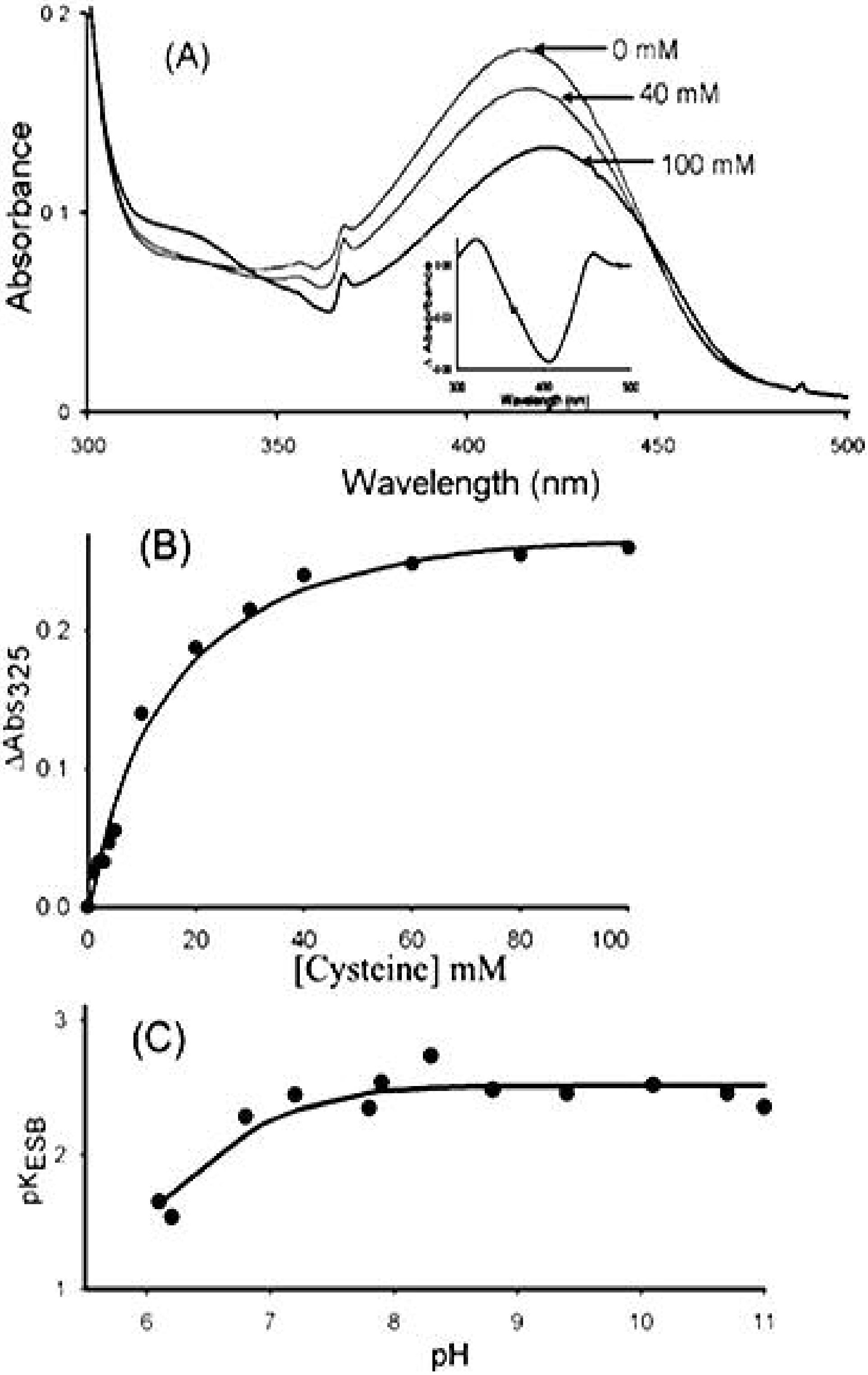
(A)
0 mM
40 mM
100 mM
Absorbance
0.2
0.1
0
300
350
400
450
500
Wavelength (nm)
(B)
ΔAbs325
0.2
0.1
0.0
0
20
40
60
80
100
[Cysteine] mM
(C)
pK$_{ESB}$
3
2
1
6
7
8
9
10
11
pH

with L-cysteine from zero to saturation causes a decrease in the absorbance at 414 nm and shift to 422 nm as a result of formation of the ketoenamine tautomer of the external Schiff base (Fig. 15A). A shoulder at 325 nm, which signals the formation of the enolimine tautomer of the external Schiff base is also observed with the OASS-A isozyme (*63*). There is no increase in absorbance at 472 nm, indicating that no significant elimination of SH^- to form the α-aminoacrylate intermediate has taken place at equilibrium. The maximum fractional changes in absorbance upon addition of cysteine was observed at 457 nm (Fig. 15A, inset), and ΔAbs_{457} were used to calculate the K_{ESB} of the external Schiff base (Fig. 15B). Experiments were repeated as a function of pH, and a plot of pK_{ESB} vs. pH (Fig. 15C) has a limiting slope of +1 and yields a pK_a value of 6.9 ± 0.3. At high pH, the reaction of L-cysteine with OASS-B was pH-independent and gave a dissociation constant value of 14 ± 3 mM at pH 9.4.

The UV-visible absorbance spectra of OASS-B with different concentrations of L-serine at pH 9.3 are shown in Fig. 16A. Addition of L-serine results in a decrease in absorbance at 414 nm and shift to 422 nm with a shoulder at 325. The maximum fractional changes in absorbance upon addition of serine was observed at 325 nm (Fig. 15 A, inset), and ΔAbs_{457} were used to calculate the K_{ESB} of the external Schiff base (Fig. 16B). The K_{ESB} of L-serine external Schiff base formation was calculated as above Fig. 16B, and a plot of pK_{ESB} versus pH was obtained (Fig. 16C). A pK_a value of 7.7 ± 0.6 obtained from the pK_{ESB} profile. At high pH, the reaction of L-serine with OASS-B was pH-independent and gave a dissociation constant value of 30 ± 1 mM at pH 9.3. The shift in absorbance is not accompanied with increase in absorbance at 472 nm when L-cysteine and L-serine are used as substrates, indicating that there is no formation of the

Figure 16. Spectral Titration of OASS-B with L-Serine. A) Titration of the enzyme with L-serine: Absorbance spectra were measured with 30 µM of OASS-B at pH 9.3 and 25°C using the concentrations indicated. Inset. Difference for free enzyme and enzyme with 160 mM serine spectra. B) A plot of ΔAbs_{457} vs. serine concentration: the concentration of serine at half the maximum ΔAbs_{457} is K_{ESB}. C) A plot of pK_{ESB} vs. pH. The curve has limiting slope of +1 on the acid side with pK_a value of 7.7 ± 0.6. Points are experimental values, while the curve is theoretical based on the fit to eq. 8.

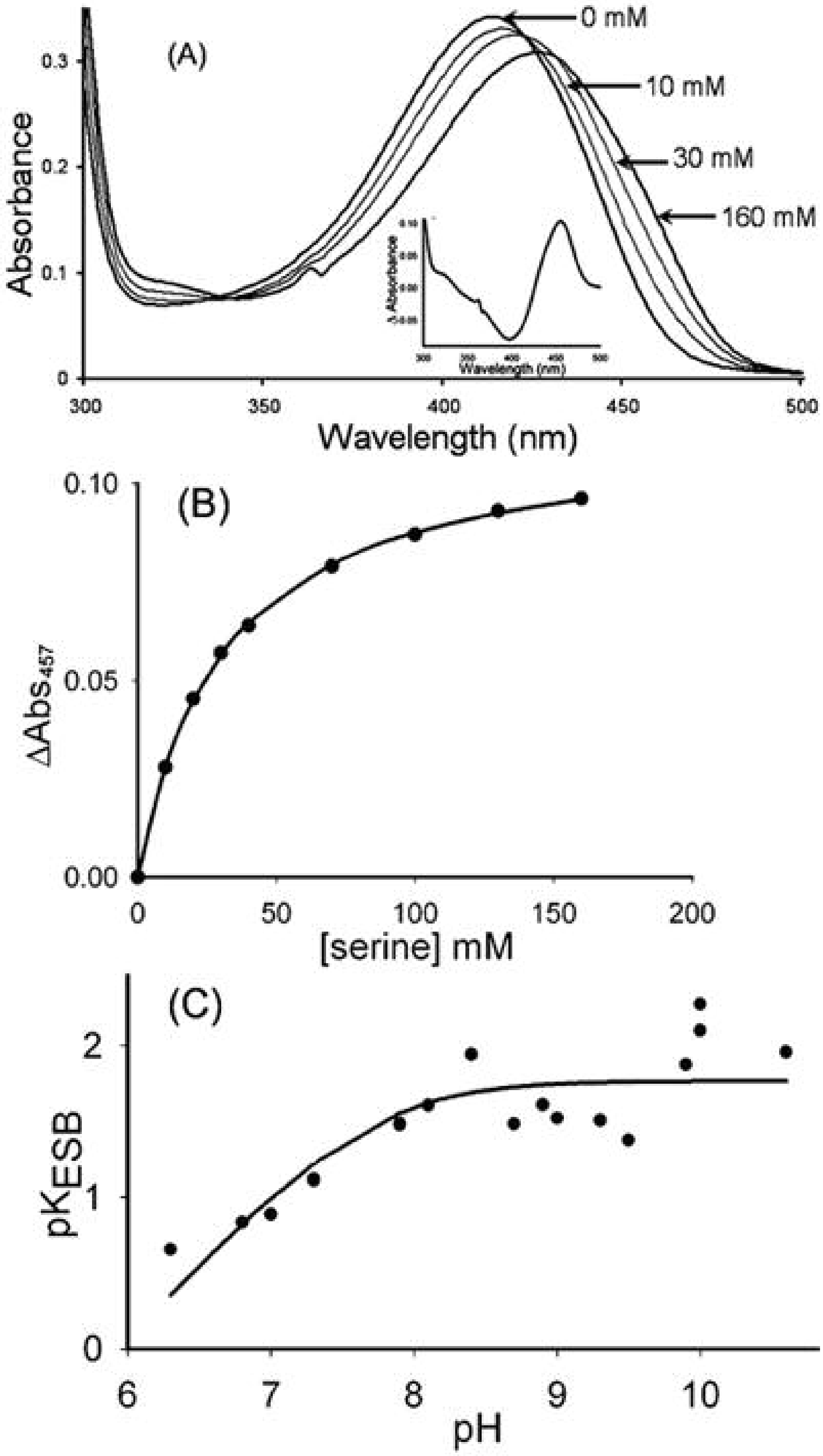
(A)
0 mM
10 mM
30 mM
160 mM
Absorbance
0.3
0.2
0.1
0
300
350
400
450
500
Wavelength (nm)
Δ Absorbance
0.10
0.05
0.00
-0.05
300
350
400
450
500
Wavelength (nm)
(B)
ΔAbs457
0.10
0.05
0.00
0
50
100
150
200
[serine] mM
(C)
pKESB
2
1
0
6
7
8
9
10
pH

α-aminoacrylate intermediate in the steady-state.

OAS:Acetate Lyase Activity. Time-dependent absorbance spectra were collected to monitor the disappearance of the α-aminoacrylate intermediate at 472 nm and the appearance of the free enzyme at 414 nm as a function of pH. The α-aminoacrylate intermediate was formed by mixing equimolar amounts of enzyme and OAS. The 472 nm band disappears with time in a first-order process Fig. 17A, indicating the presence of an OAS/acetate lyase activity in which the product of the reaction is free enzyme, pyruvate, and ammonia as was observed with the OASS-A isozyme (*60*). A plot of log k_{obs} versus pH (Fig. 17B) has a limiting slope of +1 and yields an average pK_a of 8.9 ± 0.9 on the acid side. At low pH, the rate is pH-independent and increases with pH.

Rapid-Scanning-Stopped-Flow Studies. RSSF measurements were carried out to obtain information on the identity and rates of appearance and decomposition of transients in the pre-steady-state. Kinetic parameters for the formation of the α-aminoacrylate intermediate for the first half of the OASS-B reaction were obtained as a function of pH with free enzyme reacted with different concentrations of OAS and varying pH (5.5-7.5). In Fig. 18A, spectra 1 and 9 are the absorbance spectra of the internal Schiff base and α-aminoacrylate intermediate, respectively. The spectra exhibit two clear isosbestic points, which suggest that the internal Schiff base (E) (λ_{max} at 414 nm) is converted to the α-aminoacrylate intermediate with two tautomeric forms with λ_{max} at 325 and 472 nm. The rates observed at 414 and 472 nm are identical, Fig. 18B, suggesting that there is no additional detectable intermediate between the two forms of the enzyme under the conditions used. The first order rate constants (k_{obs}) measured at different OAS concentrations did not reach maximum, Fig. 18C, and data were fitted to

Figure 17. A) Absorbance spectra of the decay of the α-aminoacrylate intermediate (AA, λ_{max} 325 and 472 nm) to free enzyme (E, λ_{max} 414 nm) ammonia, and pyruvate at pH of 8.9. The spectra are labeled according to the enzyme species. Total time is 3.5 min with first order rate of $(1.2 \pm 0.1)\text{x}10^{-2}$ s^{-1} measured at 414 nm and $(9.5 \pm 1.0)\text{x}10^{-3}$ s^{-1} measured at 472 nm. B) A plot of the pH-dependence of the decay of the α-aminoacrylate intermediate. Points are experimental values, while the curve is theoretical based on the fit to eq. 8. The curve has a limiting slope of +1 on the acid side with a pK_a value of 8.9 ± 0.9.

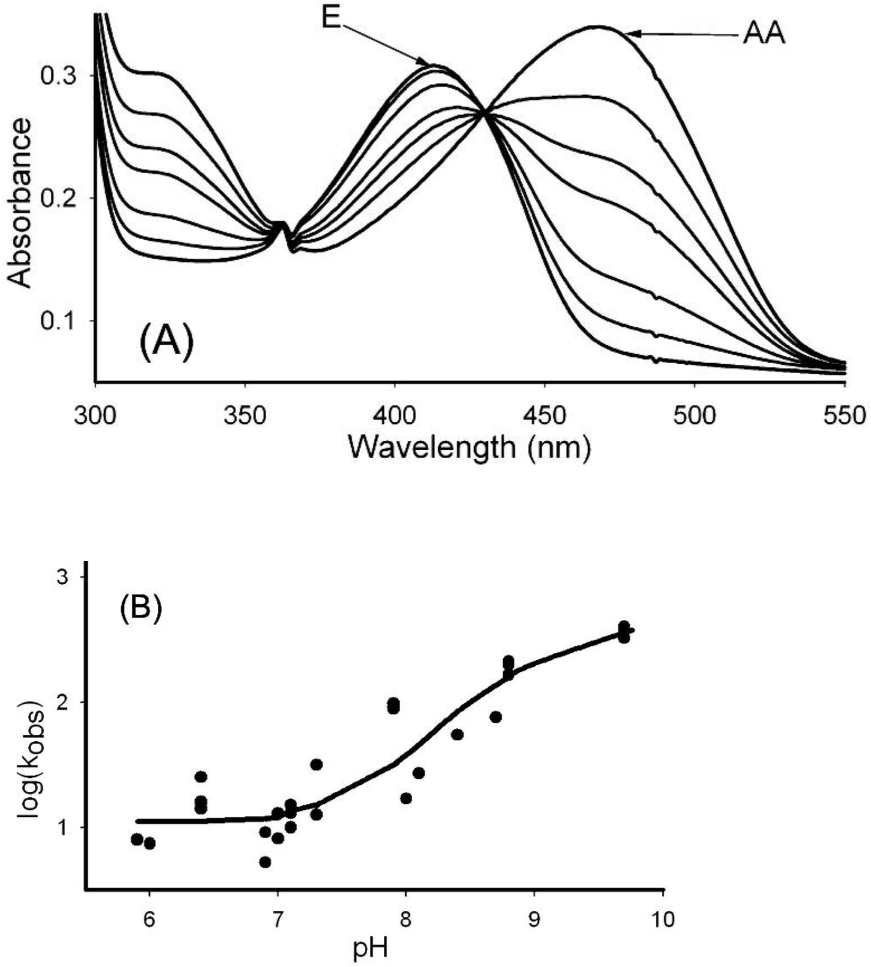
E
AA
0.3
0.2
0.1
Absorbance
(A)
300
350
400
450
500
550
Wavelength (nm)
3
2
1
(B)
log(k_obs)
6
7
8
9
10
pH

Figure 18. Rapid-scanning-stopped-flow spectra obtained upon reaction of OASS-B and OAS at pH 6.3. A) Spectrum 1 represent free enzyme and spectrum 9 represent α-aminoacrylate intermediate. The time between spectra is 0.6 s. The concentration of OASS-B is 10 μM and OAS is 0.1 mM. The reaction was carried out in 200 mM Mes buffer at pH 6.3. B) The rate of the disappearance of free enzyme measured at 414 nm (2.8 ± 0.1 s^{-1}) is identical to the rate of appearance of the α-aminoacrylate intermediate measured at 472 nm. C) A plot of the first order rate constant (k_{obs}) vs. OAS concentration: The slope of the line represents the second order rate constant (k_{obs}/K_{ESB}). D) A plot of $\log(k_{max}/K_{ESB})$ vs. pH: The points are experimental values, and the curve is drawn by eye. The curve has limiting slope of +2 on the acid side with an estimated pK_a >6.5.

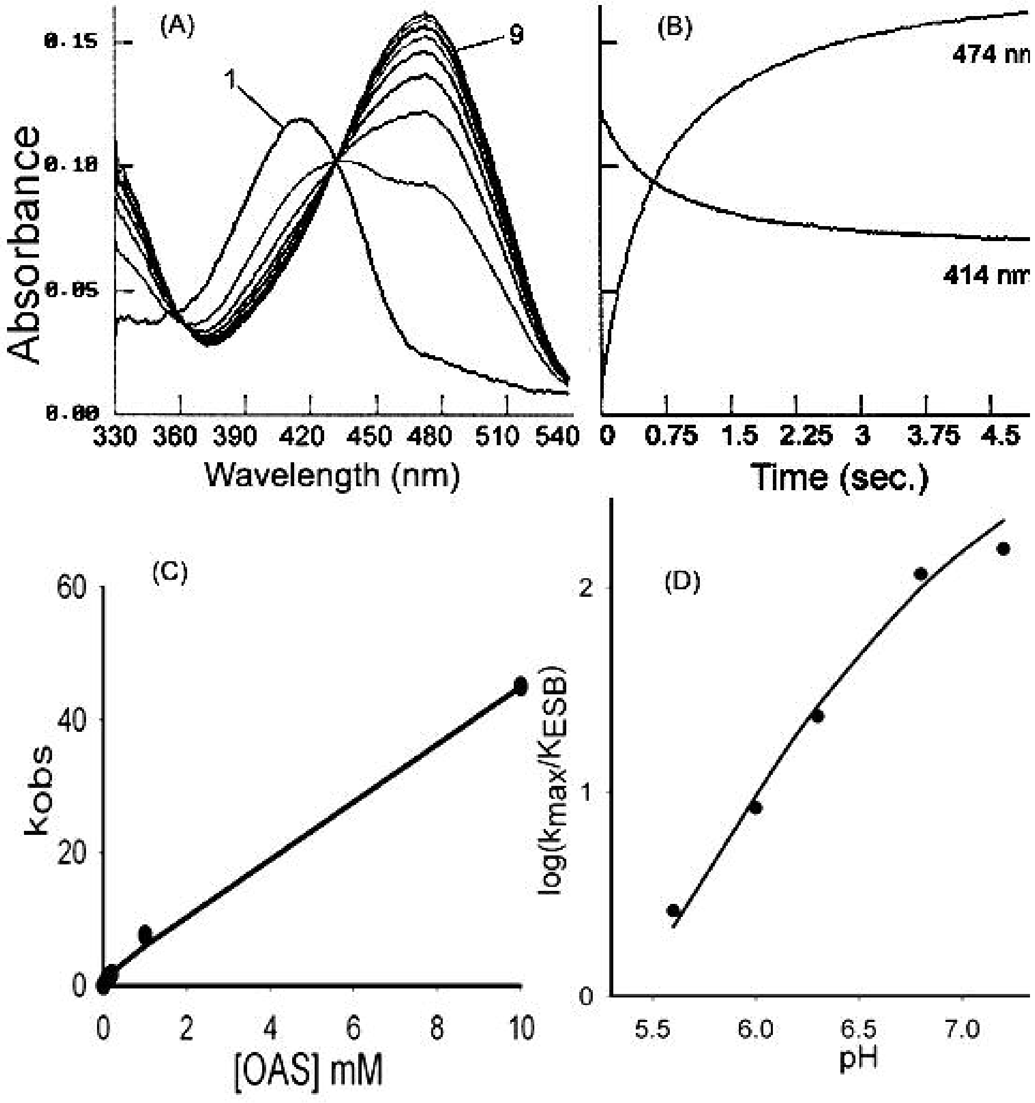
(A)
Absorbance
0.15
0.10
0.05
0.00
1
9
330
360
390
420
450
480
510
540
Wavelength (nm)
(B)
474 nm
414 nm
0
0.75
1.5
2.25
3
3.75
4.5
Time (sec.)
(C)
kobs
60
40
20
0
0
2
4
6
8
10
[OAS] mM
(D)
log(kmax/KESB)
2
1
0
5.5
6.0
6.5
7.0
pH

the equation for a straight line, to obtain the second order rate constant (k_{max}/K_{ESB}) as the slope. A plot of log k_{max}/K_{ESB} versus pH, Fig. 18D, has a limiting slope of +2. Since the pH was not high enough to reach the pH-independent value due to the fast rate of the first half-reaction at high pH values, the average pK_a for the groups titrated was not calculated.

The RSSF spectra of the L-serine or L-cysteine external Schiff base show shift in λ_{max} form 414 to 422 nm in the dead time of the instrument of 4 ms (data no shown). No formation of the α-aminoacrylate intermediate was observed at λ_{max} of 472 nm at all the concentrations tested as a function of pH.

Fluorescence Studies. The emission spectrum of free OASS-B at pH 6.5, with excitation at 298 nm, exhibits a maximum centered at 335 nm and a broad shoulder extending form 425 to >500 nm, Fig. 19A. At pH 9, an increase in fluorescence is shown by the difference spectra Fig 19A inset, with bands centered at 350, 490, and 520 nm. Addition of OAS to form the α-aminoacrylate intermediate results in a decrease in the intensity of the 335 and 425 nm peaks accompanied with the appearance of a low intensity band at 550 nm, Fig. 19B. The difference in the enzyme and the α-aminoacrylate fluorescence spectra Fig 19B inset, show a major decrease in intensity centered at 350, and a minor increase in intensity centered at 550 nm. The acetate emission spectrum is similar to that of free enzyme with theexception that the intensity at 335 nm is lower with minor enhancement at 425 nm, Fig. 20A.

L-cysteine and L-serine external Schiff base emission spectra show decreases in the intensity of the 335 and 425 nm peaks accompanied with the appearance of a band at

Figure 19. Fluorescence emission spectra of OASS-B in the absence and presence of ligands. A) Spectrum for free enzyme at pH 6.5 (100 mM Mes) and 9 (100 mM Ches). Inset. Difference for pH 6.5 and 9 spectra. B) Spectrum for free enzyme at pH 6.5, and that after addition of 10 mM OAS. Inset. Difference for free enzyme and α-aminoacrylate Schiff base spectra. Excitation was 298 nm and emission intensity was measured form 300 to 600 nm as described in methods. The temperature was maintained at 25˚C.

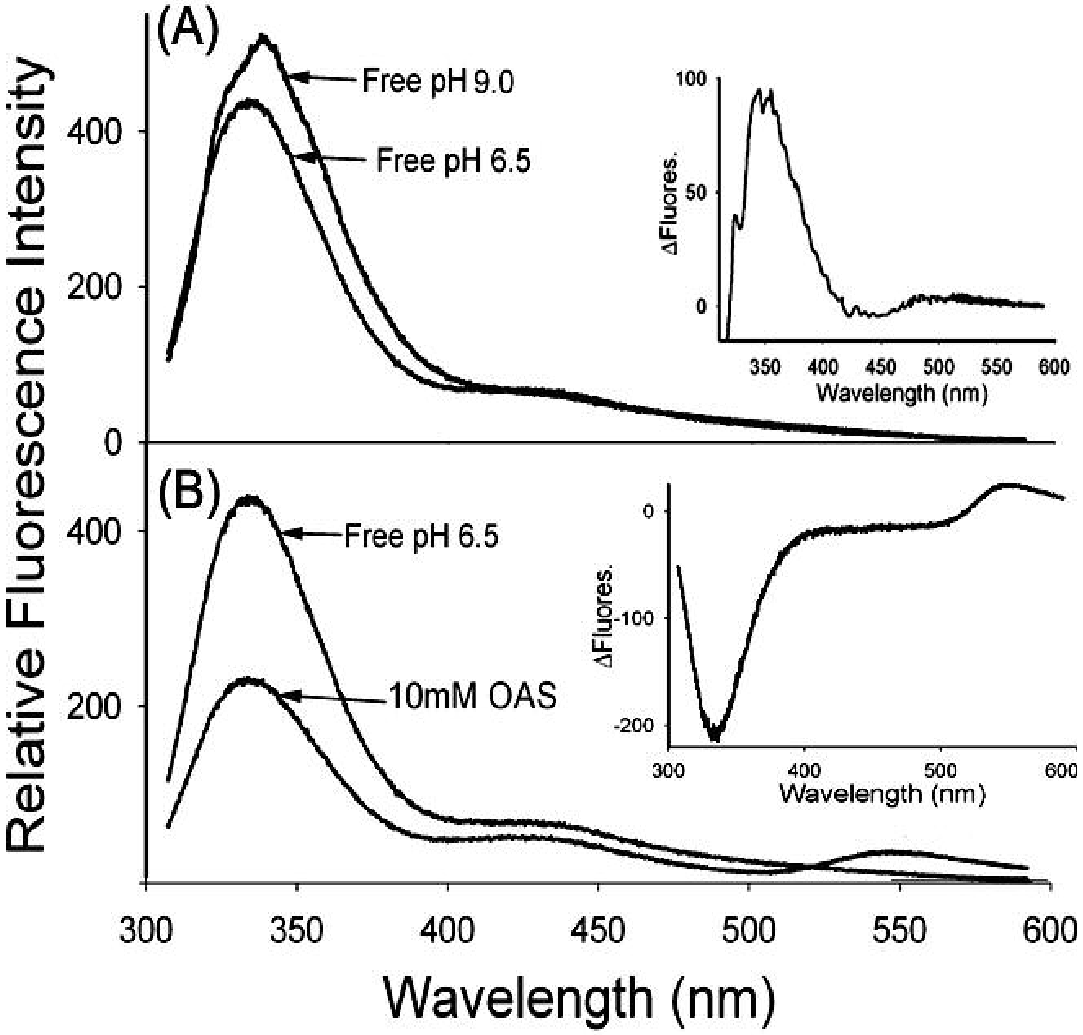
(A)
Free pH 9.0
Free pH 6.5
Relative Fluorescence Intensity
400
200
0
ΔFluores.
100
50
0
350 400 450 500 550 600
Wavelength (nm)
(B)
Free pH 6.5
10mM OAS
400
200
ΔFluores.
0
-100
-200
300 400 500 600
Wavelength (nm)
300 350 400 450 500 550 600
Wavelength (nm)

Figure 20. Fluorescence emission spectra of OASS-B in the absence and presence of ligands. A) Spectrum for free enzyme at pH 9 in the absence and presence of acetate, serine and cysteine as indicated. B) The fluorescence spectra difference of enzyme in the presence and absence of 50 mM cysteine. C) The fluorescence spectra difference of enzyme in the presence and absence of 100 mM serine. Excitation was 298 nm and emission intensity was measured form 300 to 600 nm as described in methods. The temperature was maintained at 25˚C.

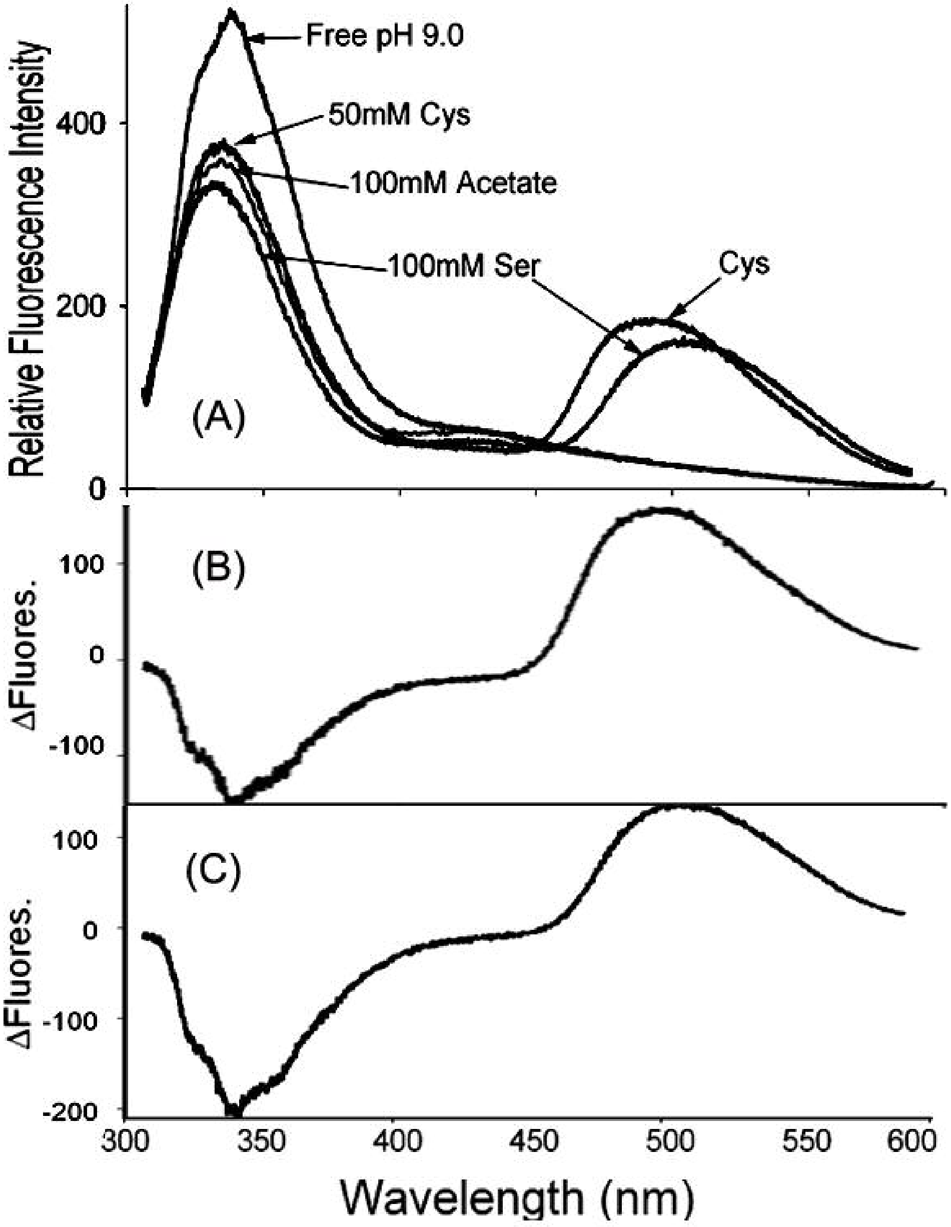
Free pH 9.0
50mM Cys
100mM Acetate
100mM Ser
Cys
(A)
Relative Fluorescence Intensity
400
200
0
(B)
ΔFluores.
100
0
-100
(C)
ΔFluores.
100
0
-100
-200
300
350
400
450
500
550
600
Wavelength (nm)

475-500 nm, Fig 20A. The difference fluorescence spectra of enzyme in the absence and presence of L-serine and L-cysteine, Fig 20B,C, show decrease in intensity around 340nm, and increase in intensity for bands around 390 and 500 nm.

Excitation spectra collected with the emission monochromator fixed at 425 nm for free OASS-B, the α-aminoacrylate intermediate, and L-serine external Schiff base show one major band centered at 317 nm and a shoulder at 290 nm, Fig. 21A, B, D. In the case of L-cysteine external Schiff base, a lower intensity 317 nm band was observed with a more prominent shoulder at 290 nm, Fig. 21C. The excitation spectra with emission at 500 nm (Fig. 22) and 550 nm (data not shown) are identical. All enzyme spectra collected show a major peak at 430 nm and a shoulder at 385 nm, with the intensity of the 430 nm peak differ depending on the enzyme form obtained. The L-serine external Schiff base spectrum exhibit a shift in the 430 nm peak to higher wavelength.

DISCUSSION

pH Dependence of the UV-Vis Spectra. The absorbance spectrum of free OASS-B is characterized by a band at 414 nm, which attribute to the internal Schiff base formed between PLP and Lys-42 as was observed for the A-isozyme, Scheme 10, Chapter II (*60*). The free enzyme spectrum is pH-dependent. At low pH, the enolimine tautomer (λ_{max} 325 nm) of the internal Schiff base predominates, while at high pH, the ketoenamine tautomer (λ_{max} 414 nm) dominates, Scheme 12. The reaction of OAS with OASS-B leads to the appearance of two bands centered at 325 and 472 nm, attributed to the enolimine and ketoenamine tautomers of the α-aminoacrylate Schiff base, Scheme 12

Figure 21. Fluorescence excitation spectra of OASS-B in the absence and presence of ligands. A) Free enzyme at ph 6.5 and 9. B) Absence and presence of 2 mM OAS at pH 6.5. C) Absence and presence of 50 mM L-cysteine at pH 9. D) Absence and presence of 100 mM serine at pH 9.0. The excitation spectra were recorded from 250-500 nm, wih the emission monochromator fixed at 425 nm. The temperature was maintained at 25˚C.

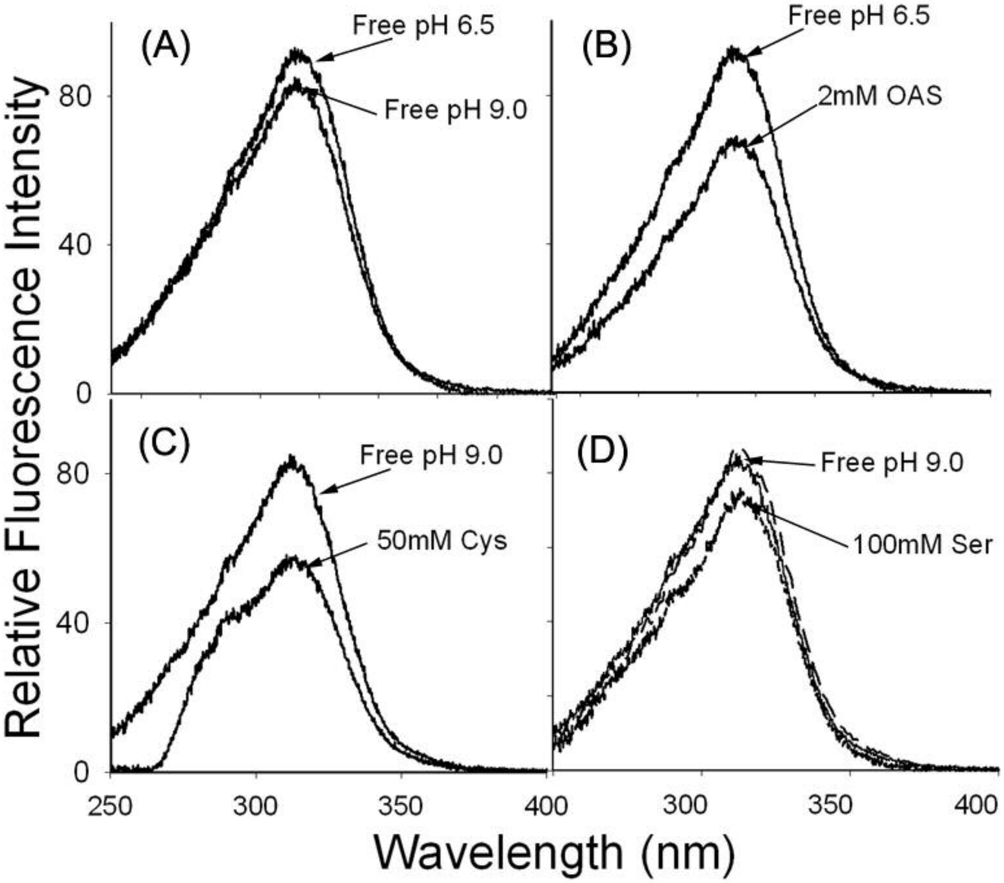
(A)
Free pH 6.5
Free pH 9.0
(B)
Free pH 6.5
2mM OAS
(C)
Free pH 9.0
50mM Cys
(D)
Free pH 9.0
100mM Ser
Relative Fluorescence Intensity
0
40
80
250
300
350
400
Wavelength (nm)

Figure 22. Fluorescence excitation spectra of OASS-B in the absence and presence of ligands as indicated on the figure. The excitation spectrum was recorded from 250-500 with the emission monochromator fixed at 500 nm. The temperature was maintained at 25˚C.

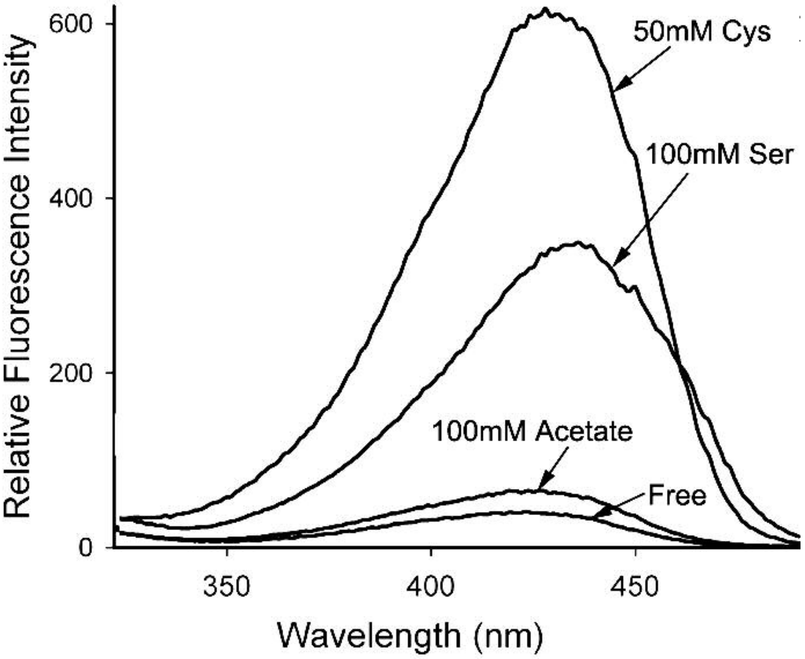

Relative Fluorescence Intensity
600
400
200
0
350
400
450
Wavelength (nm)
50mM Cys
100mM Ser
100mM Acetate
Free

(*16,60*). At low pH, the α-aminoacrylate Schiff base favors the ketoenamine tautomer (λ_{max} 472 nm), and at high pH, the enolimine tautomer (λ_{max} 325 nm) is formed. Thus, it appears the free enzyme active site, at low pH, is somewhat non-polar, and the uncharged enolimine tautomer is formed, while the active site is more polar at high pH. On the other hand, the situation is opposite for the α-aminoacrylate intermediate. At low pH, the α-aminoacrylate intermediate has a polar active site environment and favors the charged ketoenamine tautomer, while at high pH, the site is more non-polar.

Scheme 12.

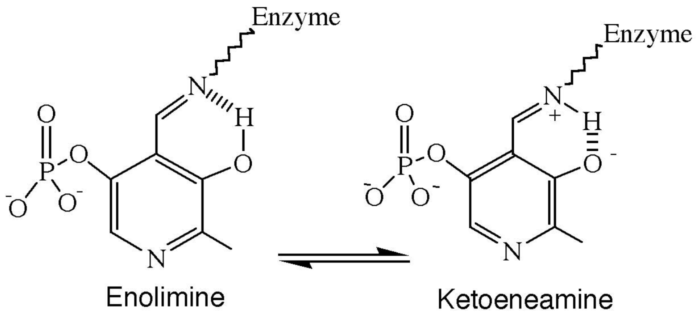

The difference in enzyme spectra upon pH titration is an indication of titrating enzyme group in which the enzyme active site favors one tautomer of the Schiff base over the other depending on the polar environment of the active site. In the case of free enzyme, a cationic enzyme group has been titrated a long the pH range in which the group is uncharged at low pH (enolimine tautomer is favored), and at high pH the, the same enzyme group is charged (ketoenamine tautomer is favored). In the case of the α-aminoacrylate intermediate, a carboxylic enzyme group has been titrated; therefore, the active site is charged at low pH and uncharged at high pH. This behavior was not observed with the A-isozyme, which shows pH-independence upon titration of free enzyme and the α-aminoacrylate external Schiff base.

Amino Acid Titration Spectra. The addition of L-cysteine or L-serine to OASS-B (λ_{max} at 414 nm) results in the formation of two new absorption bands (λ_{max} at 325 and 422 nm) suggesting the establishment of an equilibrium between two tautomeric forms of the external Schiff base, Scheme 10, Chapter III. Absorbance at 472 nm was not observed, indicating that the α-aminoacrylate intermediate is not formed in steady-state, as for the A-isozyme. In addition, the RSSF spectra with both amino acid substrates did not show the formation of the α-aminoacrylate intermediate. In the case of the A-isozyme, the α-aminoacrylate intermediate is formed with cysteine but it disappear very rapidly as another cysteine residue attack the α-aminoacrylate intermediate to form the cystathionine complex (*68*). The pH dependence of the dissociation constants (K_{ESB}) for both amino acid substrates exhibit a slope of +1 and yield a pK_a values of 6.9 (L-cysteine) and 7.7 (L-serine) on the acid side of the profile for a group that is required to be unprotonated, but its function is unknown.

In the B-isozyme, the pK_a of the amino acid α-amino group is not observed for either amino acid pH profiles. The α-amino group is required to be unprotonated to facilitate attack on the internal Schiff base of the enzyme to form the external Schiff base form of the enzyme. The pK_a should be observed on the acid side of the profile with a pK_a value >8. The pH-independence of the K_{ESB} is not understood at this point, and requires additional experiments to clarify groups that involve in catalysis and/or binding of substrates.

OAS/Deacetylase Activity for the α-aminoacrylate Intermediate. The addition of OAS to the free enzyme results in the formation of the α-aminoacrylate intermediate and releases acetate. If the nucleophilic substrate that catalyzes the second half-reaction was not available, the α-aminoacrylate intermediate decomposes back to free enzyme, pyruvate and ammonia via transimination by the active site lysine that is initially found in Schiff base linkage with PLP (*60*). The free α-aminoacrylate nonenzymically tautomerizes to iminopyruvate, which is then hydrolyzed to pyruvate and ammonia (*60*). The decomposition rate of the α-aminoacrylate intermediate increases as function of pH, as the active site lysine is deprotonated at high pH to facilitate the transimination reaction. The pH profile obtained Fig. 17B, is pH-independent at low pH values, suggesting that some other process that also regenerates free enzyme is observed once the rate of the lyase has decreased by a factor of 20. Since the rate is pH-independent an acid-base mechanism can be ruled out. It is possible that nucleophilic attack of a water molecule on C_β of the α-aminoacrylate intermediate occurs, forming the serine external Schiff base (*72*).

Rapid-Scanning Stopped-Flow. The addition of OAS to free enzyme results in the disappearance of the 414 nm band and the appearance of 325 and 472 nm bands, which are characteristics of the α-aminoacrylate intermediate. The pre-steady state data do not show the formation of any intermediates along the first half-reaction and the two clear isosbestic points observed in the RSSF spectra indicate the conversion of the two species. The pH dependence of the RSSF spectra of the first half-reaction has a slope of +2, which shows the requirement for two groups that must be unprotonated for reaction. Since the rate of formation of the α-aminoacrylate intermediate is very fast, limited data were collected at pH <7.0. As a result, the pK_a values of the groups observed were not calculated. If, as for the A-isozyme, formation of the α-aminoacrylate intermediate is slow, one of the groups observed in the pH profile is likely Lys-42, which found in Schiff base linkage with PLP. A detailed analysis requires additional experimental evidence.

Fluorescence Spectra. The emission spectrum of the holo-enzyme(no substrate bound to enzyme only cofactor, PLP) exciting at 298 nm exhibits a peak centered at 335 nm, which is typical for tryptophan, which emit maximally at 350 nm in aqueous environment, and at 325 nm in a non-polar environment (*89*). The OASS-B isozyme has three tryptophan residues (Trp-27, 158, and 211) in which the 335 nm emission band is for tryptophan residues that are partially exposed to solvent. Another emission band was observed at 425 nm, which attribute to a tautomer of the internal Schiff base that absorb maximally at 325 nm, likely the enolimine tautomer of the internal Schiff base that is stable in a non-polar environment, Scheme 12 (*90*).

The addition of L-cysteine or L-serine to free OASS-B results in formation of the external Schiff base, showing a major peak at shorter wavelength (centered at 335 nm) due to direct tryptophan emission, and a shoulder at longer wavelength centered at 425 nm attributed to the PLP enolimine tautomer that absorbs maximally at 325 nm (*90*). The 490 nm emission peak observed with the internal Schiff base of the A-isozyme upon excitation at 298 nm has been attributed to the emission of the ketoenamine tautomer as a result of energy transfer from a tryptophan to the cofactor (*90-92*). An enhancement of the long wavelength emission is observed upon formation of the external Schiff base as a result of conformational change that optimizes the orientation of the tryptophan with respect to the cofactor. The Förster energy transfer results from overlap of the tryptophan emission band with the ketoenamine absorption band. A similar triplet-singlet energy transfer might occur with the B-isozyme, as indicated by the emission band centered at 490 nm (*93*). The 550 nm peak observed in the emission spectra is a characteristic of the PLP Schiff base that is exposed to aqueous solvent, which reflects a fuller exposure of the PLP Schiff base to water molecules (*91).* In PLP-model compounds, the 550 nm emission band has been attributed to a dipolar Schiff base formed by imine proton dissociation in the excited state (*91, 92*), where the 550 nm emission band suggests a more stable ketoenamine species, Scheme 12.

A significant quenching of the tryptophan fluorescence emission maximum of OAS- B is observed in the presence of OAS, i.e., the formation of the α-aminoacrylate external Schiff base, may be due to an exposure of one or more tryptophan residues to solvent as a result of conformational change. A 550 nm emission band was observed upon formation of the α-aminoacrylate external Schiff base suggesting a more stable ketoenamine tautomer and a more polar environment in agreement with the steady-state absorption spectrum obtained at low pH, Fig. 14, spectrum 2. Acetate enhances the long wavelength emission in the case of the A-isozyme, presumably because of occupying the α-carboxylate site of the external Schiff base, and causing a change in the orientation of the cofactor (*93*). This is not observed in the case of the B-isozyme in the presence of 100 mM acetate, Fig. 20A.

From the excitation spectra of OASS-B, the emission peak at 425 nm is produced by excitation at 317 nm and 290 nm. The 290 nm absorbing band is that of tryptophan residues of the protein matrix, and the 317 nm absorbing band is that of the enolimine tautomer of the internal Schiff base (*94*). Emission peaks at 490 and 550 nm are produced upon excitation at 385 and 430 nm, which represent bands for different cofactor tautomers. In conclusion, ligand binding affects the emission spectrum at longer wavelength with minor changes in the shorter wavelength region.

APPENDIX A

A Three Dimensional Homology Model of the *O*-Acetylserine Sulfhydrylase-B

OASS-B was over-expressed, as discussed in Chapter III, and purified as the N-terminal His-tagged enzyme. The enzyme has been crystallized in the lab of Dr. Peter Burkhard at the University of Connecticut and the structure is being solved. To date, no 3D structure is available for OASS-B, and a theoretical model of the enzyme was built with the help of Dr. Tim Mather from the Oklahoma Medical Research Foundation.

Construction of the Model. Homology comparative modeling was used to build the model of OASS-B using three homology templates (OASS-A, cystathionine β-synthase (CBS), and the β-subunit of tryptophan synthase). The amino acid sequence alignment with OASS-B shows a 40% identity and 71% homology to OASS-A, 35% identity to CBS, and 19% identity to the β-subunit of tryptophan synthase, Fig. A1. As a result, the A-isozyme was used as the template to build the theoretical model of OASS-B, and CBS and the β-subunit of tryptophan synthase were used as a reference to assist in building the B-isozyme model.

Alignment of the 3D structures of the three homology templates yields structurally conserved regions (SCRs; represent the α-helices and β-sheets of the structures) and variable regions (VRs; represent the loop regions of the structures), Fig. A2. The OASS-A template was used as the backbone and its amino acid residues were mutated to match the OASS-B amino acid sequence. The SCRs are conserved in the three homology templates, and all amino acid additions and deletions were done in the VRs. The conformations in the SCR of the model are the most reliable since they contain all the conserved regions. The model was then introduced into an energy minimization program to relieve steric contacts and to optimize the bond angles and torsional angles. Main and Discover 3 were the two programs used for energy minimization.

Figure A1. Multiple amino acid sequence alignment of OASS-B, OASS-A, CBS, and the β-subunit of tryptophan synthase. The amino acid sequence alignment of OASS-B shows a 40% identity and 71% homology to OASS-A, 35% identity to CBS, and 19% identity to the β-subunit of tryptophan synthase

```
OASS-B          ------------------------------------------------------------
OASS-A          ------------------------------------------------------------
CBS             MPSETPQAEVGPTGCPHRSGPHSAKGSLEKGSPEDKEAKEPLWIRPDAPSRCTWQLGRPA 60
βTry-Syn        -----------------------MTTLLNPYFGEFGGMYVPQILMPALN---------QL 28


OASS-B           ------------MNTLEQ----TIGNTPLVKLQRLGPDNGS--EIWVKLEGNNPAGSVKD 42
OASS-A           ------------MSKIYEDNSLTIGHTPLVRLNRIG--NG---RILAKVESRNPSFSVKC 43
CBS              SESPHHHTAPAKSPKILPDILKKIGDTPMVRINKIGKKFGLKCELLAKCEFFNAGGSVKD120
βTry-Syn         EEAFVSAQKDPEFQAQFADLLKNYAGRPTALTKCQNITAGTRTTLYLKREDLLHGGAHKT 88
                                      . .  * .  :  .   *    :  * *    . : *

OASS-B          RAALSMIVEAEKRGEIKPGDVLIEATSGNTGIALAMIAALKGYRMKLLMPDNMSQERRA- 101
OASS-A          RIGANMIWDAEKRGVLKPGVELVEPTSGNTGIALAYVAAARGYKLTLTMPETMSIERRK- 102
CBS             RISLRMIEDAERDGTLKPGDTIIEPTSGNTGIGLALAAAVRGYRCIIVMPEKMSSEKVD- 179
βTry-Syn        NQVLGQALLAKRMG---KSEIIAETGAGQHGVASALASALLGLKCRIYMGAKDVERQSPN 145
                .        *:: *    .  : *. :*: *:. *  :*  * :  : *  .   .:

OASS-B          --AMRAYGAELILVTK-EQGMEGARDLALAMS--ERGEGK--LLDQFNNPDNP------- 147
OASS-A          --LLKALGANLVLTEG-AKGMKGAIQKAEEIV--ASDPQKYLLLQQFSNPANP------- 150
CBS             --VLRALGAEIVRTPT-NARFDSPESHVGVAWRLKNEIPNSHILDQYRNASNP------- 229
βTry-Syn        VFRMRLMGAEVIPVHSGSATLKDACNEALRDWSGSYETAHYMLGTAAGPHPYPTIVREFQ 205
                   ::  **::: .      :... . .           :  :         *

OASS-B          YAHYTTTGPEIWRQTSGRITHFVSSMGTTGTITGVSRFLR--EQEKPVTIVGLQPEE--- 202
OASS-A          EIHEKTTGPEIWEDTDGQVDVFISGVGTGGTLTGVTRYIKGTKGKTDLITVAVEPTDSPV 210
CBS             LAHYDTTADEILQQCDGKLDMLVASVGTGGTITGIARKLK--EKCPGCRIIGVDPEGS-I 286
βTry-Syn        RMIGEETKAQILDKEGRLPDAVIACVGGGSNAIGMFADFIN---DTSVGLIGVEPGGHGI 262
                      *  :*  . .     .:: :*  ..  *:   :           :.::*

OASS-B          ------GSSI-PG---IRRWPAEYMP-------------------------GIFNASLVD 227
OASS-A          IAQALAGEEIKPGPHKIQGIGAGFIP-------------------------GNLDLKLID 245
CBS             LAEPEELNQTEQTTYEVEGIGYDFIP-------------------------TVLDRTVVD 321
βTry-Syn        ETGEHGAPLKHGRVGIYFGMKAPMMQTADGQIEESYSISAGLDFPSVGPQHAYLNSIGRA 322
                                        :                            ::

OASS-B          EVLDIHQNDAENTMRELAVREGIFCGVSSGGAVAGALRVAR--ATPGAIVVAIICDRGDR 285
OASS-A          KVVGITNEEAISTARRLMEEEGILAGISSGAAVAAALKLQEDESFTNKNIVVILPSSGER 305
CBS             KWFKSNDEEAFTFARMLIAQEGLLCGGSAGSTVAVAVKAAQ-ELQEGQRCVVILPDSVRN 380
βTry-Syn        DYVSITDDEALEAFKTLCRHEGIIPALESSHALAHALKMMREQPEKEQLLVVNLSGRGDK 382
                . .   :::*    : *  .**:: . .:. ::* *::  .         *. : .   .

OASS-B          YLSTGVFGEEHFSQGAGI------------------------------------------ 303
OASS-A          YLSTALFADLFTEKELQQ------------------------------------------ 323
CBS             YMTKFLSDRWMLQKGFLKEEDLTEKKPWWWHLRVQELGLSAPLTVLPTITCGHTIEILRE 440
βTry-Syn        --DIFTVHDILKARGEI------------------------------------------- 397
                             :

OASS-B          ------------------------------------------------------------
OASS-A          ------------------------------------------------------------
CBS             KGFDQAPVVDEAGVILGMVTLGNMLSSLLAGKVQPSDQVGKVIYKQFKQIRLTDTLGRLS 500
βTry-Sy         ------------------------------------------------------------
```

Figure A2. Overlay of the monomer of OASS-A (red for α-helix, aquamarine for β-sheet, and white for loops), and CBS (orange) in ribbon representation. PLP is shown as a space-filling model in the active site. Both enzymes are examples of a fold type II enzyme (*24*), where OASS-A has an overall fold that is similar to the CBS. Both enzymes are homodimeric with N- and C-terminal domains in each monomer. Each domain has an overall α/β fold with a central twisted β-sheet surrounded by α-helices. The C-terminal domain is identical in both structures. On the other hand, the N-terminal domain, where all the conformational changes take place upon binding of substrate, does not align very well as in the C-terminal domain. The α-helices and β-sheets are the SCRs and the loop regions are the VRs in both structures. The figure was prepared using DS Viewer 5.0 from Accelrys.

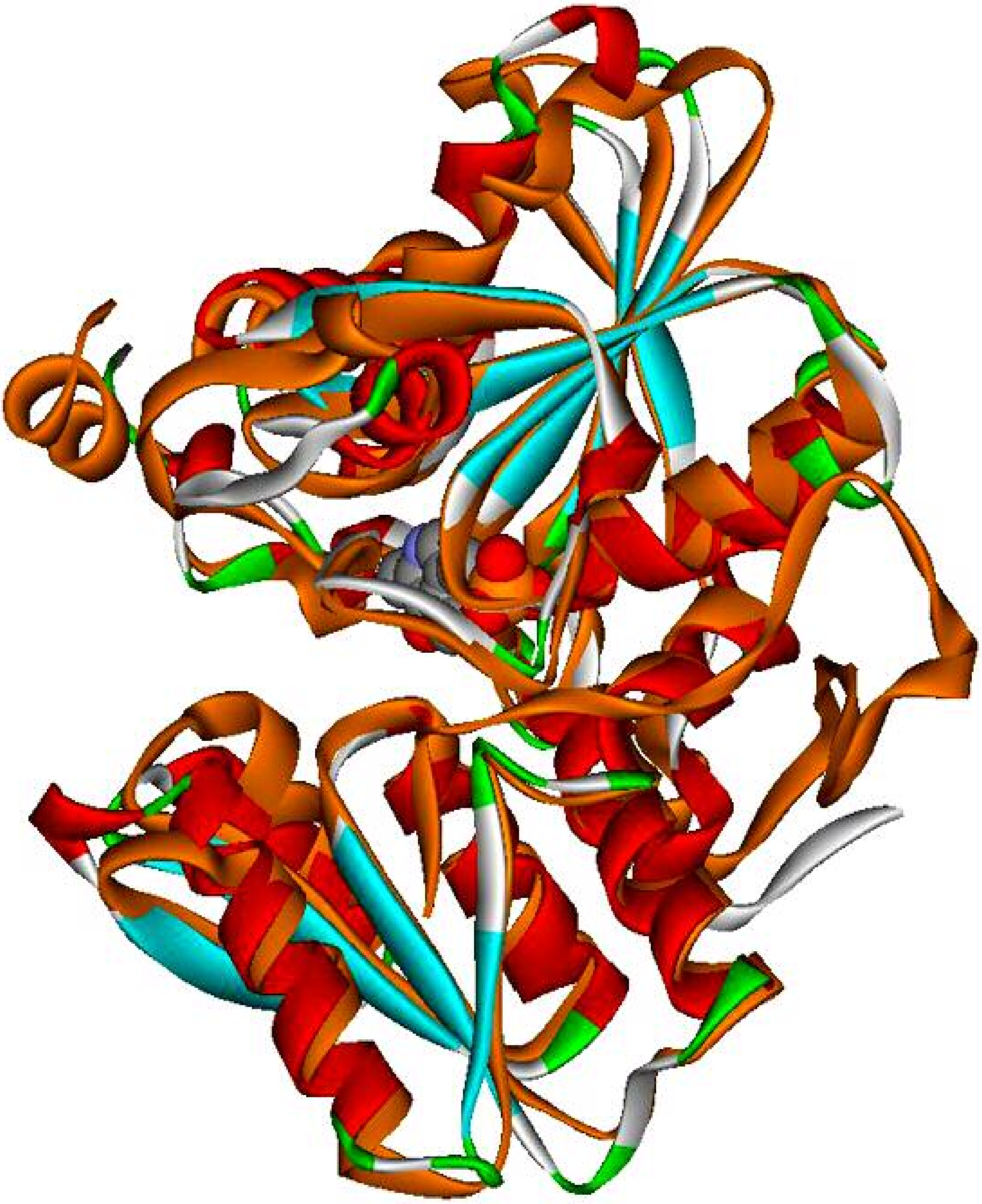

Homology Model. The OASS-B model has an overall fold that is similar to the A-isozyme, with the exception that OASS-B is missing helix 8 (Fig A3 and A4), and with minor differences found in the loop regions. Both isozymes are examples of a fold type II enzyme (*24*), where OASS-B is a homodimer containing two domains per monomer with one PLP moiety bound between the two domains. Each domain is composed of an α/β fold with a central twisted β-sheet surrounded by α-helices, Fig. A4. The active site is located at the interface of the two domains, deep within the protein. Enzyme residues involved in substrate and PLP binding, catalysis, and proper orientation of substrate and cofactor are identical to those found in OASS-A.

The PLP cofactor of OASS-B is in Schiff base linkage with the ε-amino group of Lys-42, Fig. A5. The charge on the 5'-phosphate of PLP is partially neutralized by the dipole of helix 7, in the C-terminal domain, Fig. A4, and is anchored by H-bonds to main chain and side chain functional groups in the threonine loop, Fig. A5. The threonine loop is similar in both isozymes, but with T177 in OASS-B replacing G178 in OASS-A, Fig. A5. As a result, the interactions to neutralize the negative charge of the 5'-phosphate of PLP are the same in both isozymes. The phenolic O3' of PLP is within H-bonding distance to the amide nitrogen of an asparagine side chain (N71 in OASS-A and N72 in OASS-B) and the Schiff base nitrogen (K41 in OASS-A and K42 in OASS-B), Fig. A5. The asparagine residue is part of a loop structure called the asparagines loop, and along with a glutamine side chain (Q142 in OASS-A and Q141 in OASS-B) binds the substrate α-carboxylate group, Fig. A5. The dipole of helix 2 helps to neutralize charge of the substrate α-carboxylate and provide part of the driving force for closing the active site. The pyridine nitrogen of PLP is within H-bonding distance to a serine hydroxyl (S272 in

Figure A3. Topology diagram of OASS-A (left) and OASS-B (right). The B-isozyme has a fold similar to that of OASS-A, with the exception of the absence of helix 8.

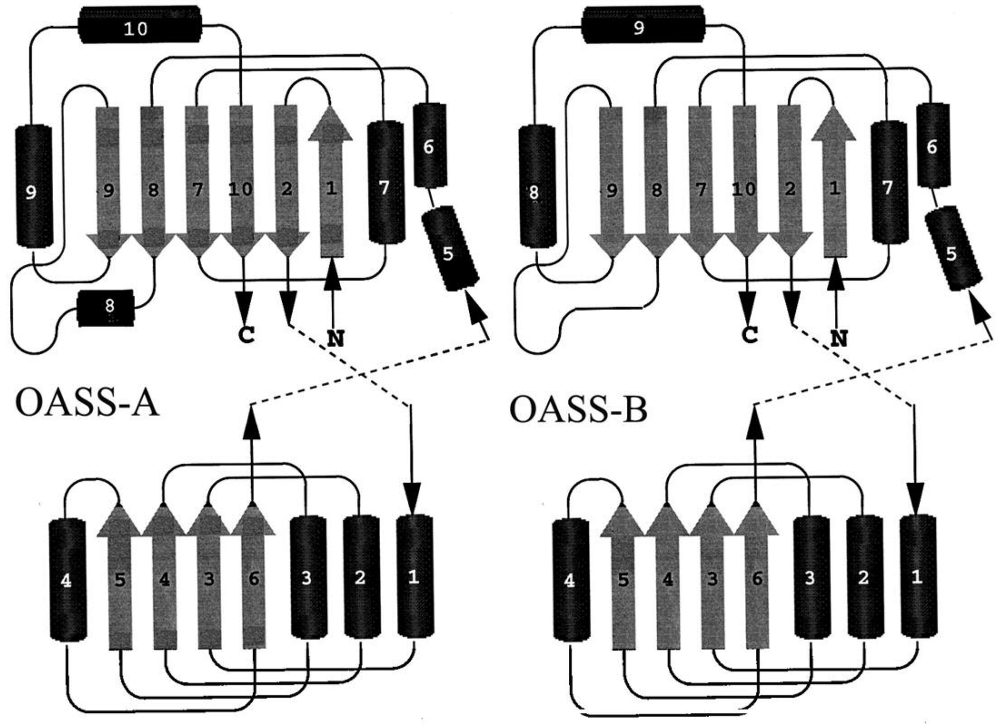
OASS-A
C
N
OASS-B
C
N

Figure A4. Ribbon representation of the structure of a monomer of the OASS-B model (right) and the monomer of OASS-A (left). PLP is in space-filling representation. The entry to the active site is on the left of the monomer. In OASS-B, β-strand 8 and α-helix 8 are not observed. α-Helix 8, observed in the A-isozyme, has been extended to a loop structure to accommodate the amino acid deletions introduced by the OASS-B model. β-strand 8 is present as a loop region and more energy minimization may be required to align it with its β-sheet. The dipole of helix 2 helps to neutralize charge of the substrate α-carboxylate and provides part of the driving force for closing the active site. The charge on the 5'-phosphate of PLP is partially neutralized by the dipole of helix 7, in the C-terminal domain. The pyridine nitrogen of PLP is in close proximity to the dipole of a helix (helix 10 in OASS-A and helix 9 in OASS-B). The figure was prepared using DS Viewer 5.0 from Accelrys.

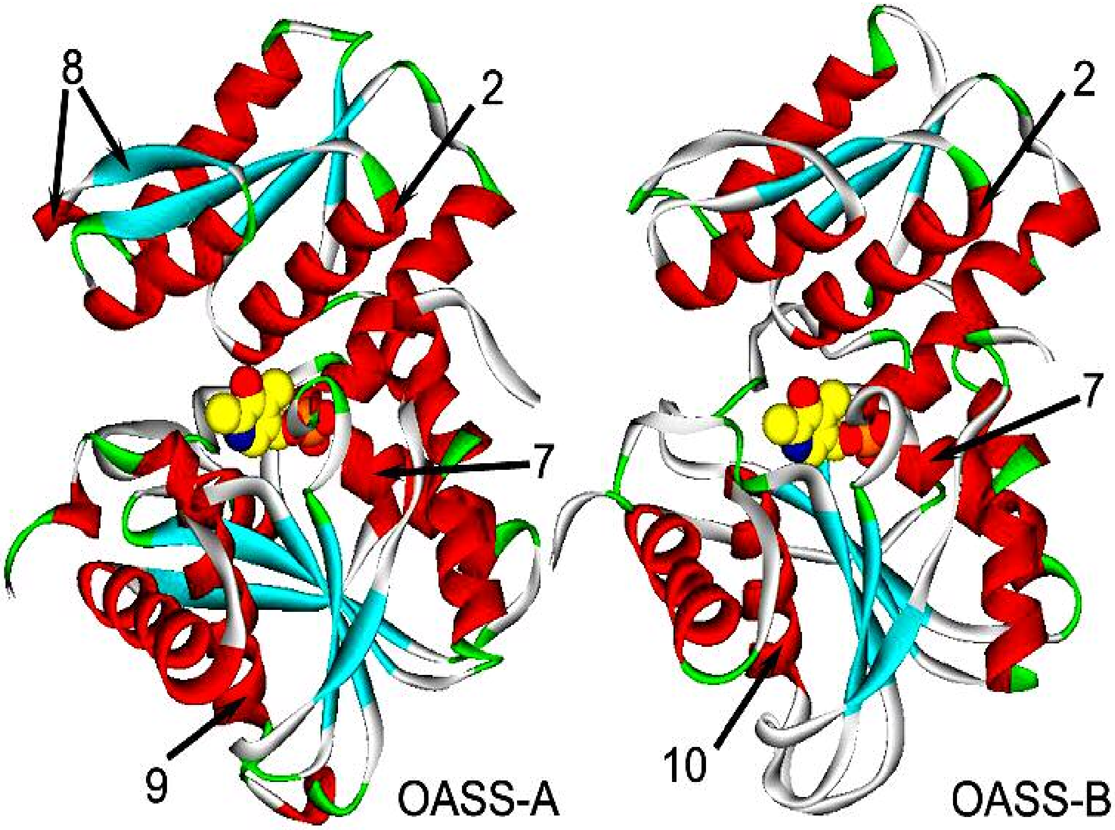
8
2
7
9
OASS-A
2
7
10
OASS-B

Figure A5. Stereo view looking into the active site of OASS-B (yellow) overlayed onto the active sites of OASS-A (aquamarine). The *re* face of the cofactor is visible at the bottom of the active site cleft. The Schiff base linkage is shown between C4’ of PLP and Lys-42. Ser-256 is within H-bonding distance to N1 of the pyridine ring. The asparagines loop, which interacts with the α-carboxylate group of the amino acid substrate, is shown in the right inset and the threonine loop, which interacts with the 5’-phosphate, is shown in the left inset. The side chain of N72 interacts with O3’ of the PLP cofactor. N69 in OASS-A changes position as the asparagines loop moves upon binding of the amino acid substrate to allow it to interact with the amino acid substrate α-carboxylate group and O3’ of the PLP. N69 (observed in OASS-A) is replaced by S70 in the B-isozyme. The figure was prepared using DS Viewer 5.0 from Accelrys.

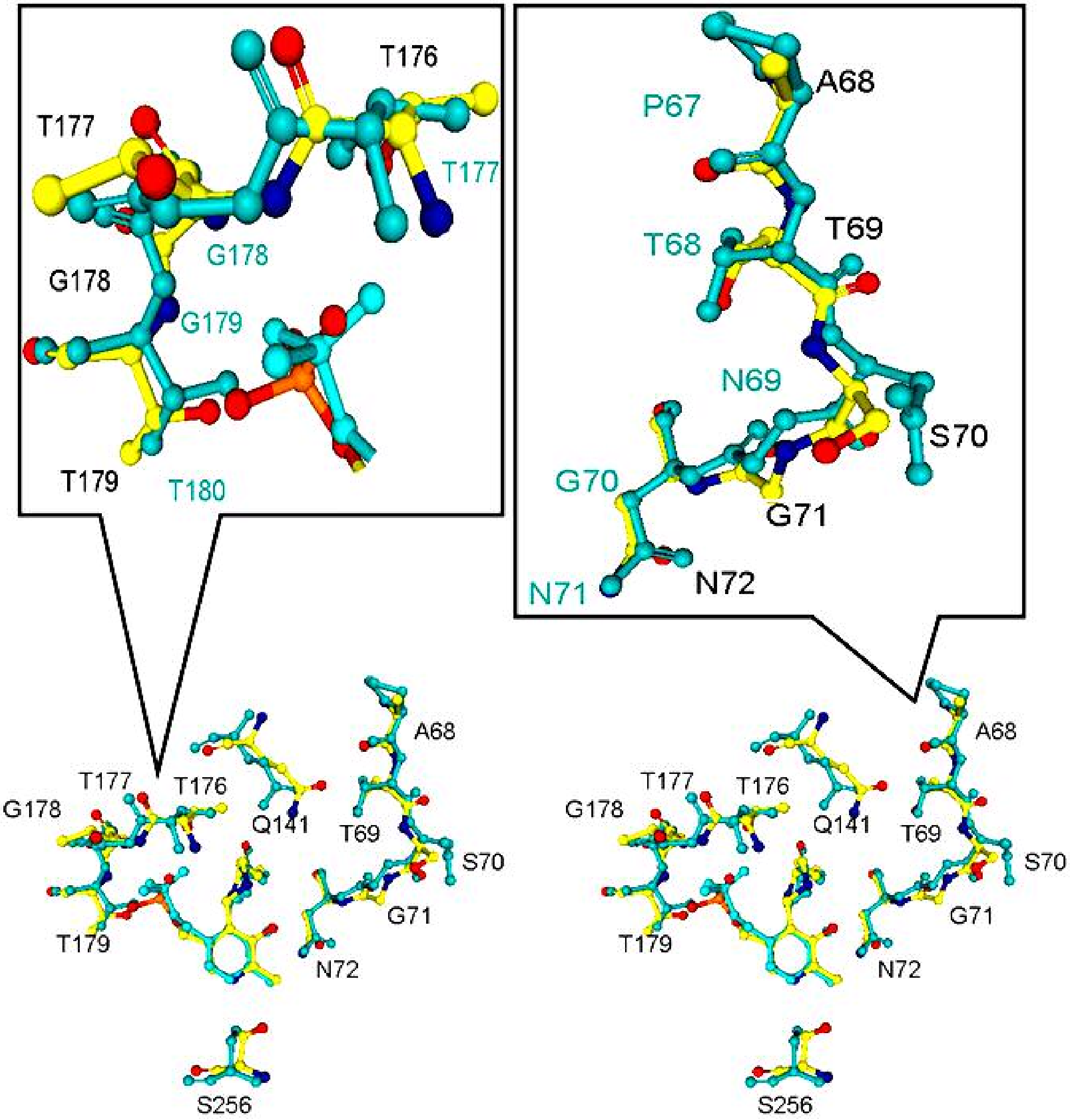
T176
T177
T177
G178
G178
G179
T179
T180
P67
A68
T68
T69
N69
S70
G70
G71
N71
N72
G178
T177
T176
Q141
A68
T69
S70
G71
N72
T179
S256
G178
T177
T176
Q141
A68
T69
S70
G71
N72
T179
S256

OASS-A and S256 in OASS-B), and the dipole of a helix (helix 10 in OASS-A and helix 9 in OASS-B). In the OASS-A, the pyridine ring of PLP is supported from the back by Val-40, but this is not observed in the B-isozyme.

An overlay of the overall structures of WT and K41A mutant OASS-A isozyme shows a large conformational change in a sub-domain of the N-terminal domain to close the active site of OASS-A (Fig. 3, Chapter I). In OASS-A, N69 moves 7Å compared to its position in the open conformation to make two new H-bonds, one with the α-carboxylate of amino acid substrate and the other with O3' of PLP. It is thought that the interaction between the asparagines loop and the α-carboxylate is the trigger that causes the movement of the sub-domain consisting of β-strands 4 and 5 and α-helices 3 and 4 and as a result, reducing the twist of the central β-sheet and closing the active site. In OASS-B, N69 is replaced with S70 to accommodate the OASS-B amino acid sequence. S70 is not expected to play the same role in the conformational changes as does N69 in OASS-A. As a result, the conformational changes to close the active site in OASS-A might not be the same in the B-isozyme.

REFRENCES

(1) Odom, J. M. S., R. (1993) *The Sulfate-Reducing Bacteria: Contemporary Perspectives.*, Springer-Verlag New York Berlin Heidelberg.

(2) Barton, L. L. (1995) *Sulfate Reducing Bacteria*, Plenum Press, New York.

(3) Hulanicka, M. D., Garrett, C., Jagura-Burdzy, G., and Kredich, N. M. (1986) Cloning and Characterization of the *cys*AMK Region of *Salmonella typhimurium. J. Bacteriol. 168*, 322-327.

(4) Postgate, J. R. (1980) *Sulphur in Biology*, Ciba Foundation Symposium 72, Casparie, Amesterdam, Netherland.

(5) Griffith, O. W. (1987) Cysteinesulfinate Decarboxylase. *Meth. Enzymol. 143*, 366-376.

(6) Kredich, N. M., Hulanicka, M. D., and Hallquiest, S. G. (1979) Synthesis of L-Cysteine in *Salmonella typhimurium, 72, 87-99.*

(7) Hell, R. (1997) Molecular Physiology of Plant Sulfur Metabolism *Planta. 202*, 138-148.

(8) Kredich, N. M. (1971) Regulation of L-Cysteine Biosynthesis in *Salmonella typhimurium. J. Biol. Chem. 246*, 3474-3484.

(9) Warrilow, A. G. S., and Hawkesford, M. J. (2000) Cysteine Synthase (*O*-Acetylserine (Thiol) Lyase) Substrate Specificities Classify the Mitochondrial Isoform as a Cyanoalanine Synthase. *J. Experimental Botany 51*, 985-993.

(10) Brunold, C. (2000) Sulfur Nutrition and Sulfur Assimilation in Higher Plants: Molecular, Biochemical, and Physiological Aspects, Berne: Haupt.

(11) Kredich, N. M., Becker, M. A., and Tomkins, G. M. (1969) Purification and Characterization of Cysteine Synthetase, a Bifunctional Protein Complex, from *Salmonella typhimurium*. *J. Biol. Chem. 244*, 2428-2439.

(12) Bogdanova, N., and Hell, R. (1997) Cysteine Synthesis in Plants: Protein-Protein Interactions of Serine Acetyltransferase from Arabidopsis thaliana. *The Plant Journal 11*, 251-262.

(13) Schneider, G. K., H.; and Lindqvist, Y. (2000) The Manifold of Vitamin B_6 Dependent Enzymes. *Structure 8*, R1-R6.

(14) Alexander, F. W., Sandmeier, E., Metha, P. K., and Christen, P. (1994) Evolutionary Relationships Among Pyridoxal 5'-phosphate-dependent Enzymes: Regio-specific α, β, and γ families. *Eur. J. Biochem. 219*, 953-960.

(15) Braunstein, A. E., and Goryachenkova, E. V. (1984) The Pyridoxal-Phosphate-Dependent Enzymes Exclusively Catalyzing Reactions of β-Replacement. *Adv. Enzymol. 56*, 1-89.

(16) Tai, C.-H., and Cook, P. F. (1998) O-Acetylserine Sulfhydrylase. *Adv. Enzymol. Related Areas Mol. Biol. 74*, 185-234.

(17) Morozow, Y. V. (1985) Spectroscopic Properties, Electronic Structure and Photochemical Behavior of Vitamin B_6 and Analogs, in *Coenzymes and Cofactors Vol. 1 Vitamin* B_6 *Pyridoxal Phosphate* pp 131-222, John Wiley & Sons.

(18) Dunn, M. F., Aguilar, V., Brzovíc, P., William F. Drewe, J., Houben, K. F., Leja, C. A., and Roy, M. (1990) The Tryptophan Synthase Bienzyme Complex Transfers Indole Between the α- and β-Sites via a 25-30 Å Long Tunnel. *Biochemistry. 29*, 8598-8607.

(19) Miles, E. W. (1995) Tryptophan Synthase, Structure, Function, and Protein Engineering. *Sub-Cellular Biochemistry 24*, 207-254.

(20) Hyde, C. C., Ahmed, S. A., Padlan, E. A., Miles, E. W., and Davies, D. R. (1988) Three-dimensional Structure of the Tryptophan Synthase $\alpha_2\beta_2$ Multienzyme Complex from *Salmonella typhimurium*. *J. Biol. Chem. 263*, 17857-17871.

(21) Miles, E. W. (2001) Tryptophan Synthase: A Multienzyme Complex with an Intramolecular Tunnel. *The Chemical Record 1*, 140-151.

(22) Lane, A. N., Paul, C. H., and Kirschner, K. (1984) The Mechanism of Self-Assembly of the Multi-Enzyme Complex Tryptophan Synthase from *E. Coli*. *EMBO J. 3*, 279-287.

(23) Banik, U., Zhu, D. M., Chock, P. B., and Miles, E. W. (1995) The Tryptophan Synthase $\alpha_2\beta_2$ Kinetic Studies with a Mutant Enzyme (β K87T) To Provide Evidence for Allosteric Activation by an Aminoacrylate Intermediate. *Biochemistry 34*, 12704-12711.

(24) Grishin, N. V., Phillips, M. A., and Goldsmith, E. J. (1995) Modeling of the Spatial Structure of Eukaryotic Ornithine Decarboxylases. *Protein Science 4*, 1291-1304.

(25) Woehl, E. U., and Dunn, M. F. (1995b) The Roles of Na^+ and K^+ in Pyridoxal Phosphate Enzyme Catalysis *Coord. Chem. Rev. 144*, 147-197.

(26) Ruvinov, S. B., A., A. S., McPhie, P., and Miles, E. W. (1995) Monovalent Cations Partially Repair a Conformational Defect in a Mutant Tryptophan Synthase $\alpha_2\beta_2$ Complex. *J. Biol. Chem. 270*, 17333-17338.

(27) Miles, E. W. (1991) Structural Basis for Catalysis by Tryptophan Synthase. *Adv. Enzymol. Related Areas Mol. Biol. 64*, 93-172.

(28) Drewe, W. F., Jr., and Dunn, M. F. (1985) Detection and Identification of Intermediates in the Reaction of L-Serine with *Escherichia coli* Tryptophan Synthase via Rapid-Scanning Ultraviolet-Visible Spectroscopy. *Biochemistry. 24*, 3977-3987.

(29) Brzovic, P. S., Kayastha, A. M., Miles, E. W., and Dunn, M. F. (1992) Substitution of Glutamic Acid 109 by Aspartic Acid Alters the Substrate Specificity and Catalytic Activity of the β-Subunit in the Tryptophan Synthase Biencyme complex from *Salmonella typhimurium*. *Biochemistry 31*, 1180-1190.

(30) Kayastha, A. M., Sawa, Y., Nagata, S., and Miles, E. W. (1991) Site-directed mutagenesis of the β-subunit of tryptophan synthase from *Salmonella typhimurium. J. Biol. Chem. 266*, 7618-7625.

(31) Strambini, G. B., Cioni, P., Peracchi, A., and Mozzarelli, A. (1992) Characterization of Tryptophan and Coenzyme Luminescence in Tryptophan Synthase from *Salmonella typhimurium. Biochemistry. 31*, 7527-7534.

(32) Skye, G. E., Potts, R., and Floss, H. G. (1974) Stereochemistry of the Tryptophan Synthase Reaction. *J. Am. Chem. Soc. 96*, 1593-1595.

(33) Schleicher, E., Mascaro, K., Potts, R., Mannn, D. R., and Floss, H. G. (1976) Stereochemistry and Mechanism of Reactions Catalyzed by Tryptophanase and Tryptophan Synthetase. *J. Am. Chem. Soc. 98*, 1043-1044.

(34) Miles, E. W., Houck, D. R., and Floss, H. G. (1982) Stereochemistry of Sodium Borohydride Reduction of Tryptophan Synthase of *Escherichia coli* and its Amino Acid Schiff's Bases. *J. Biol. Chem. 257*, 14203-14210.

(35) Steegborn, C., Clausen, T., Sondermann, P., Jacob, U., Worbs, M., Marinkovic, S., Huber, R., and Wahl, M. C. (1999) Kinetics and Inhibition of Recombinant Human Cystathionine γ-Lyase. *J. Biol. Chem. 274*, 12675-12684.

(36) Banerjee, R., Evandi, R., Kabil, O., Ojha, S., and Taoka, S. (2003) Reaction Mechanism and Regulation of Cystathionine β-Synthase. *Biochim. Biophys. Acta 1647*, 30-35.

(37) Meier, M., Janosik1, M., Kery1, V., Kraus1, J. P., and Burkhard, P. (2001) Structure of Human Cystathionine ß-Synthase: a unique Pyridoxal 5'-Phosphate-Dependent Heme Protein. *EMBO J. 20*, 3910-3916.

(38) Shan, X., Dunbrack Jr, R. L., Christopher, S. A., and Kruger, W. D. (2001) Mutations in the Regulatory Domain of Cystathionine β-Synthase can Functionally Suppress Patient-Derived Mutation *in cis*. *Human Molecular Genetics 10*, 635-643.

(39) Aitken, S. M., and Kirsch, J. F. (2003) Kinetics of the Yeast Cystathionine β-Synthase Forward and Reverse Reactions: Continuous Assays and the Equilibrium Constant for the Reaction. *Biochemistry 42*, 571-578.

(40) Jhee, K.-H., Niks, D., McPhie, P., Dunn, M. F., and Miles, E. W. (2001) The Reaction of Yeast Cystathionine β-Synthase is Rate-Limited by the Conversion of Aminoacrylate to Cystathionine. *Biochemistry 40*, 10873-10880.

(41) Taoka, S., and Banerjee, R. (2002) Stopped-flow Kinetic Analysis of the Reaction Catalyzed by the Full-Length Yeast Cystathionine β-Synthase. *J. Biol. Chem. 277*, 22421-22425.

(42) Gallagher, D. T., Chinchilla, D., Lau, H., and Eisenstein, E. (2004) Local and Global Control Mechanisms in Allosteric Threonine Deaminase. *Methods Enzymol. 380*, 85-106.

(43) Eisenstein, E., Yu, H. D., and Schwarz, F. P. (1994) Threonine Deaminase. *J. Biol. Chem. 269*, 29423-29429.

(44) Wessel, P. M., Graciet, E., Douce, R., and Dumas, R. (2000) Evidence for Two Distinct Effector-Binding Sites in Threonine Deaminase by Site-Directed Mutagenesis, Kinetic, and Binding Experiments. *Biochemistry 39*, 15136 -15143.

(45) Sharma, R. K., and Mazunder, R. (1970) Purification, Properties, and Feedback Control of L-Threonine Dehydratase from Spinach. *J. Biol. Chem. 245*, 3008-3014.

(46) Burkhard, P., Rao, G. S. j., Hoehenester, E., Schnackerz, K. D., Cook, P. F., and Jansonius, J. N. (1998) Three-Dimensional Structure of *O*-Acetylserine Sulfhydrylase from *Salmonella typhimurium*. *J. Mol. Biol. 283*, 121-133.

(47) Chinchilla, D., Schwarz, F. P., and Eisenstein, E. (1998) Amino Acid Substitutions in the C-terminal Regulatory Domain Disrupt Allosteric Effector Binding to Biosynthetic Threonine Deaminase from *Escherichia coli*. J. Biol. Chem. *273*, 23219-23224.

(48) Tomoyoshi-Nozaki, T., Shigeta, Y., Saito-Nakano, Y., Imada, M., and Kruger, W. D. (2001) Characterization of Transsulfuration and Cysteine Biosynthetic

Pathways in the *Protozoan Hemoflagellate*, and *Trypanosoma cruzi*. *J. Biol. Chem. 276*, 6516–6523.

(49) Becker, M. A., Kredich, N. M., and Tomkins, G. M. (1969) The Purification and Characterization of *O*-Acetylserine Sulfhydrylase-A from *Salmonella typhimurium*. *J. Biol. Chem. 244*, 2418-2427.

(50) Hulanicka, M. D., Hallquist, S. G., Kredich, N. M., and Mojica-A, T. (1979) Regulation of *O*-Acetylserine Sulfhydrylase-B by L-Cysteine in *Salmonella typhimurium*. *J. Bacteriol. 140*, 141-146.

(51) Mino, K., and Ishikawa, K. (2003) Characterization of a Novel Thermostable *O*-Acetylserine Sulfhydrylase from *Aeropyrum pernix* K1. *J. Bacteriol. 185*, 2277-2284.

(52) Cook, P. F., and Wedding, R. T. (1976) A Reaction Mechanism from Steady-State Kinetic Studies for *O*-Acetylserine Sulfhydrylase from *Salmonella typhimurium* LT-2. *J. Biol. Chem. 251*, 2023-2029.

(53) Tai, C.-H., Nalabolu, S. R., Jacobson, T. M., Minter, D. E., and Cook, P. F. (1993) Kinetic mechanisms of A and B isozymes of *O*-acetylserine sulfhydrylase from *Salmonella typhimurium* LT-2 using the natural and alternative reactants. *Biochemistry 32*, 6433-6442.

(54) Tai, C.-H., Burkhard, P., Gani, D., Jenn, T., Johnson, C., and Cook, P. F. (2001) Characterization of the Allosteric Anion-Binding Site of *O*-Acetylserine Sulfhydrylase. *Biochemistry 40*, 7446-7452.

(55) Hwang, C.-C., Woehl, E. U., Dunn, M. F., and Cook, P. F. (1996) Kinetic Isotope Effects as a Probe of the β-Elimination Reaction Catalyzed by *O*-Acetylserine Sulfhydrylase. *Biochemistry 35*, 6358-6365.

(56) Gallagher, D. T., Gilliland, G. L., Xiao, G., Zondlo, J., Fisher, K. E., Chinchilla, D., and Eisenstein, E. (1998) Structure and Control of Pyridoxal Phosphate Dependent Allosteric Threonine Deaminase. *Structure 6*, 465-475.

(57) Yao, M. (2000) Crystal Structure of L-Aminocyclopropane-L-Carboxylate Deaminase from *Hansenula saturnus*. *J Biol Chem 275*, 34557-34565.

(58) Burkhard, P., Tai, C.-H., Jansonius, J. N., and Cook, P. F. (2000) Identification of an Allosteric Anion-Binding Site on *O*-Acetylserine Sulfhydrylase: Structure of the Enzyme with Chloride Bound. *J. Mol. Biol. 303*, 279-286.

(59) Burkhard, P., Tai, C.-H., Ristroph, C., Cook, P. F., and Jansonius, J. N. (1999) Ligand Binding Induces a Large Conformational Change in *O*-Acetylserine Sulfhydrylase from *Salmonella typhimurium*. *J. Mol. Biol. 291*, 941-953.

(60) Cook, P. F., Hara, S., Nalabolu, S., and Schnackerz, K. D. (1992) pH-Dependence of the Absorbance and ^{31}P NMR Spectra of *O*-Acetylserine Sulfhydrylase in the Absence and Presence of *O*-Acetyl-L-Serine. *Biochemistry. 31*, 2299-2303.

(61) Cook, P. F., Tai, C.-H., Hwang, C.-C., Woehl, E. U., Dunn, M. F., and Schanckerz, K. D. (1996) Substitution of Pyridoxal 5'-Phosphate in the *O*-Acetylserine Sulfhydrylase from *Salmonella typhimurium* by Cofactor Analogs Provides a Test of the Mechanism Proposed for Formation of the α-Aminoacrylate Intermediate. *J. Biol. Chem. 271*, 25842-25849.

(62) Rege, V. D., Karsten, W. E., Schnackerz, K. D., Kredich, N. M., and Cook, P. F. (1996) Involvement of Lys-41 in the β-Elimination Reaction Catalyzed by *O*-Acetylserine Sulfhydrylase-A from *Salmonella typhimurium. FASEB J. 10*, A1382.

(63) Schnackerz, K. D., Tai, C.-H., Simmons, J. W., III, Jacobson, T. M., Rao, G. S. J., and Cook, P. F. (1995) Identification and Spectral Characterization of the External Schiff base of the *O*-Acetylserine Sulfhydrylase Reaction. *Biochemistry 34*, 12152-12160.

(64) Tai, C.-H., Nalabolu, S. R., Simmons, J. W., III, Jacobson, T. M., and Cook, P. F. (1995) Acid-Base Chemical Mechanism of *O*-Acetylserine Sulfhydrylase-A and -B from pH Studies. *Biochemistry 34*, 12311-12322.

(65) Strambini, G. B., Cioni, P., and Cook, P. F. (1996) Tryptophan Luninescence as a Probe of Enzyme Conformation Along the *O*-Acetylserine Sulfhydrylase Reaction Pathway. *Biochemistry 35*, 8392-8400.

(66) Benci, S., Maccari, S., Mozzarelli, A., and Cook, P. F. (1997) Time-Resolved Fluorescence of *O*-Acetylserine Sulfhydrylase Catalytic Intermediates. *Biochemistry 36*, 15419-15427.

(67) Benci, S., Vaccari, S., Mozzarelli, A., and Cook, P. F. (1999) Time-Resolved Fluorescence of O-Acetylserine Sulfhydrylase. *Biochim. Biophys. Acta 1429*, 317-330.

(68) Woehl, E. U., Tai, C.-H., Dunn, M. F., and Cook, P. F. (1996) Formation of the α-Aminoacrylate Intermediate Limits the Overall Reaction Catalyzed by *O*-Acetylserine Sulfhydrylase. *Biochemistry 35*, 4776-4783.

(69) Tai, C.-H., Cook, P. F., and Schnackerz, K. D. (2000) Conformation of the a-Aminoacrylate Intermediate of *O*-Acetylserine Sulfhydrylase from *Salmonella typhimurium* as Inferred from ^{31}P NMR Spectroscopy. *Protein & Peptide Lett. 7*, 207-210.

(70) Tai, C.-H., and Cook, P. F. (2001) Pyridoxal 5'-Phosphate-Dependent α,β-Elimination Reactions: Mechanism of *O*-Acetylserine Sulfhydrylase. *Accts. Chem. Res. 34*, 49-59.

(71) Karsten, W. E., Tai, C.-H., and Cook, P. F. (2002) Detection of Intermediates in the Reactions Catalyzed by PLP-Dependent Enzymes. *Methods Enzymol. 354*, 223-237.

(72) Daum, S., Tai, C.-H., and Cook, P. F. (2003) Characterization of the S272A,D Site-Directed Mutations of *O*-Acetylserine: Involvement of the Pyridine Ring in the α,β-Elimination Reaction. *Biochemistry 42*, 106-113.

(73) Westheimer, F. H. (1961) The Magnitude of the Primary Kinetic Isotope for Compounds of Hydrogen and Deuterium. *Chem. Rev. 61*, 265-273.

(74) Streitweiser, A., Jr., Jagow, R. H., Fahey, R. C., and Suzuki, S. (1958) Kinetic Isotope Effects in the Acetolysis of Deuterated Cyclopentyl Tosylates. *J. Am. Chem. Soc. 80*, 2326-2332.

(75) Ostrowski, J., Jagura-Burdzy, G., and Dredich, N. M. (1987) DNA Sequences of the *cys*B Regions of *Salmonella typhimurium* and *Escherichia coli*. *J. Biol. Chem. 262*, 5999-6005.

(76) Kredich, N. M. (1992) The Molecular Basis for Positive Regulation of *cys* Promoters in *Salmonella typhimurium* and *Escherichia coli*.

(77) Ostrowski, J., and Kredich, N. M. (1989) Molecular Characterization of the *cys*JIH Promoters of *Salmonella typhimurium* and *Escherichia coli*: Regulation by *cys*B Protein and *N*-acetyl-L-Serine. *J. Bacteriol. 171*, 130-140.

(78) Tai, C.-H., Nalabolu, S. R., Jacobson, T. M., Minter, D. E., and Cook, P. F. (1993) Kinetic Mechanisms of the A and B Isozymes of *O*-Acetylserine Sulfhydrylase from *Salmonella typhimurium* LT-2 Using the Natural and Alternative Reactants. *Biochemistry 32*, 6433-6442.

(79) Nakamura, K., Iwahashi, H., and Eguchi, Y. (1983) Evidence that thiosulfate assimilation by *Salmonella typhimurium* is catalyzed by cysteine synthase B. *J. Bacteriol. 156*, 656-662.

(80) Tai, C.-H., Jacobson, T. M., and Cook, P. F. (1993) Chemical Mechanism of the *O*-Acetylserine Sulfhydrylase-B from *Salmonella typhimurium*. *FASEB J. 7*, A1062.

(81) Hara, S., Payne, M. A., Schnackarz, K. D., and Cook, P. F. (1990) A Rapid Purification Procedure and Computer-Assisted Sulfide Ion Selective Electrode Assay from *O*-Acetylserine Sulfhydrylase from *Salmonella typhimurium*. *Prot. Express. and Purif. 1*, 70-76.

(82) Cleland, W. W. (1979) Statistical Analysis of Enzyme Kinetic Data. *Methods Enzymol. 63*, 103-138.

(83) Schowen, K. B., and Schowen, R. L. (1982) Solvent isotope effects on enzyme systems. *Methods Enzymol. 87*.

(84) Silverstein, R. M., and Webster, F. X. (1998) *Spectrometric Identification of Organic Compounds*, Sixth ed., Wiley, New York.

(85) Cleland, W. W. (1977) Determining the chemical mechanisms of enzyme-catalyzed reactions by kinetic studies. *Adv. Enzymol. Related Areas Mol. Biol. 45*, 273-387.

(86) Monroe, R. S., and Kredich, N. M. (1988) Isolation of *Salmonella typhimurium cys* Genes by Transduction with a Library of Recombinant Plasmids Packaged in Bacteriophage P22HT Capsids. *J. Bacteriol. 170*, 42-47.

(87) Tai, C.-H., and Cook, P. F. (1993) Kinetic and Chemical Mechanism of *O*-Acetylserine Sulfhydrylase-B from *Salmonella typhimurium*. *Ph.D. Dissertation*.

(88) Cook, P. F., and Wedding, R. T. (1976) Release of the Intermediate Product, *O*-Acetylserine-L-Serine, by the Multienzyme Complex, Cysteine Synthetase. *Fed. Proc. 35*, 1672.

(89) Cantor, C. R., and Schimmel, P. R. (1980) *Biophysical Cemistry. Part II: Techniques for the Study of Biological Structure and Function.*, Vol. II, Academic Press, New York.

(90) Arrio-Dupont, M. (1970) Etude Par Fluorescence De Bases De Schiff Du Pyridoxal, Comparaison Avec La L-Aspartate-Aminotransferase. *photochem. Photobiol. 12*, 297-315.

(91) Cheng, S., Michuda-Kozak, C., and Martinez-Carrion, M. (1971) Effects of Anions on the Substrate Affinities of the Pyridoxal and Pyridoxamine Forms of Mitochondrial and Supernatant Aspartate Transaminases. *The J. Biol. Chem. 246*, 3623-3630.

(92) Sevilla, F. M., Cambron, G., Pineda, T., and Blazquez, M. (1995) Electroreduction of the Schiff Base of Pyridocal-5'-Phosphate and Hexylamine in

Dimethylformamide and Methanol. Effect of the Self-Protonation. *J. Electroanal. Chem. 381*, 179-186.

(93) McClure, G. D., Jr., and Cook, P. F. (1994) Product Binding to the a-Carboxyl Subsite Results in a Conformational Change at the Active Site of *O*-Acetylserine Sulfhydrylase-A: Evidence from Fluorescence Spectroscopy. *Biochemistry 33*, 1647-1683.

(94) Benci, S., Bettati, S., Vaccari, S., Schianchi, G., Cook, P. F., and Mozzarelli, A. (1999) Conformational Probes of *O*-Acetylserine Sulfhydrylase: Fluorescence of Tryptophans 50 and 161. *J. Photochem. Photobiol. B: Biol. 48*, 17-26.

(95) Schneider, T. R., Gerhardt, E., Lee, M., Liang, P. H., Anderson, K., and Schlichting, I. (1998) Loop Closure and Intersubunit Communication in Tryptophan Synthase. *Biochemistry 37*, 5394 -5406.